

**INVESTIGATIONS ON MACHINABILITY
CHARACTERISTICS OF EN47 SPRING STEEL USING
OPTIMIZATION TECHNIQUES**

Thesis

Submitted in partial fulfillment of the requirements for the degree of
DOCTOR OF PHILOSOPHY

by

VASU. M



DEPARTMENT OF MECHANICAL ENGINEERING
NATIONAL INSTITUTE OF TECHNOLOGY KARNATAKA,
SURATHKAL, MANGALORE – 575025
SEPTEMBER-2019

DECLARATION

I hereby declare that the Research Thesis entitled “**Investigations on Machinability Characteristics of EN47 Spring Steel using Optimization Techniques**” which is being submitted to the **National Institute of Technology Karnataka, Surathkal** in partial fulfillment of the requirements for the award of the Degree of **Doctor of Philosophy in Mechanical Engineering** is a *bonafide report of the research work carried out by me*. The material contained in this Research Thesis has not been submitted to any other Universities or Institutes for the award of any degree.

Register Number: **155019ME15F15**

Name of the Research Scholar: **VASU M.**

Signature of the Research Scholar:

Department of Mechanical Engineering

Place: NITK-Surathkal

Date:

CERTIFICATE

This is to certify that the Research Thesis entitled “**Investigations on Machinability Characteristics of EN47 Spring Steel using Optimization Techniques**” submitted by **Mr. VASU M. (Register Number: 155019ME15F15)** as the record of the research work carried out by him, *is accepted as the Research Thesis submission* in partial fulfillment of the requirements for the award of the Degree of **Doctor of Philosophy**.

Dr. H. SHIVANANDA NAYAKA

Associate Professor

Chairman-DRPC

Date:

ACKNOWLEDGMENTS

With respectful pranamas, I express my sincere gratitude to His Holiness **Dr. Sri Sri Sri Shivakumara Swamigalu**, for his blessings on the students through many years.

I thank Lord Shiva for giving me the confidence and presence of mind throughout this endeavor and completing this work without any problem.

It is my great pleasure to express my heartfelt gratitude to my research supervisor **Dr. H. Shivananda Nayaka**, Associate Professor, Department of Mechanical Engineering, National Institute of Technology Karnataka, Surathkal, for his exemplary guidance and encouragement throughout my research work. His encouragement and the valuable suggestions have increased my knowledge level which led to the completion of my research work and is demonstrated through this thesis.

I sincerely thank the RPAC members, **Dr. Hemantha Kumar**, Associate Professor, Department of Mechanical Engineering and **Dr. B Venkatesa Perumal**, Associate Professor & Head, Department of Electrical and Electronics Engineering, for providing valuable suggestion and support extended to me on all occasion.

I wish to express my sincere gratitude to **Dr. K V Gangadharan**, Professor and, **Dr. S Narendranath**, Professor for their valuable suggestions to do this research work.

I wish to express my sincere thanks to **Dr. Shrikantha S Rao**, Professor and Head, Department of Mechanical Engineering, National Institute of Technology Karnataka, Surathkal, Mangalore, for his kind help in providing the facilities.

I wish to express my thanks to, **Dr. Anandhan Srinivasan**, Professor and, Head of Metallurgical and Materials Department for permitting me to use the Scanning Electron Microscope for characterization of the specimen and also, I thank Ms. Rashmi Banjan of Department of Metallurgical and Materials, for her support in connection with the use of scanning electron microscope.

I owe my deepest gratitude to supporting staff of the Department of Mechanical Engineering, Mr. Jaya Devadiga, Mr. C A Verghese, Mr. Pradeep and Mr. Sudhakar Naik for their help during conducting experiments.

I thank the Director and the administration of NITK Surathkal for permitting me to pursue my research work at the Institute.

I sincerely thank **NMTC-CMTI** Bangalore and **DST-PURSE** lab Mangalore University for all the testing facilities.

Timely industrial support had helped to finish a number of hurdles during the journey, I would like to thank Mr. Vasu B. Sr. Marketing Executive, for their selfless advice, assistance and contribution in this work.

The unfailing support of my colleagues had provided brilliant ideas, everlasting optimism and assistance. I would like to thank my friends Mr. Jagadish C, Dr. Pradeep V Badiger, Dr. Ashrith H. S, Dr. Vinyas M, Mr Vishwas M, Dr. G Venkatesh, Dr. P Sivaiah, Dr. Gopi K R, Mr. Praveen T R, Mr. Ramesh S, Mr. Jagadeesh C and Mr. Sachin S for their selfless advice, assistance and contribution in this work.

Lastly, I would like to immensely thank my parents **Sri. Mallesha M & Smt. Chikkamma**. My Brothers **Mr. Sathyananda M & Mr. Bharath M**.

At last, but not the least, thanks to my wife **Smt. Tejeswini M G** and my daughter baby **Hitha V** for their undying love, encouragement and moral support throughout my life and education. Without them and their wishes, achieving this goal would not have been possible.

(Vasu M.)

ABSTRACT

Challenge of any manufacturing industry to give a better quality of products to society with minimum manufacturing cost, low manufacturing time and less consumption of raw material. Manufacturing involves various processes to convert raw material into finished products and hence meet demands with high-quality products. Selection of process parameters plays a significant role to satisfy all demands to ensure the quality of the product, increased production rate, and reduced operating cost. For such cases, optimization is essential to represent manufacturing process. Process parameters have been optimized by chosen best possible optimization techniques. Before conducting any experiments, selection of workpiece and tools it is necessary, to explore the literature to know, what has happened in earlier days. A literature survey has been done thoroughly existing statistical techniques are understood and implemented to optimize speed, feed, and depth of cut. EN47 spring steel has been chosen as work material which has a hardness of 45-48HRC. Hard turning process eliminates grinding process, and EN47 steel possesses low thermal conductivity and suitably oil hardened and tempered. Hardened spring steel offers excellent toughness and shock resistance, and are considered as suitable material for automobile applications. Other applications involve such as manufacturing of die, leaf spring for a heavy vehicle, crankshaft, spindles, pumps and steering knuckles and many general engineering applications.

Experiments were performed using two different techniques, namely, one factor at a time (OFAT) approach and Design of Experiments (DOE). Cutting tool inserts are commercially available in the form of PVD coated TiAlN German make and are used during machining. Cutting forces, surface roughness, tool tip temperature, and material removal rate are estimated experimentally. From the experimental work, it is known that with an increase in nose radius, cutting forces, tool tip temperature, and material removal rate are increased, but surface roughness is decreased. Further, a tool with 0.8mm nose radius exhibits nominal performance in all output performances. 0.8mm nose radius tools are used to work in three different cutting environments, namely dry, wet and cryogenic. From the analysis, cryogenic machining showed better quality of the machined surface, tool wear also reduced and tool tip temperature decreased.

Experiments were performed and analyzed using design of experiments (DOE) technique L₂₇ full factorial design. A second order regression model was developed to know the interaction effect of output responses. Tool wear was analyzed by confocal microscope and SEM, with varying cutting time. ANOVA was used to identify the significant factor and percentage contribution for a particular output. Results from machining reveal that cutting force is mainly influenced by feed rate and depth of cut. Surface roughness was influenced by cutting speed and feed rate. Tool tip temperature was influenced by cutting speed and depth of cut. Material removal rate was influenced by speed, feed, and depth of cut.

3D response surface plots show interaction effect on each output response. Main effects plots show optimum condition for each output performance. Normal probability plots showed that the developed models are adequate by observing normal error distribution. Determination coefficient (R^2) value should be in between 1 or 100% in the model. Multi-objective optimization was identified by Desirability Approach (DA) and Particle Swarm Optimization (PSO). Also, Artificial Neural Network (ANN) is used to predict experimental results and compared with RSM model, as well as, experimental value. Statistical analysis was done by Minitab and Design Expert Software. Validation was performed by ANN. MATLAB is used to develop artificial neural network model, as well as; codes are developed for PSO. From the experimental analysis, the developed model showed a significant and good agreement between the experimental value and predicted value.

Keywords: EN47 Spring Steel, Coated tungsten carbide tool, Cutting forces, Surface roughness, Wet machining, Cryogenic machining, Tool wear, Material removal rate, Chip morphology, Surface integrity, Artificial neural network, Particle Swarm Optimization, Response Surface Methodology, tool tip temperature, Desirability Approach.

Outline of the thesis

Present thesis has been divided into five chapters which are as follows.

Chapter 1: This chapter explains the background of the machining process, applications of metal alloys of spring steel EN47, basic techniques of Design of Experiments (DOE). Different cutting environments like dry, wet and cryogenic conditions. Modeling and optimization techniques and need for the present study.

Chapter 2: Deals with literature review, in which metal cutting process, the design of experiment, different cutting environments and modeling and optimization techniques are discussed in brief. Also, gain knowledge and familiar with the existing techniques and methodology, research gaps and objectives of research work.

Chapter 3: This chapter explains the methodology of research work, description of all machines, measuring instruments, work piece material and cutting tool inserts used in the present work.

Chapter 4: In this chapter explains result and discussion of experimental work. Machinability study of EN47 spring steel with tool inserts of different nose radii; 0.4, 0.8 & 1.2 mm. One factor at a time approach was used to identify cutting forces, surface roughness, tool tip temperature, and material removal rate. From the comparative study based on the performance of output response, tool insert with best nose radius was selected for further work.

Using the selected tool insert, turning experiments were conducted at different cutting environments; dry, wet & cryogenic condition using full factorial design (FFD) L_{27} orthogonal array optimization technique to measure cutting forces, surface roughness, tool tip temperature, machined surface analysis, machined surface topography, chip morphology, and tool wear.

Further modeling and optimization of cutting parameters were performed, multi-objective optimization was done by composite desirability approach and PSO technique. Validation has been performed with a new set of cutting condition. Also, an artificial neural network was used to predict the experimental result.

Chapter 5: Explains conclusions and future work.

TABLE OF CONTENTS

| | |
|---|--------------|
| DECLARATION..... | i |
| CERTIFICATE..... | iii |
| ACKNOWLEDGMENTS | v |
| ABSTRACT..... | vii |
| TABLE OF CONTENTS | xi |
| LIST OF TABLES | xv |
| LIST OF FIGURES | xix |
| NOMENCLATURE..... | xxv |
| SYMBOLS | xxvii |
| 1 INTRODUCTION..... | 1 |
| 1.1 Background | 1 |
| 1.2 DOE technique..... | 3 |
| 1.3 Cutting environments..... | 3 |
| 1.3.1 Dry Machining | 3 |
| 1.3.2 Wet Machining..... | 4 |
| 1.3.3 Cryogenic Machining..... | 4 |
| 1.4 Modeling techniques | 4 |
| 1.5 Need for the present study | 5 |
| 2 LITERATURE SURVEY..... | 7 |
| 2.1 Independent variables | 7 |
| 2.1.1 Cutting parameters | 7 |
| 2.1.2 Workpiece material..... | 8 |
| 2.1.3 Tool material..... | 8 |
| 2.1.4 Tool geometry | 9 |
| 2.2 Machinability factors | 9 |
| 2.2.1 Effect of cutting parameters on cutting forces | 9 |
| 2.2.2 Effect of cutting parameters on surface roughness | 11 |

| | | |
|----------|---|-----------|
| 2.2.3 | Effect of cutting parameters on material removal rate (MRR) | 13 |
| 2.2.4 | Effect of cutting parameters on tool tip temperature | 15 |
| 2.2.5 | Effect of cutting parameters on tool wear | 16 |
| 2.2.6 | Effect of cutting parameters on chips | 17 |
| 2.3 | Modeling and optimization technique | 18 |
| 2.3.1 | Particle Swarm Optimization (PSO)..... | 18 |
| 2.3.2 | Desirability Approach (DA) | 19 |
| 2.4 | Artificial Neural Networks (ANNs)..... | 21 |
| 2.5 | Gaps found from literature survey | 24 |
| 2.6 | Scope of the work | 24 |
| 2.7 | Objectives | 24 |
| 3 | EXPERIMENTATION | 25 |
| 3.1 | Methodology | 25 |
| 3.2 | Experimental setup..... | 26 |
| 3.3 | Experimental procedure | 26 |
| 3.4 | Workpiece material | 27 |
| 3.5 | Cutting tool material | 27 |
| 3.6 | Infrared thermometer | 28 |
| 3.7 | Panther lathe machine | 29 |
| 3.8 | Surface roughness tester | 30 |
| 3.9 | Lathe tool dynamometer | 31 |
| 3.10 | Confocal microscope | 32 |
| 3.11 | Scanning Electron Microscope | 33 |
| 4 | RESULTS AND DISCUSSION | 35 |
| 4.1 | One factor at a time of approach (OFAT)..... | 36 |
| 4.1.1 | Varying cutting speed | 37 |
| 4.1.2 | Varying feed rate..... | 38 |
| 4.1.3 | Varying depth of cut | 42 |
| 4.2 | Selection of cutting tool insert | 48 |
| 4.3 | Turning process using optimization technique | 49 |
| 4.3.1 | Analysis of variance (ANOVA)..... | 51 |

| | | |
|----------|--|------------|
| 4.3.2 | Main effects plots..... | 54 |
| 4.3.3 | Normal Probability plots..... | 60 |
| 4.3.4 | 3D surface graphs | 63 |
| 4.3.5 | Regression analysis..... | 67 |
| 4.3.6 | Machined surface analysis | 69 |
| 4.3.7 | Machined surface topography..... | 75 |
| 4.3.8 | Chip morphology | 80 |
| 4.3.9 | Tool wear analysis | 88 |
| 4.4 | Multi objective optimization using DA and PSO technique..... | 94 |
| 4.5 | Artificial Neural Networks (ANNs)..... | 99 |
| 4.6 | Validation..... | 107 |
| 5 | CONCLUSIONS | 113 |
| | SCOPE OF FUTURE WORK | 117 |
| | REFERENCES..... | 119 |
| | APPENDIX..... | 127 |
| | LIST OF PUBLICATIONS AND CONFERENCE..... | 139 |
| | BIO-DATA..... | 143 |

LIST OF TABLES

| | |
|---|----|
| Table 3.1 Chemical composition of EN47 spring steel | 27 |
| Table 3.2 Panther lathe machine specification | 30 |
| Table 3.3 Technical specifications of Kistler 9257B dynamometer..... | 32 |
| Table 4.1 OFAT Experimental conditions..... | 36 |
| Table 4.2 Relationship between varying cutting velocity on cutting forces (F_x , F_y & F_z) at different nose radius..... | 37 |
| Table 4.3 Relationship between varying cutting velocity on MRR, surface roughness and tool tip temperature at different nose radius | 37 |
| Table 4.4 Relationship between varying feed rate on cutting forces (F_x , F_y & F_z) at different nose radius..... | 39 |
| Table 4.5 Relationship between varying feed rate on MRR, surface roughness and tool tip temperature at different nose radius | 39 |
| Table 4.6 Relationship between varying depth of cut on cutting forces (F_x , F_y & F_z) at different nose radius..... | 42 |
| Table 4.7 Relationship between varying depth of cut on MRR, surface roughness and tool tip temperature at different nose radius | 42 |
| Table 4.8 Experimental plan and output responses | 50 |
| Table 4.9 ANOVA for tangential cutting force (F_z) during dry condition | 51 |
| Table 4.10 ANOVA for tangential cutting force (F_z) during wet condition..... | 51 |
| Table 4.11 ANOVA for tangential cutting force (F_z) during cryogenic condition..... | 51 |
| Table 4.12 ANOVA for surface roughness (R_a) during dry condition | 52 |
| Table 4.13 ANOVA for surface roughness (R_a) during wet condition..... | 52 |
| Table 4.14 ANOVA for surface roughness (R_a) during cryogenic condition..... | 53 |
| Table 4.15 ANOVA for tool tip temperature (T) during dry condition..... | 53 |
| Table 4.16 ANOVA for tool tip temperature (T) during wet condition | 54 |

| | |
|--|-----|
| Table 4.17 ANOVA for tool tip temperature (T) during cryogenic condition | 54 |
| Table 4.18 Optimum condition for cutting force (F_z) under different cutting environments..... | 55 |
| Table 4.19 Optimum condition for surface roughness (R_a) under different cutting environments..... | 55 |
| Table 4.20 Optimum condition for tool tip temperature (T) under different cutting environments..... | 55 |
| Table 4.21 Optimum conditions by desirability approach..... | 95 |
| Table 4.22 Parameters of MOPSO..... | 97 |
| Table 4.23 Optimum condition by PSO technique | 98 |
| Table 4.24 ANN training parameters..... | 99 |
| Table 4.25 New cutting condition for validation..... | 107 |
| Table 4.26 Error percentage of output response during experimental vs RSM under dry condition | 108 |
| Table 4.27 Error percentage of output response during experimental vs ANN under dry condition | 108 |
| Table 4.28 Error percentage of output response during experimental vs RSM under wet condition | 109 |
| Table 4.29 Error percentage of output response during experimental vs ANN under wet condition | 109 |
| Table 4.30 Error percentage of output response during experimental vs RSM under cryogenic condition..... | 110 |
| Table 4.31 Error percentage of output response during experimental vs ANN under cryogenic condition..... | 110 |
| Table 5.1 ANOVA for tangential cutting force (F_z) during dry condition | 127 |
| Table 5.2 ANOVA for tangential cutting force (F_z) during wet condition..... | 128 |
| Table 5.3 ANOVA for tangential cutting force (F_z) during cryogenic condition..... | 129 |

| | |
|---|-----|
| Table 5.4 ANOVA for surface roughness (Ra) during dry condition..... | 130 |
| Table 5.5 ANOVA for surface roughness (Ra) during wet condition | 131 |
| Table 5.6 ANOVA for surface roughness (Ra) during cryogenic condition | 132 |
| Table 5.7 ANOVA for tool tip temperature (T) during dry condition..... | 133 |
| Table 5.8 ANOVA for tool tip temperature (T) during wet condition | 134 |
| Table 5.9 ANOVA for tool tip temperature (T) during cryogenic condition | 135 |
| Table 5.10 Experimental verses predicted (RSM and ANN) during dry condition... | 136 |
| Table 5.11 Experimental verses predicted (RSM and ANN) during wet condition .. | 137 |
| Table 5.12 Experimental verses predicted (RSM and ANN) during cryogenic condition | 138 |

LIST OF FIGURES

| | |
|--|----|
| Figure 2.1 Basic motion of turning (Viktor P Astakhov 2011) | 8 |
| Figure 2.2 Cutting forces | 10 |
| Figure 2.3 Mathematical principle on a neuron (Kant and Sangwan 2015) | 21 |
| Figure 3.1 Experimental flow chart | 25 |
| Figure 3.2 Experimental setup | 26 |
| Figure 3.3 (a-c) Cutting tool inserts of nose radius (a) 0.4mm, (b) 0.8 mm and (c)1.2 mm | 28 |
| Figure 3.4 Infrared thermometer | 29 |
| Figure 3.5 Panther Lathe machine | 29 |
| Figure 3.6 Mitutoyo Talysurf roughness tester..... | 31 |
| Figure 3.7 Lathe tool dynamometer type 9257B (Kistler)..... | 31 |
| Figure 3.8 Confocal microscope | 33 |
| Figure 3.9 Scanning electron microscope | 33 |
| Figure 4.1 (a-c) Variation of cutting speed on (a) axial force (F_x), (b) thrust force (F_y) and (c) tangential force (F_z) for different nose radii. | 40 |
| Figure 4.2 (a-c) Variation of cutting speed on (a) MRR, (b) surface roughness and (c) tool tip temperature for different nose radii | 41 |
| Figure 4.3 (a-c) Variation of feed rate on on (a) axial force (F_x), (b) thrusrt force (F_y) and (c) tangential force (F_z) for different nose radii. | 44 |
| Figure 4.4 (a-c) Variation of feed rate on (a) MRR, (b) surface roughness and (c) tool tip temperature for different nose radii. | 45 |
| Figure 4.5 (a-c) Variation of depth of cut on (a) axial force (F_x), (b) thrusrt force (F_y) and (c) tangential force (F_z) for different nose radii. | 46 |
| Figure 4.6 (a-c) Variation of depth of cut on (a) MRR, (b) surface roughness and (c) tool tip temperature for different nose radii. | 47 |

| | |
|---|----|
| Figure 4.7 Flow chart showing the variuos stages of experimental work using tool insert of 0.8mm nose radius..... | 48 |
| Figure 4.8 Experimental setup during dry, wet and cryogenic condition | 49 |
| Figure 4.9 Main effects plot for tangential cutting force (F_z) during dry condition | 56 |
| Figure 4.10 Main effects plot for tangential cutting force (F_z) during wet condition.. | 56 |
| Figure 4.11 Main effects plot for tangential cutting force (F_z) during cryogenic condition | 57 |
| Figure 4.12 Main effects plot for surface roughness (R_a) during dry condition..... | 57 |
| Figure 4.13 Main effects plot for surface roughness (R_a) during wet condition | 58 |
| Figure 4.14 Main effects plot for surface roughness (R_a) during cryogenic condition | 58 |
| Figure 4.15 Main effects plot for tool tip temperature (T) during dry condition..... | 59 |
| Figure 4.16 Main effects plot for tool tip temperature (T) during wet condition | 59 |
| Figure 4.17 Main effects plot for tool tip temperature (T) during cryogenic condition | 60 |
| Figure 4.18 Normal probability plot for cutting force (F_z) during dry, wet & cryogenic condition | 61 |
| Figure 4.19 Normal probability plot for surface roughness (R_a) during dry, wet & cryogenic condition..... | 61 |
| Figure 4.20 Normal probability plot for tool tip temperature (T) during dry, wet & cryogenic condition..... | 62 |
| Figure 4.21 (a-c) 3D surface plot for cutting force (F_z) during dry, wet and cryogenic condition | 64 |
| Figure 4.22 (a-c) 3D surface plot for surface roughness (R_a) during dry, wet and cryogenic condition..... | 65 |
| Figure 4.23 (a-c) 3D surface plot tool tip temperature (T) during dry, wet and cryogenic condition | 66 |

| | |
|---|----|
| Figure 4.24 (a-c) SEM micrographs of machined surface at higher cutting speed (118 m/min) at different cutting environments (a) Dry (b) Wet & (c) Cryogenic condition | 71 |
| Figure 4.25 SEM micrographs of machined surface at lower cutting speed (59 m/min) at different cutting environments (a) Dry (b) Wet & (c) Cryogenic condition..... | 72 |
| Figure 4.26 SEM micrographs of machined surface at lower feed rate (0.070 mm/rev) at different cutting environments (a) Dry (b) Wet & (c) Cryogenic condition..... | 73 |
| Figure 4.27 SEM micrographs of machined surface at higher feed rate (0.117 mm/rev) at different cutting environments (a) Dry (b) Wet & (c) Cryogenic condition..... | 74 |
| Figure 4.28 Surface topography at lower feed rate under different cutting environments (a) Dry (b) Wet & (c) Cryogenic condition | 76 |
| Figure 4.29 Surface topography at higher feed rate under different cutting environments (a) Dry (b) Wet & (c) Cryogenic condition | 77 |
| Figure 4.30 Surface topography at lower cutting speed under different cutting environments (a) Dry (b) Wet & (c) Cryogenic condition | 78 |
| Figure 4.31 Surface topography at higher cutting speed under different cutting environments (a) Dry (b) Wet & (c) Cryogenic condition | 79 |
| Figure 4.32 SEM images of chips at $V_c=59$ m/min, $f=0.093$ mm/rev & $a_p=0.4$ mm (a) dry (b) wet & (c) cryogenic condition | 82 |
| Figure 4.33 SEM images of chips at $V_c=118$ m/min, $f=0.093$ mm/rev & $a_p=0.4$ mm (a) dry (b) wet & (c) cryogenic condition | 83 |
| Figure 4.34 SEM images of chips at $f=0.070$ mm/rev, $V_c=59$ m/min & $a_p=0.4$ mm (a) dry (b) wet & (c) cryogenic condition | 84 |
| Figure 4.35 SEM images of chips at $f=0.117$ mm/rev, $V_c=59$ m/min & $a_p=0.4$ mm (a) dry (b) wet & (c) cryogenic condition | 85 |
| Figure 4.36 SEM images of chips at $a_p=0.2$ mm, $f=0.093$ mm/rev & $V_c=75$ m/min (a) dry (b) wet & (c) cryogenic condition | 86 |

| | |
|--|-----|
| Figure 4.37 SEM images of chips at $a_p=0.6$ mm, $f=0.093$ mm/rev & $V_c=75$ m/min (a) dry (b) wet & (c) cryogenic condition | 87 |
| Figure 4.38 Tool wear analysis during dry condition | 90 |
| Figure 4.39 Tool wear analysis during wet condition..... | 91 |
| Figure 4.40 Tool wear analysis during cryogenic condition..... | 92 |
| Figure 4.41 Variation of tool wear with machining time for different conditions of machining..... | 93 |
| Figure 4.42 Desirability plot for cutting force, surface roughness and tool tip temperature during dry condition..... | 94 |
| Figure 4.43 Desirability plot for cutting force, surface roughness and tool tip temperature during wet condition | 95 |
| Figure 4.44 Desirability plot for cutting force, surface roughness and tool tip temperature during cryogenic condition | 96 |
| Figure 4.45 Principle of the particle swarm optimization..... | 97 |
| Figure 4.46 MOPSO Convergence graph | 98 |
| Figure 4.47 Artificial Neural Network..... | 100 |
| Figure 4.48 ANN Regression plots for cutting force during dry condition | 100 |
| Figure 4.49 ANN Regression plots for cutting force during wet condition..... | 101 |
| Figure 4.50 ANN Regression plots for cutting force during cryogenic condition..... | 101 |
| Figure 4.51 ANN Regression plots for surface roughness during dry condition..... | 102 |
| Figure 4.52 ANN Regression plots for surface roughness during wet condition | 102 |
| Figure 4.53 ANN Regression plots for surface roughness during cryogenic condition | 103 |
| Figure 4.54 ANN Regression plots for tool tip temperature during dry condition.... | 103 |
| Figure 4.55 ANN Regression plots for tool tip temperature during wet condition ... | 104 |

| | |
|---|-----|
| Figure 4.56 ANN Regression plots for tool tip temperature during cryogenic condition | 104 |
| Figure 4.57 (a-c) Experimental versus predicted values for cutting force, surface roughness and tool tip temperature during dry condition | 105 |
| Figure 4.58 (a-c) Experimental versus predicted for cutting force, surface roughness and tool tip temperature during wet condition..... | 105 |
| Figure 4.59 (a-c) Experimental versus predicted for cutting force, surface roughness and tool tip temperature during cryogenic condition..... | 106 |
| Figure 4.60 (a-c) Validation for cutting force, surface roughness and tool tip temperature during dry condition..... | 111 |
| Figure 4.61 (a-c) Validation for cutting force, surface roughness and tool tip temperature during wet condition | 111 |
| Figure 4.62 (a-c) Validation for cutting force, surface roughness and tool tip temperature during cryogenic condition..... | 112 |

NOMENCLATURE

| | |
|-----------------|--------------------------------|
| ANN | Artificial Neural Networks |
| ANOVA | Analysis of Variance |
| CVD | Chemical Vapor Deposition |
| DA | Desirability approach |
| DOE | Design of Experiments |
| EDS | Energy Dispersive Spectroscopy |
| EN | Euro Norms |
| FFD | Full Factorial Design |
| GRA | Gray Relational Analysis |
| LN ₂ | Liquid Nitrogen |
| MRR | Material Removal Rate |
| OA | Orthogonal Array |
| PSO | Particle Swarm Optimization |
| PVD | Physical Vapor Deposition |
| R _a | Average Roughness |
| RSM | Response Surface Methodology |
| SEM | Scanning Electron Microscope |

SYMBOLS

| | | |
|---------|------------------------------|---------------|
| Adj. SS | Adjusted Sum of Squares | |
| a_p | Depth of cut | mm |
| f | Feed rate | mm/rev |
| F | F-Ratio Value | |
| F_x | Axial force | N |
| F_y | Thrust force | N |
| F_z | Tangential force | N |
| MS | Mean square | |
| P | Probability | |
| R^2 | Coefficient of determination | |
| R_a | Surface roughness | μm |
| SS | Sequential sum of squares | |
| V_b | Tool wear | μm |
| V_c | Cutting speed | m/min |

CHAPTER 1

1 INTRODUCTION

This chapter explains the back-ground of the machining process, applications of EN47 spring steel, basic techniques of the design of experiments (DOE). It explains different cutting environments like dry, wet and cryogenic conditions, modeling and optimization techniques and explains the importance of need for the present study.

1.1 Background

In most of the cases, metals are used in industrial applications. Cutting of such metals is complex, which has resisted theoretical analysis. Machining is performed using a variety of machine tools. Economic analysis mainly depends on proper selection of cutting parameters, which is done either by the experience of the process planning or machining hand book. Selected cutting parameters, by hand book, are, not the optimum values, but range of values. Main objectives of any industry are to give a better quality of products with acceptable dimensional accuracy and better surface finish, without disturbing the product quality (Jawaid et al. 1999).

Machining is a process of removing unwanted material from a given stock of material to give the desired output (shape), and it involves a number of processes. Extracted materials are in the form of chips obtained from workpiece material. Various machining process involved are turning, milling, shaping, drilling, broaching, sawing and abrasive machining. These processes involve independent input variables and dependent output variables, and their relationship is explained in this thesis. A skilled operator or engineer has direct control over the independent input parameter. They can specify input variables and setting them for machining process. Independent input variables involve workpiece material, cutting parameters, tool material, tool geometry, work holding devices and cutting fluids, etc. Dependent variables involve cutting forces, power consumption, surface finish, tool wear and failure, size and properties of the finished product, etc.

Turning is one such machining process, used to remove excess material for generating new and smooth surfaces by the action of a stationary cutting tool against a rotating work piece, usually in a lathe machine (Richelsen 1994). Turning is the major operation

in a machining sequence, which involves centering, facing, boring, countersinking, plain turning, parting, knurling, step turning, taper turning and thread cutting, etc. Lathe machines are used in metal working, woodturning, parts reclamation, glass working, and metal spinning, etc. Turning process, having major process parameters like speed feed and depth of cut, denoted by V_c , a_p , and f , respectively, will impact production cost. Also, tool material, workpiece, tool geometry, and cutting environment, influence the production rate. Cutting forces, surface roughness, material removal rate, and tool life are strongly correlated with input parameters.

Turning of hardened steels becomes more beneficial when working in dry condition. EN47 spring steel, in oil hardened and tempering conditions, has good wear resistance, abrasion resistance and hardness of 45-48HRC, and hence are suitable for producing different parts gears, knuckles, shafts, spindles, and pumps. Also, EN47 steels are used for making leaf spring for heavy vehicles and many other general engineering applications.

Single point (SNMG) tungsten carbide tool insert is used in turning operation. Tungsten carbide (WC) tool insert was essentially used for machining of hard material, as well as, soft material at higher cutting speed. WC tools have good wear resistance, corrosion and thermal shock resistance, which is excellent for machining most steels, cast iron, nonferrous materials, stainless steel and alloys under stable conditions.

Many experiments related to cutting forces, surface roughness, tool wear, tool vibration with different alloy steel, with different cutting condition have been studied. In a few studies, single objective optimization technique was taken into consideration for optimizing the interactions of process parameters for all output responses. However, in some cases, multi-objective optimization techniques are employed, to achieve the optimized process parameters for all output responses. (Abbas et al. 2016).

1.2 DOE technique

Process parameters are optimized using Design of Experiment (DOE), which require mathematical models and predicts the behavior of the process. DOE gives systematic experimental plan and also reduce number of experiments for achieving a high quality product at low cost. (Montgomery 2012). Various application of DOE has been reported in literature review chapter, which involves machining of metallic and other alloy steels. But minimum work has been reported on spring steels with optimization technique under different cutting environments.

Response Surface Methodology (RSM) is a suitable technique to optimize the cutting conditions and to study the effects of process parameters. RSM is a collection of statistical and mathematical data, which are very useful in understanding the model and analysis of the problems. Full Factorial Design (FFD) L_{27} orthogonal array (OA) gives sequentially arranged experimental design. Also, analysis of variance (ANOVA) provides significant terms for each output response. During the past few years, statistical techniques are employed for prediction of surface roughness, cutting force, tool tip temperature and material removal rate, etc. during machining.

1.3 Cutting environments

Cutting environment is a major independent variable, which involves (dry, wet and cryogenic condition) for a particular combination of tool and workpiece material.

1.3.1 Dry Machining

Dry Machining is a process, where machining is performed in the absence of coolant. Atmospheric air will be acting as a coolant. Dry machining is preferred for hard turning, where the hardness of the material is more than 50 HRC. Hard turning eliminates a series of operations essentially to produce required finished products. But during dry machining, temperature may be very high, and friction between tool and workpiece are more, causes reduced tool life, higher surface roughness and increased cutting force.

1.3.2 Wet Machining

Wet machining is a process, in which the coolant was supplied to machining zone. Cutting fluids serve as a coolant which reduces the friction between tool and workpiece interface. But disposal of chips during cutting is very difficult in wet machining, conventional cutting fluids not only affects environments but also creates health issues to operator.

1.3.3 Cryogenic Machining

Cryogenic machining process, wherein liquid nitrogen (LN_2) is supplied to machining zone. Cryogenic machining was employed to eliminate health problems caused during wet machining. Also, improved surface finish, reduced tool tip temperature and extraction of chips during machining are the features of cryogenic machining. Cryogenic machining is a type of dry machining with evaporation of delivered cryogenic fluids. In most of the cases, liquid nitrogen (LN_2) and liquid carbon dioxide (LCO_2) are used. Many of the researchers use liquid nitrogen (LN_2) as a coolant to reduce the heat. LN_2 substantially reduce the temperature between chip-tool interface (Evans and Bryan 1991). Cryogenic cooling technique substantially improves the tool life with reduction of adhesion-dissolution-diffusion wear of tool. Also, controls the temperature of machining zone (Venugopal et al. 2007). LN_2 cooling technique improved machinability performance of Inconel 718 when compared with wet and minimum quantity lubrication (MQL) (Kaynak 2014). Cryogenic machining effectively reduced the coefficient of friction between tool and chip interface during the machining of titanium alloy Ti-6Al-4V (Hong and Ding 2001).

1.4 Modeling techniques

Particle Swarm Optimization (PSO) technique was proposed by James Kennedy and Eberhart R in 1995. These techniques were inspired by social behavior of birds flocking and fish schooling. PSO technique is used to find the optimal values which followed the work of animal society which has no leader for searching best value. In these techniques, particles will move through the multi-directional search space to find best position.

Desirability approach (DA) was demonstrated by Derringer and Suich in 1980, which was commonly used in industry for optimization of multi-objectives responses. Desirability approach was one of techniques to convert multi-objective output responses into a single objective function termed as composite desirability.

Artificial neural networks (ANNs) is a modeling and data processing technique, which was inspired by biological neuron system. This technique pursuits mathematical modeling of learning process. ANN technique is very beneficial for classification and function approximation problems.

1.5 Need for the present study

Presently, industries work for better quality of products with reduced cost. Most of the cases, metal products are required in automobile industries for general engineering applications. So, metal cutting is essential for obtaining desired components, where the workpiece materials are subjected to various machining operations like turning, drilling, grinding, etc. Machining can be performed on soft workpiece material, as well as, hard materials so that final component can be obtained. In the present work, machinability characteristics of EN47 spring steel (45-48 HRC), will be studied. EN47 spring steel has many engineering applications such as manufacturing of dies, knuckles, gears, shafts and leaf spring for heavy vehicles. From the literature survey, it is shown that limited work has been reported on EN47 spring steel. The main importance of this research work is to optimize the process parameters. Comparative studies are carried out with tool insert of different nose radius, with different cutting environments like dry, wet and cryogenic conditions. EN47 spring steel requires a high cutting conditions, which leads to higher tool wear and poor surface finish and hence resulting in difficulty in cutting. In such situations, an optimization technique should be employed. In the present investigation, a full factorial design (FFD), L_{27} orthogonal array (OA) was used to conduct the experiments. Three factors and three levels $[(3^3)$ total of 27 experiments] are carried out from the design. The combination of cutting conditions is sequentially arranged, according to design. Experiments are conducted for every condition and are repeated three times, and average values are considered for analysis.

As reported by many researchers, metal cutting, is coupled with different cutting environments, for achieving a better quality of products like machining with coolants, machining with minimum quantity lubrication (MQL) and machining with liquid nitrogen (LN₂), and thermally assisted machining (TAM). Some of the restrictions that have been observed during machining are usage and disposal of conventional coolants, which has more conscious regulations in the view of health and environmental issue. For overcoming these problems, industries are looking for alternative cooling techniques which can improve productivity and reduce environmental issues.

CHAPTER 2

2 LITERATURE SURVEY

This chapter gives brief discussion about metal cutting process, design of experiment (DOE), different cutting environments, modeling and optimization techniques. And also provides knowledge and familiarize with the existing techniques and methodologies. A brief discussion of published research work done by experts has been analyzed. Metal cutting involves many operations such as turning, drilling, grinding, milling, etc. According to DOE, experiments are conducted in sequential order, and the data is analyzed, according to the orthogonal array. Analysis of variance (ANOVA) is used to identify percentage contribution for each response. Main effects plots are used to know individual significant terms and response surface plots (3D plots) are used to understand the interaction effects for each output response. A second order regression model is developed to predict the output response. Different cutting environments have been reported, like machining with the dry condition, wet condition, and cryogenic machining. Also, machined surface topography, chip morphology, and tool wear analysis have been reported. Modeling and optimization involve desirability approach (DA), particle swarm optimization (PSO) and artificial neural network (ANN) have been studied.

2.1 Independent variables

2.1.1 Cutting parameters

During machining, it is required to select appropriate input parameters (feed, speed, and depth of cut). In most cases, input parameters strongly depend on output responses and machine tool condition. By selecting proper cutting conditions, better quality of the product can be achieved. Speed, feed and depth of cut are the primary parameters. Workpiece and tool materials also influence the output performance. Cutting speed is normally denoted as revolution per minute (rpm) and represents workpiece rotation in a number of turns completed in one minute around a fixed axis. Feed rate can be defined as the total distance traveled by tool during one spindle revolution and it represented in mm/rev. Depth of cut is the distance, the tool is moving towards the workpiece in a single pass and is represented in mm. These three parameters (speed, feed, and depth

of cut) play a major role in material removal. Turning is a machining process to obtain cylindrical surfaces, by removing the excess material in the form of chips. In turning, two types of motions were observed: primary motion is rotary motion, and secondary motion is translation motion called as feed motion. Figure 2.1 shows the motions of turning. Workpiece rotates in symmetry about the rotation axis of the lathe machine. On lathe, different turning operation can be performed, and the sequence involves, facing, centering, plain turning, drilling, knurling, step turning, taper turning and thread cutting, etc. Lathe machines are used in metal working, woodturning, parts reclamation, glass working, and metal spinning, etc.

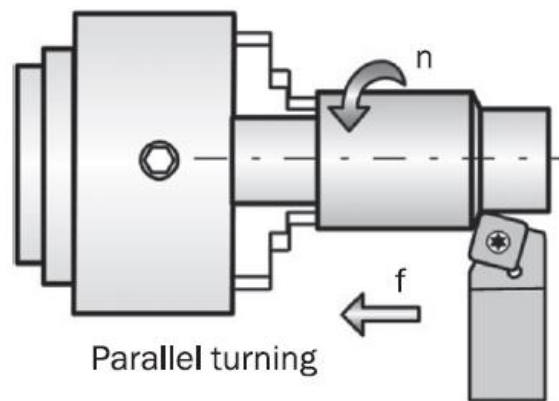


Figure 2.1 Basic motion of turning (Viktor P Astakhov 2011)

2.1.2 Workpiece material

Proper selection of workpiece material for an application, depends upon metallurgical aspects and chemical compositions of workpiece. The dimensions of workpiece are major restriction during machining, for avoiding chatter and vibration the length and diameters (L/D) ratio not exceed 10 as per ISO 3685. For hard materials has large cutting force and poor surface finish is obtained during machining, which results in reduced tool life. For such cases, proper selection of cutting parameters is essential for machining.

2.1.3 Tool material

Selection of tool materials plays a vital role in machining. Usually tool material is harder than the workpiece. Commonly used tool materials are in production are high-

speed steel (HSS), Carbide and coated tools, ceramics, cubic boron nitride (CBN) and diamond tipped tools. HSS tool is used for general purpose cutting, ceramic and carbide tools are used for cutting at higher cutting speeds which are available with a variety of grades and geometries. Higher cutting speed leads to higher tool tip temperature and reduced tool life. Nowadays, coated cutting tool inserts one replacing HSS and carbide tools which fulfill the functional requirement. Coated tool material have to wear resistant property at higher cutting speed and longer tool life.

2.1.4 Tool geometry

Tool geometry is essential for cutting tool to perform a cutting action. Tool geometry consists of rake angles, cutting edge angles, relief angles or clearance angle and nose radius. Large rake angle and clearance angles are preferred for HSS tools and small angles for carbide, ceramics tools which keep cutting tool material in compression, to avoid fracture of the tool, and tensile failure during machining. Cutting nose radius also influencing more during machining, higher nose radius leads a better surface finish but increased cutting forces and higher tool tip temperature. The better geometry of the cutting edge leads to an improved output performance and longer tool life.

2.2 Machinability factors

2.2.1 Effect of cutting parameters on cutting forces

In metal working process, cutting force is the most important factor for machinability study. Cutting force is obtained by performing cutting action at specified cutting parameters (speed, feed, and depth of cut). It is necessary to identify cutting force while machining. Higher cutting force leads to reduced tool life and it affects the machined surface. So, it is necessary to optimize the cutting parameters. In machining, three cutting forces, namely, axial force (F_x), thrust force (F_y) and tangential force (F_z), are observed. From the Figure 2.2, it is observed that tangential force is the main cutting force and hence considered for the analysis.

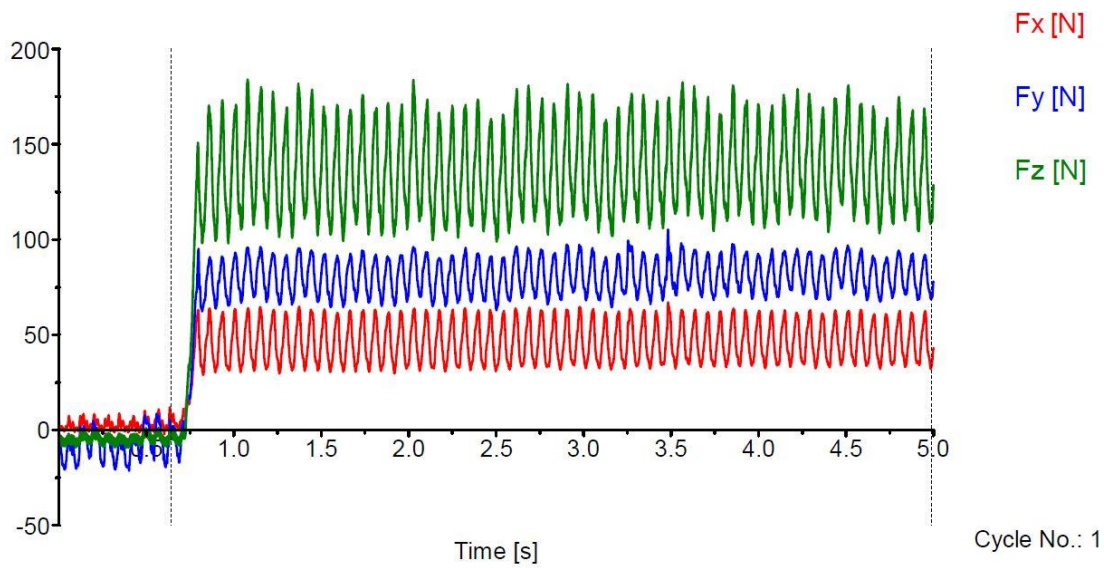


Figure 2.2 Cutting forces

Suresh et al. (2012) employed design of experiment (DOE) technique to optimize process parameters to identify cutting force and surface roughness by machining of AISI 4340 steel. From the experimental work, it is observed that low machining force and improved surface roughness obtained with machining combination of low machining time, low depth of cut, low feed rate and high cutting speed.

Chen et al. (2014) investigated machinability study on GCr15 bearing steel with PCD tool, to identify the cutting force, surface topography and surface roughness. It was found that feed rate influenced more on surface roughness while minimum cutting force and reduced surface roughness values are obtained with higher cutting speed and lower feed rate.

Pugazhenthii et al. (2018) employed design of experiment (DOE) to conduct experiments based on Central Composite Rotatable Design (CCRD) to, identify the cutting forces and surface roughness by machining AA7075/ (0-12%) TiB₂ aluminum matrix composites. From the analysis, a downward trend was observed, while increasing cutting speed and TiB₂ content. It was observed that cutting force increased with increase of depth of cut and feed rate.

Mahamani et al. (2014) investigated machinability characteristics of AA2219-TiB₂/ZrB₂ with uncoated tool insert, to identify surface roughness and machining force. Experiments were conducted based on L₂₇ full factorial design to optimize the

process parameters. From the analysis, it was revealed that feed rate is a more influencing factor for surface roughness and cutting forces.

Kishore et al. (2014) studied the effects of process parameters namely speed, feed, and depth of cut, during turning of Al6061 with 2wt% of TiC and Al6061 4 wt% of TiC with PCD and uncoated WC tool under dry condition, and output response being cutting force and surface roughness. From the experimental result, it was observed that the cutting force and surface roughness decreased with an increase in cutting speed and also to understand PCD is the best tool than the uncoated tungsten carbide.

Kosaraju and Chandraker (2015) conducted turning experiments on MDN 350 steel using a cemented carbide tool. Experiments were conducted based on L₉ orthogonal array. Cutting force and surface roughness were investigated. It was concluding that cutting speed and feed rate are more significant for cutting force and surface roughness respectively.

Sayed Ahmed et al. (2015) investigated the feed force and radial force by using Taguchi design approach. In this work, turning is carried out on mild steel with an HSS tool. To optimize the cutting parameters, experiments are conducted based on Taguchi L₉ orthogonal array (OA). The analysis was done by Minitab software to identify the significant terms. It was concluded, that feed rate and depth of cut are influencing factors for feed force and radial force.

Bensouilah et al. (2016) investigated the surface roughness and cutting force. Taguchi L₁₆ orthogonal array was employed. AISI D3 cold worked tool steel is workpiece material, and CC6050 and CC650 are ceramic inserts used. ANOVA, S/N ratio, and RSM were adopted for acquiring data. It was concluding that the coated CC6050 showed better for surface roughness and uncoated CC650 ceramic insert showed reduced cutting force.

2.2.2 Effect of cutting parameters on surface roughness

The machined surface has two important aspects, surface finish, and surface integrity. Surface finish is related to geometrical irregularities on the surface. Surface integrity deals with the metallurgical alterations of surface. Surface finish plays a vital role in

manufacturing sector, as it has most important quality characteristics which influence performance of machine part and hence the production rate. Better surface finish leads to the elimination further process like honing lapping and buffing. Most of the industries achieve a better quality of the products with less operating cost and shorten manufacturing time. Generally, surface roughness is a measure of fine irregularities in surface texture of machined parts and defined in terms of average roughness (R_a), waviness, lay and flaws. Surface roughness can be measured by comparing all the peaks and valleys from mean line and then averaging all the values. Surface Tester Probe measures vertical deviation of a real machined surface. When the deviations are large, the surface will be rough, and the value of roughness will be high, while deviations are small, surface will be smooth. During surface roughness measurement, different roughness parameters are present: R_a is arithmetic mean roughness, R_z is ten points mean roughness and R_t is maximum height of surface profile. Most of the cases R_a is considered for analysis according to Standard ISO 468:1982. During the analysis, arithmetic means roughness (R_a) is considered.

Aruna and Dhanalaksmi (2012) revealed that the optimization technique reduces the cost and time of machining. In the present experimental work, nickel-based super alloy and Inconel 718 are the workpiece materials with cermet inserts as a tool. Response surface method and 2nd order quadratic models are employed to investigate the surface roughness. Central composite design was used to determine the machining parameters. Experiments of all the parameters are validated, and the response values reasonably agree with predicted value.

Nithyanandam et al. (2014) studied machinability of titanium alloy (workpiece) using nano-carbide insert (tool). Taguchi method was used to optimize the surface roughness with, speed, feed, depth of cut and nose radius, as cutting parameters. Optimum condition surface roughness was determined by using S/N ratio and ANOVA. It was concluded that the feed was the most influential parameter.

Taguchi L_9 orthogonal array was employed by Nikam and Kadam (2016) to investigate the effect of tool geometry and surface roughness of 08040 steel with CVD coated carbide inserts CNMG and TNMG respectively. Experiments are conducted on a CNC machine, at low, medium and high levels of 3 factors namely, cutting speed, feed and

depth of cut. It was concluded that TNMG insert gave better surface roughness when compared to CNMG coated carbide insert and feed rate was the most significant parameter for obtaining better surface roughness.

Hua and Liu (2018) studied the machinability of Inconel 718. Effects of process parameters and nose radius on machined surface, microhardness and work hardening during dry turning were investigated. Results revealed that feed rate and nose radius influence the machined surface, but there was no clear tendency of cutting speed. Work hardening was influenced by cutting speed and feed rate. Increased nose radius tends to reduce work hardening.

Sharman et al. (2015) investigated machinability characteristics of Inconel 718 to identify surface integrity. It was found that feed rate influenced surface integrity, whereas no clear tendency for cutting speed.

Pawade et al. (2007) studied machinability characteristics of Inconel 718 to investigate the surface integrity during dry turning. Results revealed that the tool cutting edge geometry and depth of cut, mainly influenced the work hardening beneath the subsurface of machined part of Inconel 718, whereas cutting speed had less significant.

Lalbondre et al. (2013) studied the machinability of AISI51100 & AISI52100 steel with triangular P-30 inserts as a cutting tool. Face turning was carried out according to ISO 3685: 1993(E). Effectiveness of this method was assessed by studying the cutting time required for flank wear (0.3mm). It was concluded that face turning was a simple and effective method of machining.

Siddesh Kumar et al. (2017) conducted a turning process on different composite materials, to investigate machinability characteristics such as surface roughness and cutting force. Experiments were conducted with coated and uncoated tool insert. From the analysis it was concluded that cutting force and surface roughness are mainly influenced by feed rate, machining with coated tool inserts exhibits better performance.

2.2.3 Effect of cutting parameters on material removal rate (MRR)

Material removal rate can be defined as amount of material removed per unit time. $[(\text{initial weight} - \text{final weight})/\text{machining time}]$. Main goal of machining is to increase

MRR which results in higher production rate with improved accuracy and precision of final product. Cutting parameters like speed, feed, and depth of cut influence MRR. Depth of cut is a significant factor for MRR. From the analysis, increased depth of cut leads to a higher MRR. Achieving a desired goal of productivity and increased material removal rate requires an advanced machining process, equipment, and control system. Specifically, improved productions are obtained with increased depth of cut and feed rate with higher cutting speed.

Kaladhar et al. (2011), used Taguchi approach combined with utility concept of L_8 orthogonal array to conduct the experiments on AISI 202 steel with coated carbide tool, identify material removal rate and surface roughness. It was concluded that higher cutting speed and nose radius increased MRR and lower feed rate tends to improve surface roughness.

Choudhuri et al. (2014) employed Taguchi L_9 orthogonal array (OA) with utility concept for turning of aluminum 6061 with coated carbide insert, and it was stated that the single response results were not optimum values. So multi-characteristics response optimization such as surface roughness and material removal rate were employed during turning. It was concluded that higher levels of feed and depth of cut were used to maximize MRR and lower level of spindle speed was used to minimize surface roughness.

Gupta and Kumar (2015) investigated the machinability characteristics on UD-GFRP material with PCD tool, using principle component analysis with Taguchi Method. Six input parameters such as speed, feed, depth of cut, nose radius, rake angle, and cutting environment and the output response are surface roughness and material removal rate. From the experiments, it was concluded that the surface roughness increases with an increase in feed rate.

Kamble et al. (2015) performed turning operation on AISI 4340 with both coated and uncoated tool inserts based on the Fuzzy logic method, and it was used to convert multiple objectives into single objective, and a regression model was developed. It was concluded that quality characteristics such as MRR, R_a and cutting force were simultaneously improved by multi optimization.

Jewlikar et al. (2015) employed Taguchi technique L₉ orthogonal array for the analysis. Turning process was carried out on HPT of Bohler K110 steel with carbide tipped tool insert. Speed, feed, and depth of cut are the input cutting parameters and the output parameters are cutting force and material removal rate. It was concluded that an increase in cutting speed decreased in surface roughness and also with an increase in feed rate, surface roughness also increases.

2.2.4 Effect of cutting parameters on tool tip temperature

Temperature is one of significant factors during machining, when, there is physical contact between tool and the work piece, heat will be generated on tool tip along with chip interface. Cutting temperature can be defined as the measure of heat developed at tool-chip interface. From experimental analysis and by literature survey, cutting speed was a most significant term for tool tip temperature. High temperature affects the tool tip and will reduce the tool life. Due to higher cutting temperature, tool material softens and deform plastically. Many methods are used to measure the temperature, like a tool-workpiece thermocouple, implanted thermocouple, radiation method, and inserted thermocouple, etc. Nowadays, temperature is measured using a non-contact infrared thermal heat gun.

El Hakim et al. (2015) studied the secondary hardening on tool steel AISI T15 high-speed steel and AISI D2 cold work with multi-layer coated carbide insert, the effect of secondary hardening on machinability of cutting force, cutting temperature and tool wear are investigated. It was concluded that secondary hardening occurs during turning operation of HSS, which causes increased cutting force and temperature.

Gosai and Bhavsar (2016) investigated the temperature measurement in turning of hardened EN36 material with CNMG 4325 coated carbide insert. Cutting temperature was measured by inserting a K-type thermo-couple sensor within the tool. LABVIEW software through Arduino R3 controller board was used to analyze the temperature and also mathematical model and equation are generated by using CCD-based RSM.

Sivaiah and Chakradhar (2017a) conducting turning experiments on 17-4 PH Stainless steel with dry, wet, MQL and cryogenic conditions. to study the output performance of cutting force, surface roughness, chip morphology and tool tip temperature with

varying cutting velocities. Results reveal that cryogenic machining performs better than other cutting environments.

Mia and Dhar (2016) developed a predictive model for temperature of tool and workpiece interface by turning of AISI 1060 steel with a coated carbide insert. RSM and ANN are used to predict tool tip temperature to optimize the process parameters.

2.2.5 Effect of cutting parameters on tool wear

Tool wear also plays an important role in machinability characteristics, which will affect the production rate. Normally tool wear refers to the gradual failure of tool, due to its continuous operation. Tool wear measurement is essential, to know how long a tool lasts its life. From ISO-3685, V_b max is 0.6mm, and V_b average is 0.3mm. Tool wear is affected by cutting parameters, machining condition, cutting tool geometry, workpiece material, tool material, and cutting environment, etc. There are two types of tool wear occur during machining operation; (i) crater wear and (ii) flank wear. Crater wear is formed the rake face of tool, while flank wear occurs on flank of the tool. From the experimental analysis, most of the cases flank wear was considered for tool wear analysis.

Gaitonde et al. (2009) investigated the machinability characteristics of AISI D2 cold work tool steel, to identify cutting forces, surface roughness, and tool wear. Turning process was carried with two different tool material CC650 & CC650WG. Results reveal that CC650WG produced better surface roughness and minimum tool wear. CC650 perform well for cutting force and power.

Sreerama Reddy et al. (2009) investigated surface roughness, cutting force and flank wear of cutting tool insert during turning of C45 workpiece material with coated tungsten carbide. Flank wear of deep cryogenic treatment of tool insert is less than the untreated tool inserts. Cutting forces reduced during cryogenic machining and surface finished improving.

Satyanarayana et al. (2013) studied Taguchi based Grey relational analysis during turning of Inconel 718 work material with uncoated cemented carbide tool inserts. Taguchi based Grey relational analysis was used to obtain optimum value by employing

Taguchi L₉ orthogonal array, which minimizes the cutting force, surface roughness and tool wear. Optimum value was obtained at 90m/min speed, 0.18mm/rev feed and 0.5mm depth of cut and the process parameters have been optimized by ANOVA.

Sahu and Choudhury (2015) predicted surface roughness and tool wear by employing Taguchi method. This research work, AISI 4340 steel was considered workpiece material and coated, and uncoated tool material are used. The influencing cutting parameters are speed, feed, and depth of cut. Turning process was performed using coated and uncoated tool material. Machining of hard material at a higher speed and lower feed was improved by coated inserts.

Kaynak (2014) compared the machining performance of Inconel 718 with dry, MQL and cryogenic machining. The author concludes that the progression of flank wear and crater wear rate can be minimized using cryogenic machining

2.2.6 Effect of cutting parameters on chips

During machining, material is removed in the form of chips, and hence fresh surface is obtained on the workpiece. Chip formation helps to control machining condition, turning costs, surface finish and tool life which often lead to better process and increased productivity. Extraction of chips from machined surface affects production rate. Chips are separated in three ways: chips break against a workpiece; chips break against tool, and chips break by themselves. Chips formed at lower cutting speed are irregular in shape and shortened, while higher at cutting speed, chips are continuous and spring shape. Disposal of chips are essential; if not controlled, chips may affect machined surface and tool performance.

Chinchanikar and Choudhury (2013) investigated machinability characteristics of AISI 4340 with CVD and PVD tool material, to identify cutting forces, surface roughness, and chip morphology. Results reveal that CVD coated tool performs better than that PVD coated tool.

Palanisamy et al. (2016) studied the microstructure properties of 15-5PH stainless steel at different aging conditions. The treated samples were machined to study the machinability aspects namely tool wear, surface roughness, cutting force and chip

morphology. Experimental investigations revealed that air-cooled samples exhibit higher cutting forces compare to furnace cooled samples, surface finishes were also good in at air cooled samples, whereas higher hardness was observed in unprocessed samples.

2.3 Modeling and optimization technique

2.3.1 Particle Swarm Optimization (PSO)

Kennedy and Eberhart developed the particle swarm optimization (PSO) technique through imitating the preying behavior of birds or fishes. In PSO, for every solution in the searching space is seen as a ‘bird,’ known as ‘particle.’ All the particles have fitness values; and evaluated through a fitness function to be optimized. Particles are move through the search space with its best practice of personal and social experience. The personal experience embodied the individual effort to find the best solution, while social experience is taking help from neighbors to achieve best solution. Some of the experts work on PSO and are summarized.

Gaitonde and Karnik (2012) used particle swarm optimization (PSO) developed by an artificial neural network (ANN) to optimize the process parameters to minimize the burr height and thickness during drilling of AISI 316L stainless steel.

Hanafi et al. (2016) investigated machinability characteristics of Ploy Ether Ketone (PEEK), to identify cutting forces, cutting power and specific cutting pressure. Taguchi method DOE is used and to arrange for optimizing the process parameters by employing the PSO technique. Developed PSO program gives minimum values of output response with corresponding optimum conditions.

Bharathi Raja and Baskar (2011) conducted experiments on turning of copper, brass, aluminum and mild steel using CNC lathe. PSO technique was used for optimizing the cutting condition to identify the surface roughness.

Mohanty et al. (2016) investigate machinability characteristics of Inconel 718. To identify the MRR, electrode wear rate, radial over cut and surface roughness during electric discharge machining. Multi-objective particle optimization (MOPSO) algorithm are used to find the optimal process parameters.

2.3.2 Desirability Approach (DA)

Desirability approach was demonstrated by Derringer and Suich, in 1980. It is widely used in industry for optimization of multi-response problems. Desirability approach is one of techniques used to convert multi-objective output responses into a single objective function which is termed as composite desirability. A composite desirability value is obtained for multi responses from desirability approach. Optimum process parameters and optimal value for each output performance are obtained from desirability approach. If the composite desirability value lies in between 1 or 100% then developed model is adequate.

Methodology for desirability approach Equation 2.1 to 2.4 (Azizi et al. 2012)

Step-1: Calculate individual desirability index (d_i).

There are three forms of desirability approaches.

a. Smaller is better

Value of y expected to be smaller is better.

$$d_i = \begin{cases} 1, & \hat{y} \leq y_{\min} \\ \left(\frac{\hat{y} - y_{\max}}{y_{\min} - y_{\max}} \right), & y_{\min} \leq \hat{y} \leq y_{\max}, \quad r \geq 0 \\ 0, & \hat{y} \geq y_{\max} \end{cases} \quad 2.1$$

b. Nominal is better

Value of y is required to achieve a particular target (T)

$$d_i = \begin{cases} \left(\frac{\hat{y} - y_{\min}}{T - y_{\min}} \right)^s, & y_{\min} \leq \hat{y} \leq T, \quad s \geq 0 \\ \left(\frac{\hat{y} - y_{\max}}{T - y_{\max}} \right)^t, & T \leq \hat{y} \leq y_{\max}, \quad t \geq 0 \\ 0, & \text{otherwise} \end{cases} \quad 2.2$$

Where y_{\max} and y_{\min} represent upper and lower tolerance limits of y . s and t represent weights.

c. Larger is better

The value y expected to be larger is better

$$d_i = \begin{cases} 0, & \hat{y} \leq y_{\min} \\ \left(\frac{\hat{y} - y_{\min}}{y_{\max} - y_{\min}} \right), & y_{\min} \leq \hat{y} \leq y_{\max}, r \geq 0 \\ 1, & \hat{y} \geq y_{\max} \end{cases} \quad 2.3$$

Step-2: Compute composite desirability index (d_G).

$$d_G = \sqrt[n]{d_1^{w_1} * d_2^{w_2} \dots * d_i^{w_i}} \quad 2.4$$

Where d_i = Individual desirability; W_1, W_2 sum of individual weights; W_i weight of property

Step-3: Determine optimum process parameters, higher composite desirability value implies a better quality of product.

Step-4: Perform ANOVA for significant terms and percentage contribution for independent variable.

Step-5: Calculate predicted optimum condition.

Malghan et al. (2016) carried out milling process on aluminum metal matrix composite (MMC). To identify the cutting force, surface roughness and power consumption. The cutting parameters are analyzed by response surface method (RSM) of desirability approach (DA) and particle swarm optimization (PSO). Result reveals that predicted results shows very close to experimental results. PSO technique achieves significantly improved than DA technique.

Meddour et al. (2018) turning process were carried out on AISI 4140 steel with ceramic tools. To identify the surface roughness and cutting force, modeled by an artificial neural network (ANN) and response surface method (RSM). Multi-objective optimization was performed with desirability approach (DA), and Non-dominated

sorting genetic algorithm (NGSA-II) is coupled with ANN. Result reveals that (NGSA-II) provide more efficient than DA.

Amel Chabbi et al. (2017) performed experiments on polyoxymethylene (POM C) polymer. Experimental analysis was divided into three steps such as unifactorial tests, modeling with RSM and ANN, and last step, multi-objective optimization by desirability approach (DA). Result reveals that to minimize output responses of cutting forces, cutting power and surface roughness.

2.4 Artificial Neural Networks (ANNs)

Artificial Neural Network (ANNs) is a modeling and data processing technique, which is inspired from biological neuron system. This technique pursuits mathematical modeling of learning process. ANN technique is very useful for classification and function approximation problems.

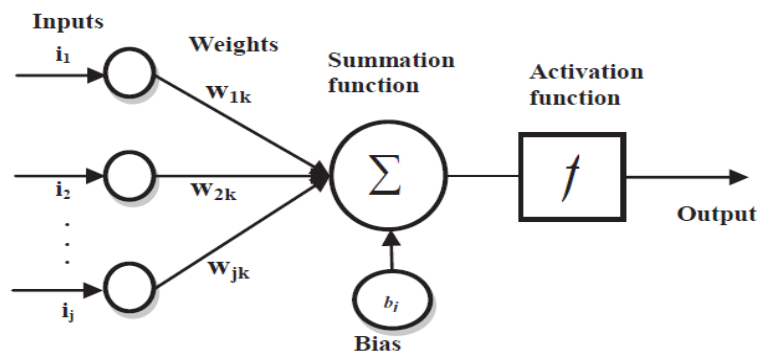


Figure 2.3 Mathematical principle on a neuron (Kant and Sangwan 2015)

In a biological system, brain stores all information by adjusting the linking patterns. In the same way that ANN can be trained to store the information in network by adjusting synaptic weights. Neural networks have three parameters namely, training, validating and testing. Determination of coefficient R^2 value should be 100% or 1, so trained network is adequate. ANN model consists of three layers namely, input layer, hidden layer and output layers. The diagram for a network with a single neuron is shown in Figure 2.3.

Kumar and Chauhan (2015) investigated machinability study on different composite materials of Al7075 with PCD tool, to optimize process parameters of approach angle,

speed and feed rate. Experiments are conducted based on design of experiments to identify surface roughness of different composite material. Researchers developed predicted models by using response surface method and artificial neural network. From the analysis, feed rate influence more on machined surface of all the composite materials.

Hanief et al. (2017) employed design of experiments for turning of on red brass material using HSS tool. Full factorial design is used make experimental plan. Artificial neural network and regression models are comparing with each other. From the analysis, it was concluded that more accurate result was obtained with ANN model as compare to regression model.

Ciurana et al. (2009) adopted PSO technique for pulsed laser micromachining of AISI H13 hardened steel to optimize the process parameters. PSO technique was coupled with ANN, to minimize surface roughness and volume error. Result reveals that developed models are suitable for optimizing the process parameters.

Muthukrishnan and Davim (2009) investigated machinability characteristics of metal matrix composite (MMC) during turning with PCD tool. Experiments were conducted based on DOE technique and validated with artificial neural network (ANN). Result reveals that predicted results much closer to experimental results.

Umbrello et al. (2007) used artificial neural network (ANN) for predicting subsurface residual stress during hard turning of 52100 bearing steel. To optimize cutting condition and the results shows that predicted errors ranged between 4 to 10%.

Davim et al. (2008) studied machinability characteristics of 9SMnPb28k(DIN) free machining steel, to identify the surface roughness (R_a and R_t). Full factorial design L_{27} orthogonal array are used to carry out the experiments. ANN training models were developed to study interaction effects of input cutting condition on surface roughness. Result reveals that feed rate (f) and cutting speed (V_c) influence more on surface roughness.

Mia and Dhar (2016) conducted experimental work on EN24T steel during turning process with high pressure coolant (HPC). ANN was used for prediction of surface

roughness. Experiments were conducted based on full factorial design (FFD). Results reveal that Bayesian Regularization (BR), gives least Root Mean Square Error (RMSE). Hua and Liu (2018) reported machinability studies on Inconel 718 in order to identify microhardness, surface roughness and degree of work hardening. Experiments are conducted with three different feed rate, three different cutting speed, different nose radius during dry machining. From the experimental work result reveals that feed rate and nose radius having dominant effect on surface roughness. While there is no much effect of cutting speed on surface roughness. Increased cutting speed and feed rate are degree of work hardening strengthened.

Meddour et al. (2018) investigated machinability studies on AISI 4140 hardened steel with different nose radius of tool insert. In this work an attempt is made to improve the prediction by ANN technique in order to identify cutting force and surface roughness. From the analysis result reveals that a better surface roughness obtained with larger nose radius and low feed rate while increased cutting speed. In addition to that Desirability approach and Non-Dominated Sorting Genetic Algorithm (NSGA-II) coupled with ANN is used solve multi-optimization problems. From the analysis it was observed that NSGA-II is more efficient than desirability approach.

Okokpujie et al. (2018) employed design of experiment, develop mathematical model using least square method. Experiments are conducted based on L_{27} orthogonal array in order to optimize cutting parameters such as cutting speed, feed rate and depth of cut. Aluminum 1061 is used as a work material with high speed steel (HSS) to investigate tool wear.

From the literature survey it is observed that a lot of research work have been report on machine ability studies of different kinds of alloy, and optimization techniques. Limited work has been reported on machinability studies on EN47 spring steel using different cutting environments. In the present investigation, experiments are conducted based on full factorial design (FFD). Present work deals with the hard turning of EN47 spring steel with PVD coated tungsten carbide tool insert of three different nose radii 0.4, 0.8 & 1.2mm. Experiments are conducted with three different cutting environments namely, dry, wet and cryogenic condition. Present work, has been carried out systematically, to study the effects of process parameters such as cutting speed (V_c),

feed rate (f) and depth of cut (a_p) using various cutting environments, to identify cutting force (F_z), surface roughness (R_a) and tool tip temperature (T).

2.5 Gaps found from literature survey

From the literature review it is observed that lot of work has been conducted on AISI 4340, mild steel, Al6061, AISI series, MDN series, Inconel 718 and as well as the EN series materials like EN 8, EN24, EN31, EN25 and EN353 to enhance the properties.

A very limited work has been reported on EN47 spring steel. These materials are used widely in the manufacturing of leaf spring for heavy vehicles and other application like manufacture of dies, knuckles, gears and many general engineering applications. EN47 spring steels relatively low in cost compare to other alloy steels like nickel-based steels, Inconel 718 and 17-4PH steels etc.

2.6 Scope of the work

- Prediction and validation of output responses; cutting force, surface roughness and temperature, chip morphology and tool wear during hard turning, which are essential to improve quality, productivity and tool life.

2.7 Objectives

- To carry out the turning process using tool insert of 0.4, 0.8 and 1.2mm nose radius, based on OFAT approach and select tool of best nose radius among tool inserts based on their performances.
- To optimize input process parameters; speed, feed and depth of cut in dry, wet and cryogenic condition using the tool selected using DOE technique.
- Multi optimization was done with Particle Swarm Optimization (PSO) and desirability approach (DA).
- To develop mathematical model and prediction of all the output response by using regression model and correlate with artificial neural network (ANN).

CHAPTER 3

3 EXPERIMENTATION

This chapter explains methodology of research work, description all the measuring equipment's, and work piece material, cutting tool inserts are used in the present work.

3.1 Methodology

Flow chart of methodology is mentioned in Figure 3.1

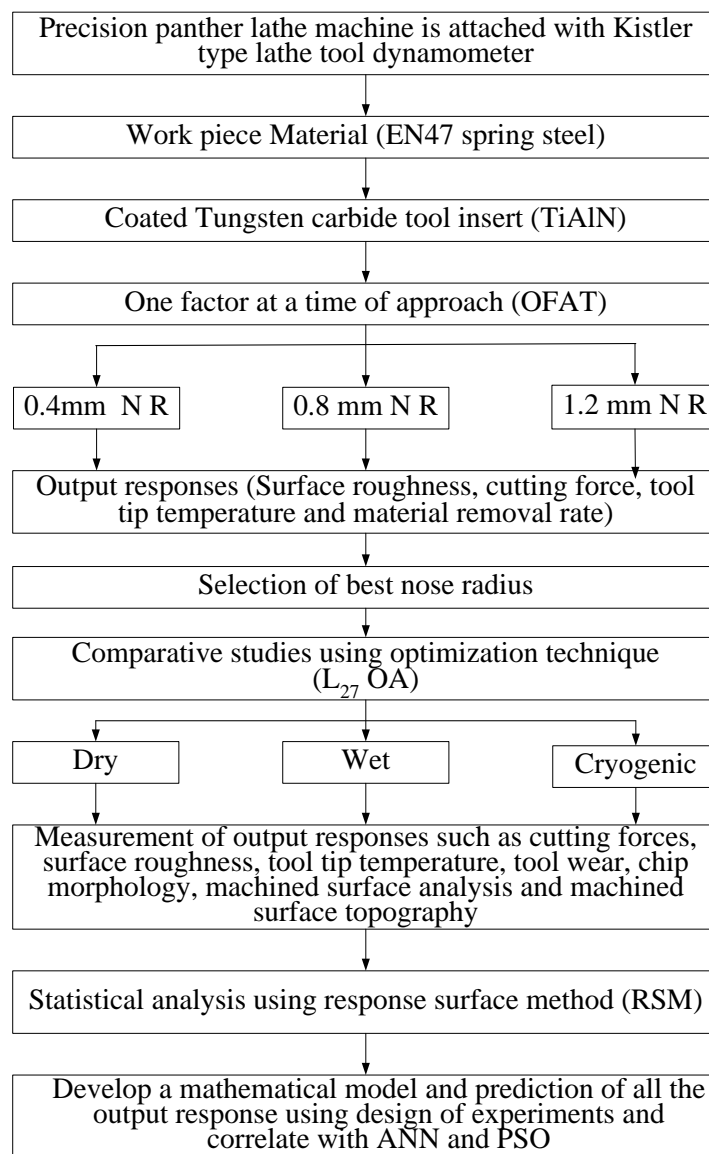


Figure 3.1 Experimental flow chart

3.2 Experimental setup

The experimental set up of precision panther lathe machine is attached with Kistler type lathe tool dynamometer as shown Figure 3.2.

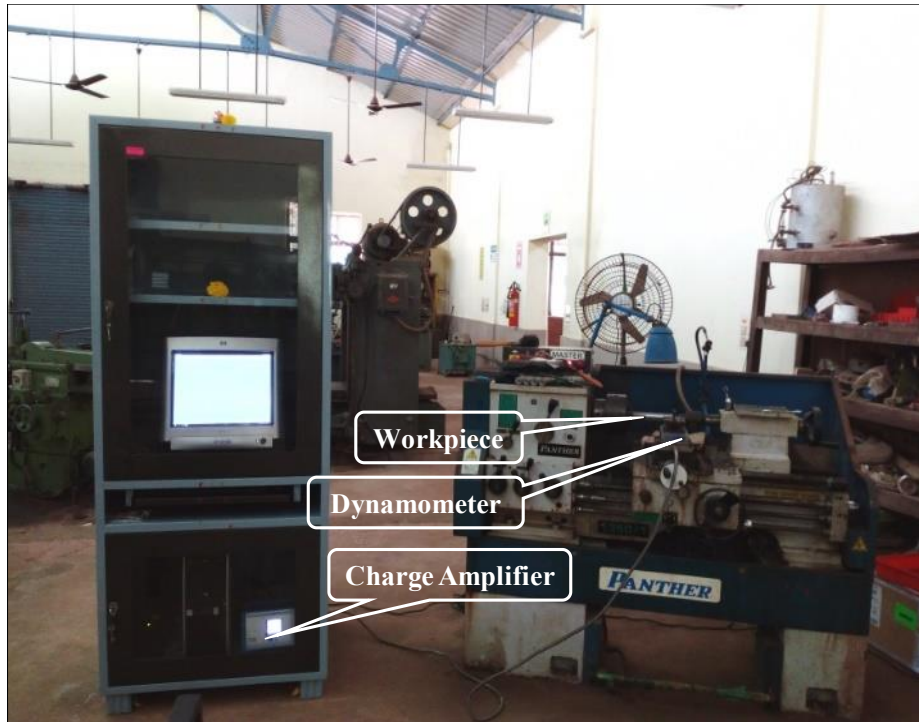


Figure 3.2 Experimental setup

3.3 Experimental procedure

1. Precision Panther lathe machine was used to turn spring steel EN47 samples using commercially available WC tools of different nose radii 0.4, 0.8 & 1.2 mm.
2. Machining will be done at different sets of cutting speed, feed rates, depth of cut and at different nose radius of cutting inserts.
3. Optimization of results are based on OFAT approach using L_{27} full factorial design.
4. Select the best tool nose radius of their performance of output result.
5. Experiments are conducted with different environment condition, namely dry, wet and cryogenic condition, using the selected tool.

6. Cutting forces are acquiring with a kistler type lathe tool dynamometer during machining for each trial as per the experimental array.
7. During machining, machining time and chip tool interface temperature are measured using stop watch and non-contact heat gun respectively.
8. Surface roughness of machined samples is measured by Mitutoyo Talysurf SJ301 roughness tester.
9. Chemical composition is confirmed by spectroscopy and flank wears on the coated carbide tools is measured using confocal microscope and SEM. Chip morphology studies are performed using SEM.
10. Regression equation for each output response is obtained by using statistical tool and predicted results are compared with experimental value. Further response is optimized and corelated with ANN and PSO technique.

3.4 Workpiece material

Spring steel is commonly delegated as low carbon steel, medium carbon steel or high carbon steel with high return quality. These materials are suitable in oil hardening and tempering conditions. Spring steel have good wear and abrasion resistance. EN47 spring steel are used to manufacture gears, knuckles, shafts, spindles and pumps. Further, EN47 spring steel is used for making leaf spring for heavy vehicles and many general engineering application. Chemical composition is confirmed by using *spectroscopy* and is mentioned in Table 3.1. Work Sample having length of 200 mm and diameter of 30mm is used for conducting turning experiments. For avoiding chatter and vibration of workpiece L/D ratio should maintain less than 10 according ISO 3685.

Table 3.1 Chemical composition of EN47 spring steel

| Material | C | Mn | Si | S | P | Cr | Fe |
|----------|---------------|---------------|-------------|------|------|---------------|-----------|
| EN 47 | 0.45- 0.55 | 0.50- 0.80 | 0.50 Max | 0.40 | 0.40 | 0.80- 1.20 | Remaining |

3.5 Cutting tool material

German make Kennametal, tungsten carbide tool inserts SNMG120404 (KUC10), SNMG120408 (K313), SNMG120412 (KCU25) with different nose radius as shown in

Figure 3.3(a-c). Cutting tool inserts are PVD coated tools mono-layer having a coating thickness of 2.939 μm , 3.156 μm and 4.659 μm for 0.4, 0.8 & 1.2mm nose radius respectively, as confirmed by calo test. From the EDS analysis, coating layer consisted of Ti, Al & N in all inserts. Hence it is confirmed that the coating layer consists of TiAlN.

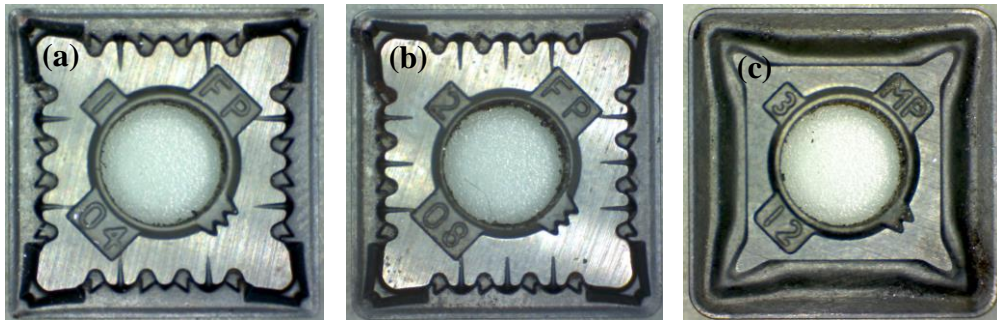


Figure 3.3 (a-c) Cutting tool inserts of nose radius (a) 0.4mm, (b) 0.8 mm and (c)1.2 mm

Turning process are carried out on precision panther lathe machine. Kistler tool dynamometer is used to measure the cutting forces which is attached to the lathe machine. Tool tip temperature is measured by non-contact type infrared thermal heat gun. Material removal rate is measured by equation 3.1. Surface roughness was measured by Mitutoyo Talysurf SJ301. Calotest is performed to know the thickness of the coating and EDS analysis was done to know the composition coating materials in the tool insert.

$$MRR = \left(\frac{W_1 - W_2}{t} \right) \frac{g}{s} \quad 3.1$$

Where W_1 is initial weight, W_2 is final weight and t is the machining time in sec.

3.6 Infrared thermometer

Calibrated non-contact infrared (IR) thermometer for accuracy $\pm 1\%$ has been used to measure the cutting zone temperature. Non-contact type infrared thermal heat gun model 'Center 350' as shown in Figure 3.4.



Figure 3.4 Infrared thermometer

3.7 Panther lathe machine

Turning process is carried out on self-center 3 jaw chuck Precision Panther lathe machine having spindle speed ranges from 30 to 1250 rpm and 10 KW power, is shown in Figure 3.5. Table 3.2 depicts technical specification of Panther lathe machine.



Figure 3.5 Panther Lathe machine

Table 3.2 Panther lathe machine specification

| SL No | Description | 1350/1 |
|-------|--------------------------------------|---------------------------|
| 1 | Type of bed | Gap bed |
| 2 | Length of bed | 1370mm |
| 3 | Width of bed | 230mm |
| 4 | Height of centre | 177mm |
| 5 | Admit between centre | 540mm |
| 6 | Swing over bed | 335mm |
| 7 | swing over Saddle | 245mm |
| 8 | Swing over cross slide | 200mm |
| 9 | Swing in gap | 535mm |
| 10 | Length of gap in front of face plate | 125mm |
| 11 | No. of Spindle RPM | 8/16* |
| 12 | Spindle RPM Range | 45-938/ 30-1250* 50-1250* |
| 13 | Taper in Spindle sleeve | MT-4 |
| 14 | Spindle Hollow | 42mm |
| 15 | Spindle Nose Detail | A2 size 4/D1 size 4* |
| 16 | No. of British Threads | 65 |
| 17 | Range of British Threads | 4-60 TPI |
| 18 | No. of Metric Threads | 54 |
| 19 | Range of Metric Threads | 0.35-6mm |
| 20 | No. of D.P. Threads | 65 |
| 21 | Range of D.P. Threads | 8-120 DP |
| 22 | No. of Module Threads | 54 |
| 23 | Range of Module Threads | 0.175- 3 mod |

3.8 Surface roughness tester

In the present work, machined surface analyzed by ‘Mitutoyo Talysurf SJ301’ roughness tester. Measurement was taken at five different places with cut off length of (λ) of 4 mm and average values are considered for analysis. Surface roughness (R_a) is a measuring of surface texture of machined part. Surface tester probe measures vertical

deviation of a real machined surface. If the deviations are large then roughness will high, while deviation are small then surface is smooth. Figure 3.6 shows Mitutoyo surface roughness tester.



Figure 3.6 Mitutoyo Talysurf roughness tester

3.9 Lathe tool dynamometer

Specific cutting forces (F_x , F_y , F_z) are measured by piezo electric based Kistler 9257B type lathe tool dynamometer as shown in Figure 3.7. and is attached to Panther lathe.

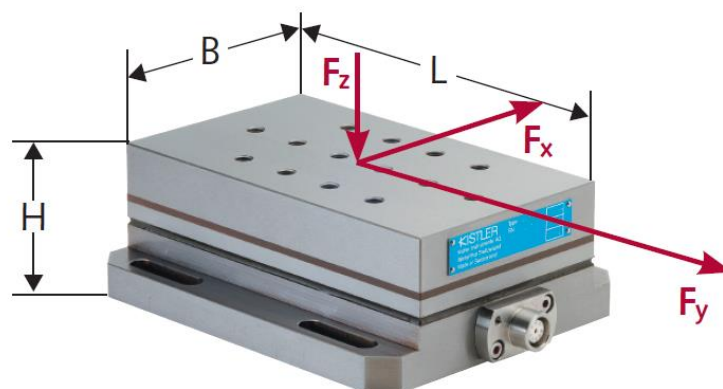


Figure 3.7 Lathe tool dynamometer type 9257B (Kistler)

Kistler dynamometer is rigidly mounted on tool post and equipped with charge amplifier 5070A. Dynoware software 2825D-02 data acquisition is used to acquire data. Cutting forces were measured in real time with three-component Kistler 9257B linked with multichannel charge amplifier 5070A to high impedance cable. Technical specification of Kistler 9257B dynamometer is depicted in Table 3.3.

Table 3.3 Technical specifications of Kistler 9257B dynamometer

| | Technical Data | Type | 9257B |
|-----------------------------------|-----------------------|------------------|-------------------------------|
| Measuring range | F_x, F_y | kN | -5 ... 5 |
| | F_z | kN | -5 ... 10 |
| Calibrated measuring range | F_x, F_y | kN | 0 ... 5 |
| | F_z | kN | 0 ... 10 |
| Sensitivity | F_x, F_y | pC/N | ≈ -7.5 |
| | F_z | pC/N | ≈ -3.7 |
| Natural frequency | $f_n(x), f_n(y)$ | kHz | ≈ 2.3 |
| | $f_n(z)$ | kHz | ≈ 3.5 |
| Pretensioning direction | | | vertical |
| Operating temperature range | | °C | 0 ... 70 |
| LxWxH | | mm | 170x100x60 |
| Weight | | kg | 7.3 |
| Degree of protection IEC/EN 60529 | | (w. conn. cable) | IP67 |
| Connection | | | Fischer flange 9 pol. neg. |

3.10 Confocal microscope

Surface roughness and surface texture was measured by confocal microscope model LEXTOLS411 shown in Figure 3.8. From the laser 3D surface tester measuring the surface topography of machined surface and measuring tool wear.

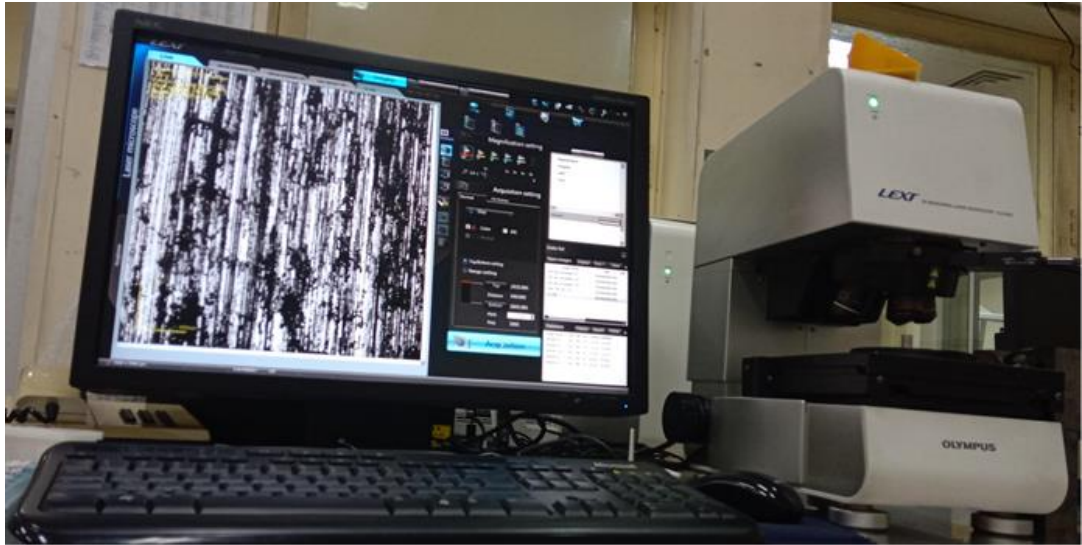


Figure 3.8 Confocal microscope

3.11 Scanning Electron Microscope

Scanning electron microscope are used analyze the surface defects of machined surface, chip morphology, tool wear analysis, microstructures and subsurface characteristics. The SEM images were taken with different magnification for extensive analysis at different locations.



Figure 3.9 Scanning electron microscope

The resolution of SEM is 30KV. X-ray spectroscopy (EDAX) has been used for elemental composition of machined samples. Figure 3.9 depicts the 'JEOL-JSM-638OLA' model SEM.

CHAPTER 4

4 RESULTS AND DISCUSSION

Stage-1

Machinability studies of EN47 spring steel with different nose radii of 0.4, 0.8 & 1.2mm using (OFAT) one factor at a time approach to identify cutting forces, surface roughness, tool tip temperature and material removal rate. From the comparative study based on performance of output response, a best nose radius of cutting tool insert is used for further work.

Stage-2

Selected cutting tools insert are used to conduct the experiments with different cutting environment; dry wet & cryogenic condition using full factorial design (FFD) L₂₇ orthogonal array for optimizing the process parameters to measure cutting force, surface roughness, tool tip temperature, machined surface analysis, machined surface topography, chip morphology and tool wear.

Stage-3

In this stage, cutting parameters are modelled and optimized. Multi objective optimization was done by composite Desirability Approach (DA) and Particle Swarm Optimization (PSO) technique. Artificial neural network was used to predict the experimental result and validation also performed with ANN and RSM.

4.1 One factor at a time of approach (OFAT)

OFAT explains the effect of individual cutting parameters like cutting speed (V_c), feed rate (f), depth of cut (a_p) and different nose radii on cutting forces, surface roughness, tool tip temperature and material removal rate.

OFAT method consists of selecting a starting point, or baseline set of levels, for each factor, and then successively vary each factor over its range with other factors held constant at the baseline level. After performing the tests, a series of graphs are usually constructed, showing the variation of response variables by varying one input factor with other input factors held constant (Montgomery 2012). One factor at a time approach (OFAT) is a technique of conducting experiments by varying one factor and maintaining other factors constant. OFAT is a kind of pilot run, to know the best condition based on the output response. In the present work, 15 sets of experiments are conducted (three factors i.e. speed, feed and depth of cut and each factor having 5 levels). Table 4.1 depicts pilot runs and experimental conditions.

Table 4.1 OFAT Experimental conditions

| SL No | V_c m/min | a_p mm | f mm/rev |
|-------|----------------|-------------|---------------|
| 1 | 24 | 0.6 | 0.093 |
| 2 | 36 | 0.6 | 0.093 |
| 3 | 59 | 0.6 | 0.093 |
| 4 | 75 | 0.6 | 0.093 |
| 5 | 118 | 0.6 | 0.093 |
| 6 | 59 | 0.2 | 0.093 |
| 7 | 59 | 0.4 | 0.093 |
| 8 | 59 | 0.6 | 0.093 |
| 9 | 59 | 0.8 | 0.093 |
| 10 | 59 | 1.0 | 0.093 |
| 11 | 59 | 0.6 | 0.062 |
| 12 | 59 | 0.6 | 0.070 |
| 13 | 59 | 0.6 | 0.093 |
| 14 | 59 | 0.6 | 0.117 |
| 15 | 59 | 0.6 | 0.125 |

Turning experiments are conducted on spring steel EN47 with dimension of 30 mm diameter, 200 mm length. Experimental cutting conditions are chosen based on pilot runs. Experiments are conducted on 3 jaw chuck PANTHER lathe machine. From the experimental work, varying cutting parameters, which influences the cutting force, tool tip temperature, surface roughness and material removal rate for different nose radii (NR) 0.4, 0.8 & 1.2 mm are studied.

4.1.1 Varying cutting speed

Figure 4.1 (a-c), shows that cutting forces reduce with increase in cutting speed. Relation between cutting velocity on cutting forces (F_x , F_y and F_z) at different nose radii (NR) are depicted in Table 4.2.

Table 4.2 Relationship between varying cutting velocity on cutting forces (F_x , F_y & F_z) at different nose radius

| V_c | F_x (N) | | | F_y (N) | | | F_z (N) | | |
|-------|-----------|-------|-------|-----------|--------|--------|-----------|--------|--------|
| | 0.4 | 0.8 | 1.2 | 0.4 | 0.8 | 1.2 | 0.4 | 0.8 | 1.2 |
| 24 | 45.27 | 57.22 | 72.89 | 190.25 | 215.75 | 248.69 | 270.45 | 350.26 | 400.26 |
| 36 | 42.85 | 52.85 | 64.56 | 160.29 | 173.25 | 200.69 | 220.1 | 276.56 | 370.56 |
| 59 | 25.89 | 34.94 | 52.13 | 133.56 | 163.87 | 200.54 | 200.36 | 240.56 | 285.69 |
| 75 | 28.65 | 41.99 | 57.86 | 128.39 | 152.96 | 178.59 | 170.56 | 205.60 | 244.56 |
| 118 | 31.23 | 45.26 | 60.28 | 112.56 | 143.89 | 168.96 | 130.28 | 160.23 | 190.40 |

Table 4.3 Relationship between varying cutting velocity on MRR, surface roughness and tool tip temperature at different nose radius

| V_c | MRR (g/s) | | | R_a (μm) | | | T ($^{\circ}\text{C}$) | | |
|-------|-----------|------|------|-------------------------|------|-----|--------------------------|-------|--------|
| | 0.4 | 0.8 | 1.2 | 0.4 | 0.8 | 1.2 | 0.4 | 0.8 | 1.2 |
| 24 | 0.16 | 0.24 | 0.26 | 3.4 | 2.69 | 2.2 | 33.59 | 39.56 | 47.05 |
| 36 | 0.22 | 0.27 | 0.36 | 2.9 | 2.44 | 2.0 | 45.69 | 52.96 | 57.96 |
| 59 | 0.41 | 0.46 | 0.53 | 2.9 | 2.34 | 1.9 | 51.94 | 58.94 | 70.94 |
| 75 | 0.45 | 0.59 | 0.64 | 2.6 | 1.78 | 1.2 | 65.58 | 73.56 | 84.58 |
| 118 | 0.57 | 0.69 | 0.73 | 2.2 | 1.04 | 0.2 | 79.59 | 90.29 | 101.29 |

From the analysis, it is observed that, at higher cutting speed, cutting forces are reduced. Some of the reasons noticed that, with increase of nose radius, increase of bluntness of tool is more, which cause larger force in plastic deformation. Furthermore, increased nose radius cause increased specific energy i.e cutting force. (Parida and Maity 2017). Increased nose radius gives higher cutting forces, which is because of higher cutting speed tends to the formation of high temperature at the tool tip, which softens the work material and reduce the shear angle. (A. Chabbi et al. 2017; El Hakim et al. 2015; Shihab et al. 2014).

Table 4.3 (a-c) depicts the relationship between varying cutting velocity on material removal rate (MRR), surface roughness (R_a) and tool tip temperature (T). From Figure 4.2 (a), it is observed that material removal rate increases with increase in cutting speed, and increased nose radius gives higher material removal rate. This is due to reduction in friction between tool and workpiece, resulting in higher material removal rate.

Figure 4.2 (b), it is observed that surface roughness reduced with increase in cutting speed, while increased nose radius gives better surface roughness. Influence of edge radius on the roughness of the machined surface. Which includes lays and grooves induced by edge chipping and built-up-edge. Periodically feed marks created by nose of the cutting tool (Hua and Liu 2018). Figure 4.2 (c) shows that tool tip temperature increases with increase in cutting speed. At increased nose radius, it was observed that there was an increase in chip thickness and chip-tool contact length. From the experimental work it is observed that increased nose radius leads to increase in the chip thickness and reduced shear angle, which is responsible for large shear plane in primary deformation zone (Parida and Maity 2017).

4.1.2 Varying feed rate

Figure 4.3 (a-c), it is observed that cutting forces (axial force (F_x), thrust force (F_y) and tangential force (F_z)) increase with increase in feed rate and are depicted in Table 4.4. From the analysis, it is observed that cutting forces gradually increase with

increase in feed rate. Cutting forces also increase with increase in nose radius. Similar results were obtained by (Chou and Song 2004a).

Table 4.5 depicts variation of feed rate on MRR, surface roughness and tool tip temperature. From Figure 4.4 (a), it is observed that material removal rate increases with increase in feed rate, and increase in nose radius. From Figure 4.4 (b), surface roughness increases with increase in feed rate. Further, increased nose radius gives better surface roughness. From Figure 4.4 (c), tool tip temperature increases with increase in feed rate, and this is due to increased contact length of tool-chip and leads to higher temperature. Further, tool tip temperature increases with increase in nose radius (Parida and Maity 2017).

Table 4.4 Relationship between varying feed rate on cutting forces (F_x , F_y & F_z) at different nose radius

| f | F_x (N) | | | F_y (N) | | | F_z (N) | | |
|----------|-----------------------------|------------|------------|-----------------------------|------------|------------|-----------------------------|------------|------------|
| | 0.4 | 0.8 | 1.2 | 0.4 | 0.8 | 1.2 | 0.4 | 0.8 | 1.2 |
| 0.062 | 20.64 | 30.64 | 49.57 | 90.23 | 117.25 | 140.25 | 145.26 | 177.7 | 215.69 |
| 0.070 | 25.065 | 36.59 | 53.89 | 125.8 | 135.8 | 162.36 | 162.53 | 195.69 | 245.86 |
| 0.093 | 25.89 | 34.94 | 52.13 | 133.56 | 163.87 | 200.54 | 200.36 | 240.56 | 285.69 |
| 0.117 | 40.54 | 50.54 | 70.54 | 166.23 | 186.35 | 215.23 | 232.06 | 266.59 | 310.96 |
| 0.125 | 53.93 | 61.58 | 82.56 | 187.27 | 197.27 | 229.56 | 256.59 | 275.89 | 368.56 |

Table 4.5 Relationship between varying feed rate on MRR, surface roughness and tool tip temperature at different nose radius

| f | MRR (g/s) | | | R_a(μm) | | | T($^{\circ}\text{C}$) | | |
|----------|------------------|------------|------------|---|------------|------------|---|------------|------------|
| | 0.4 | 0.8 | 1.2 | 0.4 | 0.8 | 1.2 | 0.4 | 0.8 | 1.2 |
| 0.062 | 0.1259 | 0.159 | 0.198 | 2.2 | 1.16 | 0.98 | 30.26 | 35.69 | 51.29 |
| 0.070 | 0.1659 | 0.329 | 0.429 | 2.68 | 1.66 | 1.34 | 37.59 | 46.12 | 65.21 |
| 0.093 | 0.4113 | 0.457 | 0.528 | 2.885 | 2.34 | 1.9 | 51.94 | 58.94 | 70.94 |
| 0.117 | 0.4982 | 0.598 | 0.642 | 2.94 | 2.45 | 2.2 | 56.29 | 67.59 | 77.28 |
| 0.125 | 0.5893 | 0.622 | 0.725 | 3.52 | 3.21 | 2.89 | 58.96 | 69.54 | 81.56 |

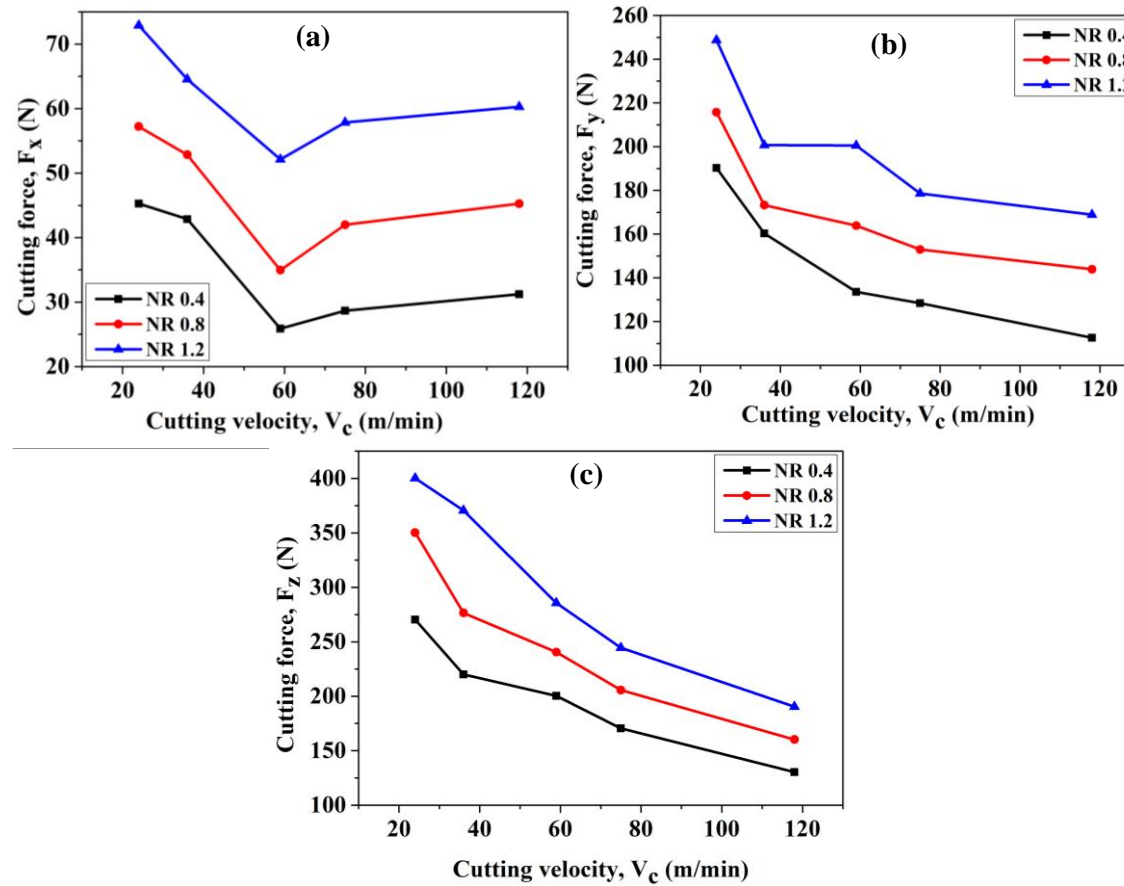


Figure 4.1 (a-c) Variation of cutting speed on (a) axial force (F_x), (b) thrust force (F_y) and (c) tangential force (F_z) for different nose radii.

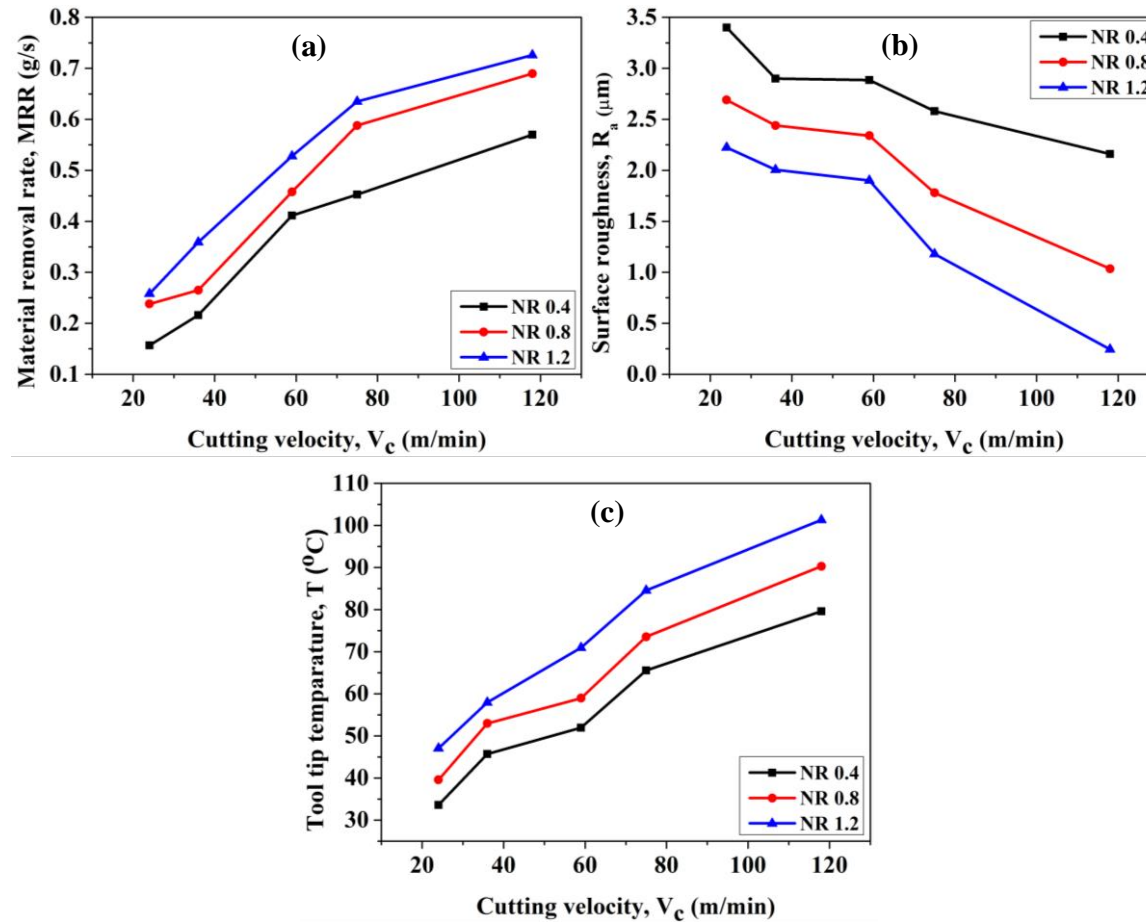


Figure 4.2 (a-c) Variation of cutting speed on (a) MRR, (b) surface roughness and (c) tool tip temperature for different nose radii

4.1.3 Varying depth of cut

From Figure 4.5 (a-c), it is observed that cutting forces (F_x , F_y & F_z) increases with increasing depth of cut. At higher depth of cut, the tool penetrates deeper into the work piece and has to remove large volumes of material and hence higher cutting forces are required. Further, with increase in nose radius, contact between the tool and the workpiece is increased and results in the formation of large cross section of chips which may require high cutting force to deform the work materials. (A. Chabbi et al. 2017). Relationship between variation of depth of cut on cutting forces (F_x , F_y & F_z) at different nose radius are depicted in Table 4.6

Table 4.6 Relationship between varying depth of cut on cutting forces (F_x , F_y & F_z) at different nose radius

| a_p | F_x (N) | | | F_y (N) | | | F_z (N) | | |
|-------|-----------|--------|---------|-----------|--------|--------|-----------|--------|--------|
| | 0.4 | 0.8 | 1.2 | 0.4 | 0.8 | 1.2 | 0.4 | 0.8 | 1.2 |
| 0.2 | 26.57 | 32.16 | 43.04 | 50.26 | 71.72 | 100.36 | 86.23 | 135.69 | 177.5 |
| 0.4 | 27.89 | 35.29 | 59.98 | 85.26 | 124 | 155.24 | 130.25 | 195.25 | 240.65 |
| 0.6 | 25.89 | 34.94 | 52.13 | 133.56 | 163.87 | 200.54 | 200.36 | 240.56 | 285.69 |
| 0.8 | 82.135 | 92.135 | 112.134 | 236.41 | 290.56 | 350.26 | 320.69 | 355.3 | 398.56 |
| 1.0 | 94.79 | 104.79 | 124.79 | 310.24 | 350.25 | 384.25 | 365.21 | 419.3 | 470.26 |

Table 4.7 Relationship between varying depth of cut on MRR, surface roughness and tool tip temperature at different nose radius

| a_p | MRR (g/s) | | | R_a (μm) | | | T($^{\circ}\text{C}$) | | |
|-------|-----------|--------|--------|-------------------------|------|------|-------------------------|-------|-------|
| | 0.4 | 0.8 | 1.2 | 0.4 | 0.8 | 1.2 | 0.4 | 0.8 | 1.2 |
| 0.2 | 0.1869 | 0.2658 | 0.2934 | 2.25 | 1.23 | 1.11 | 32.26 | 37.95 | 49.95 |
| 0.4 | 0.2359 | 0.3579 | 0.3872 | 2.56 | 2.2 | 1.86 | 36.29 | 45.26 | 59.56 |
| 0.6 | 0.4113 | 0.4572 | 0.5279 | 2.885 | 2.34 | 1.9 | 51.94 | 58.94 | 70.94 |
| 0.8 | 0.5289 | 0.5669 | 0.6289 | 3.51 | 2.89 | 2.66 | 55.78 | 65.29 | 75.86 |
| 1.0 | 0.5569 | 0.6571 | 0.7584 | 3.81 | 3.12 | 2.85 | 61.73 | 70.29 | 79.15 |

From the Figure 4.6 (a), it is observed that material removal rate increases with increase in depth of cut. Further, higher material removal rate is obtained, with increased tool nose radius. From Figure 4.6 (b), it is observed that surface roughness increases with

increase in depth of cut. But increased nose radius gives better surface finish. From Figure 4.6 (c), it is observed that tool tip temperature increases with increase in depth of cut. Increase of nose radius may breakage the tool tip, which cause rise in temperature (Parida and Maity 2017). Tool nose radius is also affected during machining, increased nose radius gives higher tool tip temperature, as the tool requires more energy to remove higher amount of material. Higher temperature reduced chip thickness and increased the chip tool contact length. Furthermore, due to rise in temperature at shear zone results reduction of flow stress. Increased nose radius tends to increase in flow stress because formation flank wear at higher nose radius (Parida and Maity 2017). Large nose radius seems to be finer surface finish and specific cutting energy is slightly higher. Maximum uncut chip thickness decreases with larger tool nose radius.(Chou and Song 2004b).Table 4.7 depicts the relationship between varying depth of cut on material removal rate (MRR), surface roughness (R_a) and tool tip temperature (T).

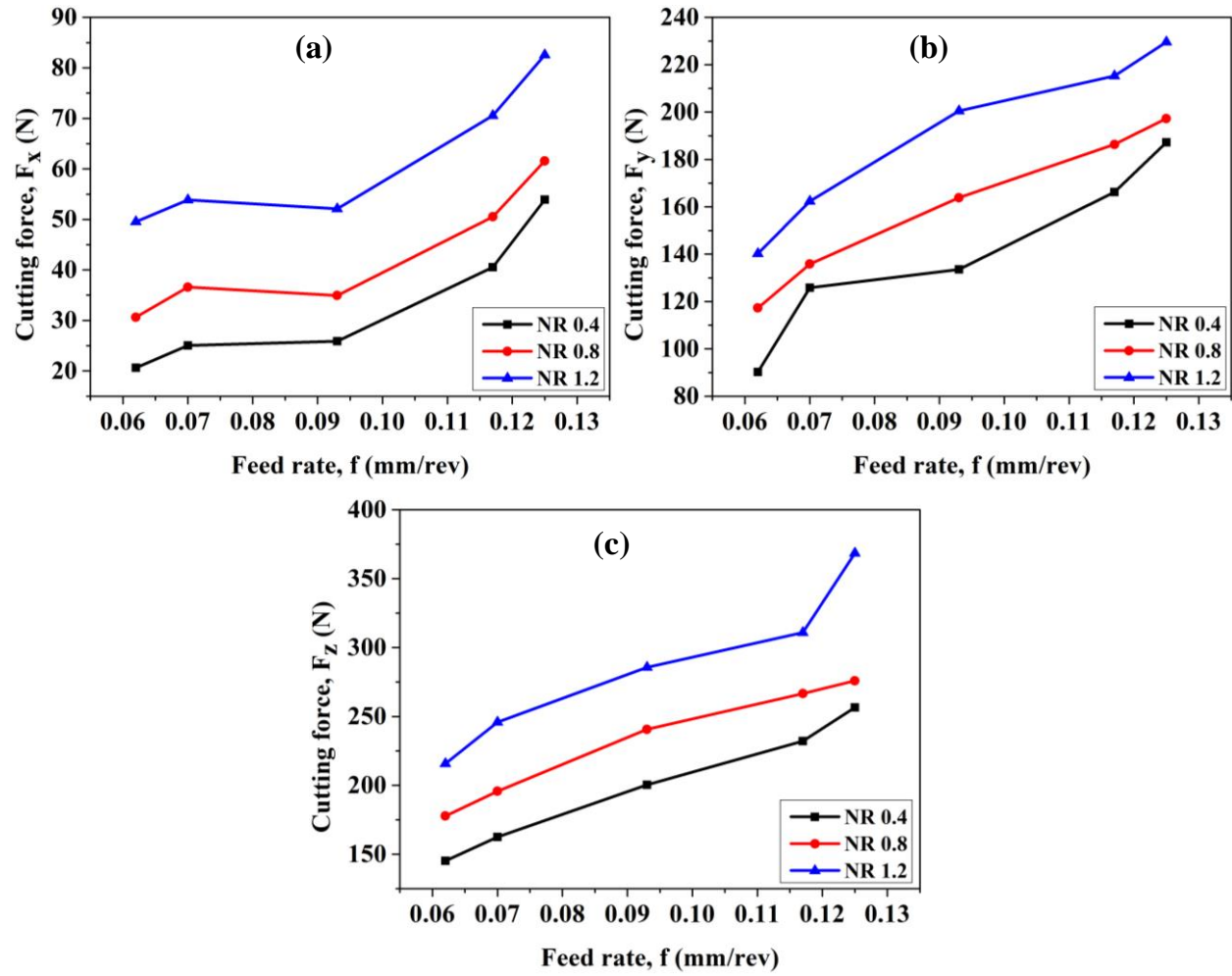


Figure 4.3 (a-c) Variation of feed rate on on (a) axial force (F_x), (b) thrust force (F_y) and (c) tangential force (F_z) for different nose radii.

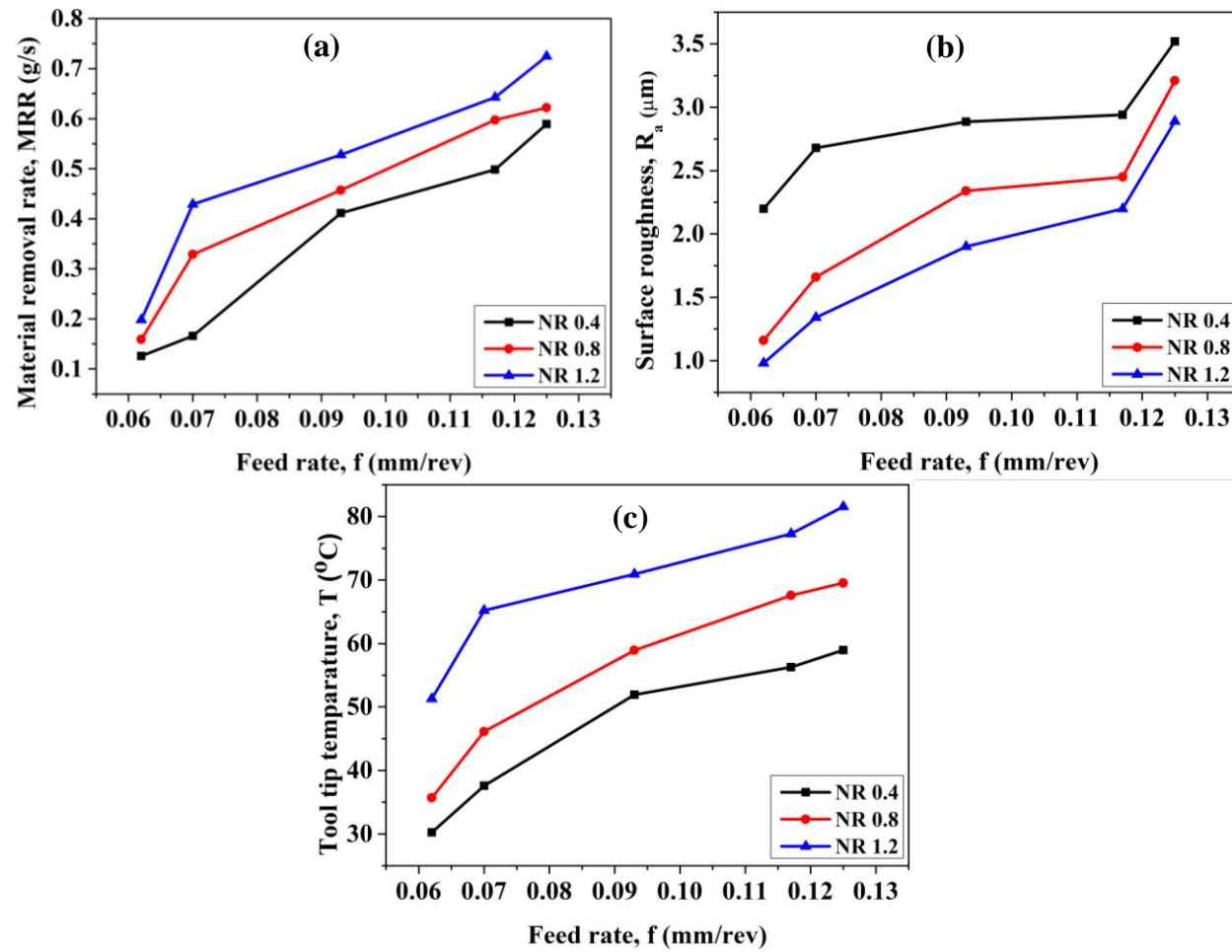


Figure 4.4 (a-c) Variation of feed rate on (a) MRR, (b) surface roughness and (c) tool tip temperature for different nose radii.

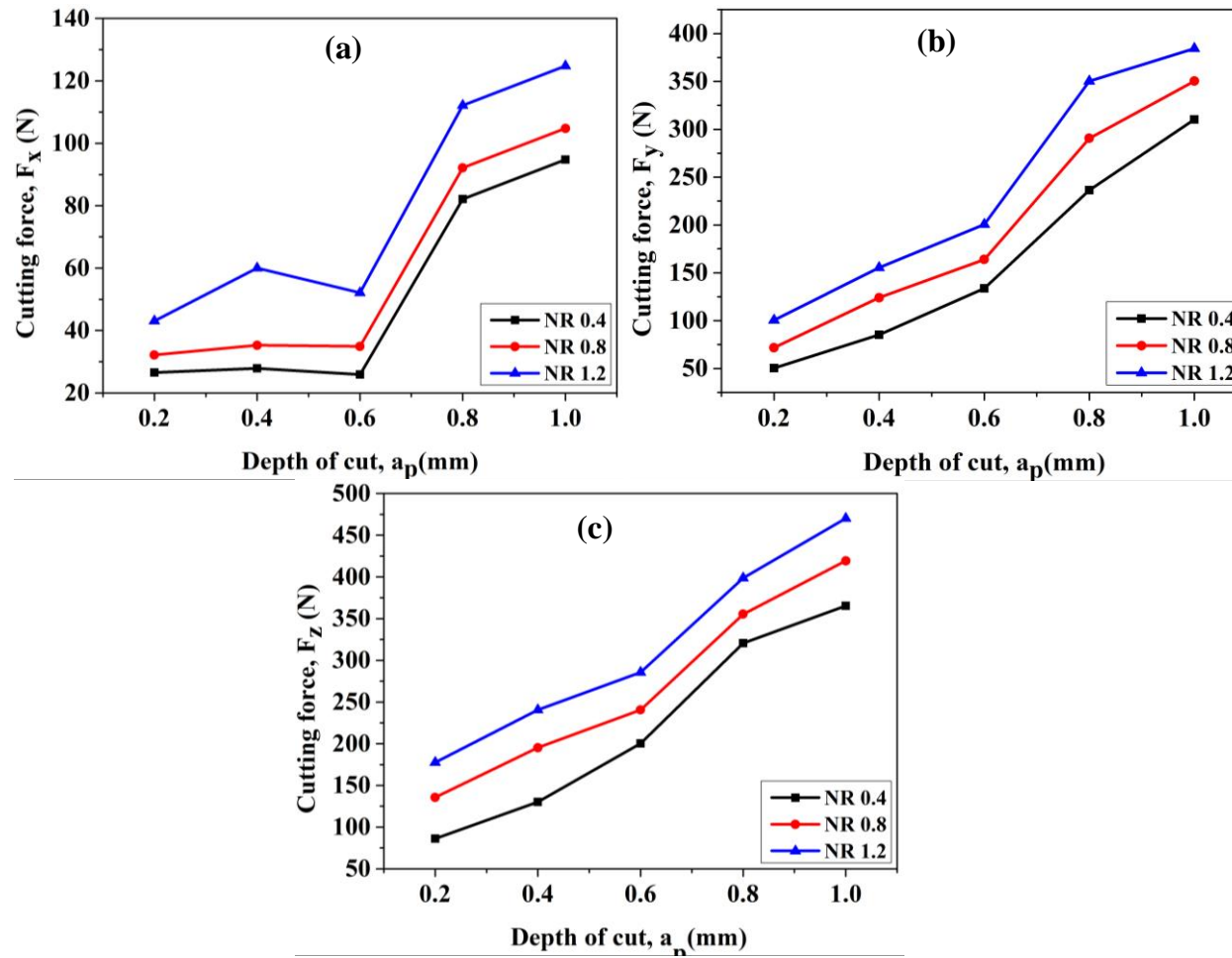


Figure 4.5 (a-c) Variation of depth of cut on (a) axial force (F_x), (b) thrust force (F_y) and (c) tangential force (F_z) for different nose radii.

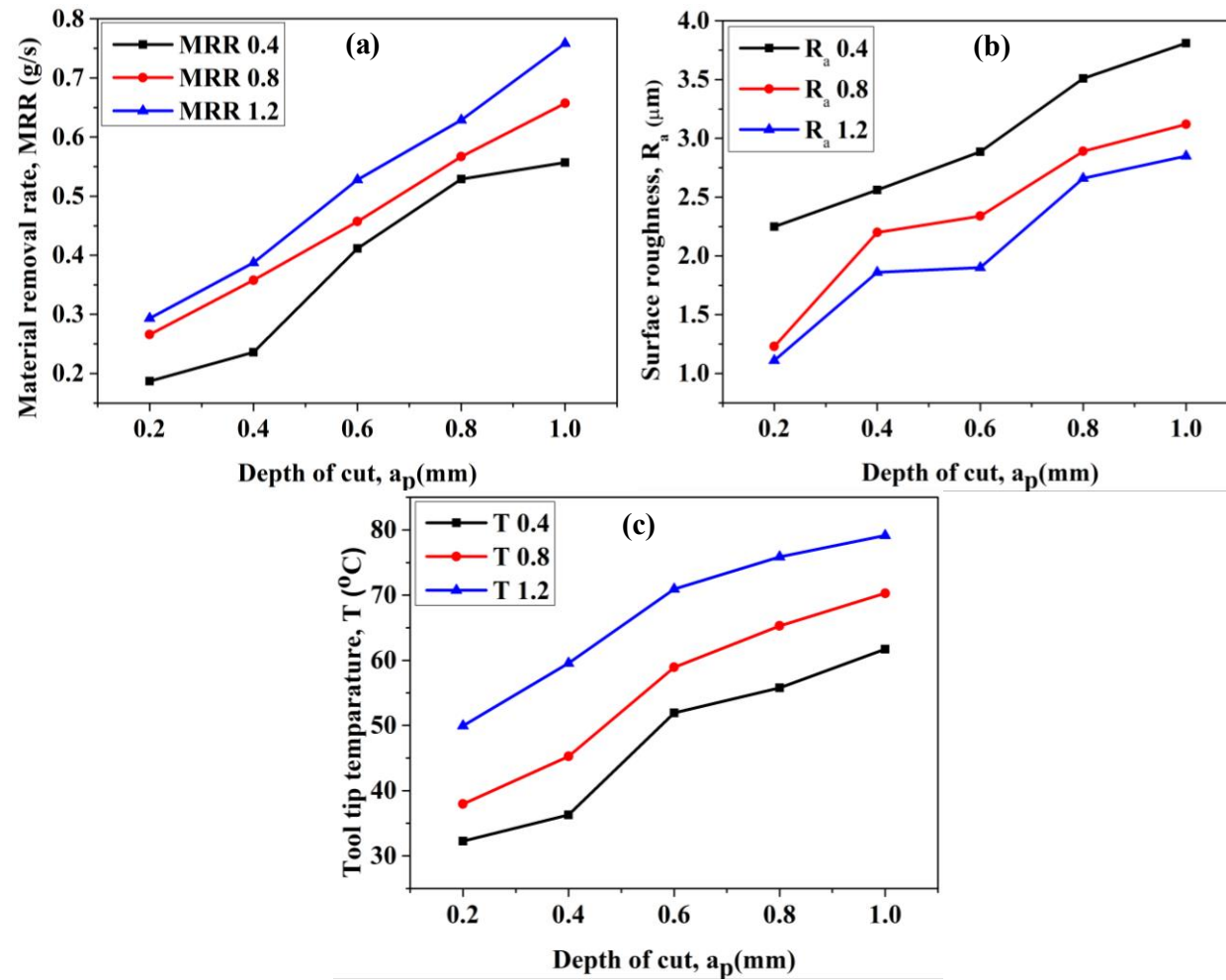


Figure 4.6 (a-c) Variation of depth of cut on (a) MRR, (b) surface roughness and (c) tool tip temperature for different nose radii.

4.2 Selection of cutting tool insert

Turning process was carried on EN47 spring steel at different tool nose radii (0.4, 0.8 & 1.2mm), during dry condition. Experiments are conducted based on one factor at a time of approach (OFAT) and compared with one another. To identify the cutting forces, surface roughness, tool tip temperature and material removal rate. From the analysis, it was observed that tool of nose radius 0.8 mm exhibited excellent performance in all the cases. Hence tool insert of 0.8mm nose radius was selected for further experimental work. Various stages of work are represented in the flow chart shown in Figure 4.7.

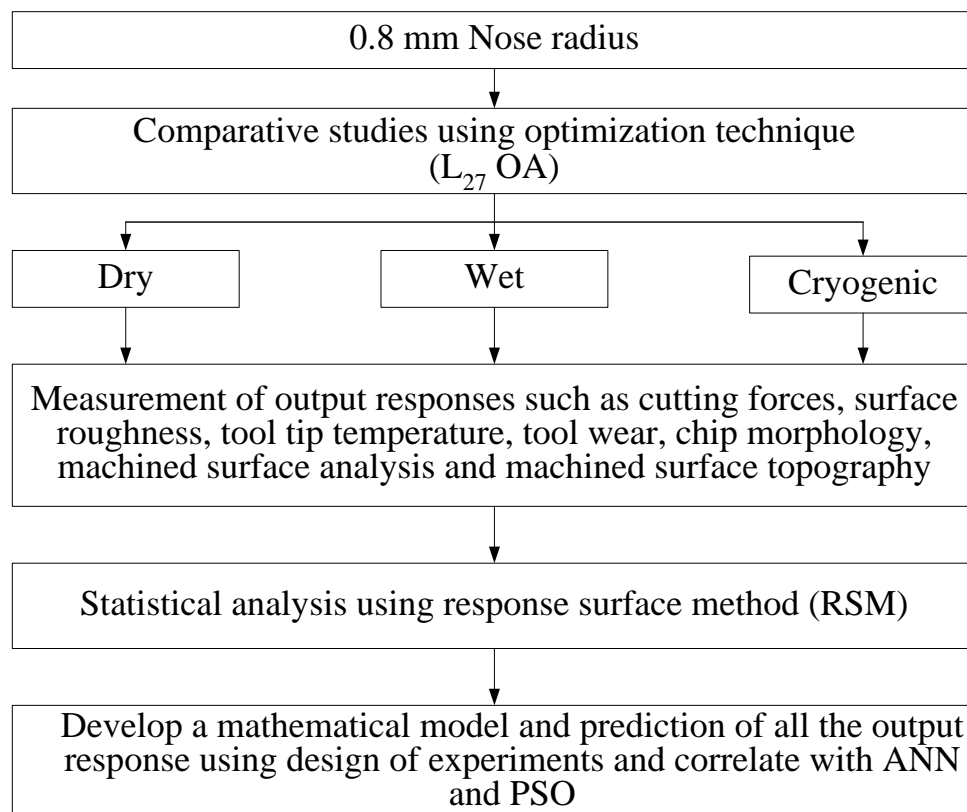


Figure 4.7 Flow chart showing the various stages of experimental work using tool insert of 0.8mm nose radius

4.3 Turning process using optimization technique

Full factorial design (FFD) L_{27} orthogonal array is used to optimize the process parameters. 27 experiments are performed with different cutting environment such as dry, wet and cryogenic environments. Various experimental set up are depicted in Figure 4.8. Cutting force, surface roughness and tool tip temperature are experimentally estimated at different cutting environments using a tool insert of 0.8mm nose radius by using DOE technique. Further, the results are analyzed by Minitab software tool and design expert software tool (A. Chabbi et al. 2017; Davim et al. 2008; Elbah et al. 2013). Table 4.8 depicts experimental plan and corresponding outputs under different cutting environments.

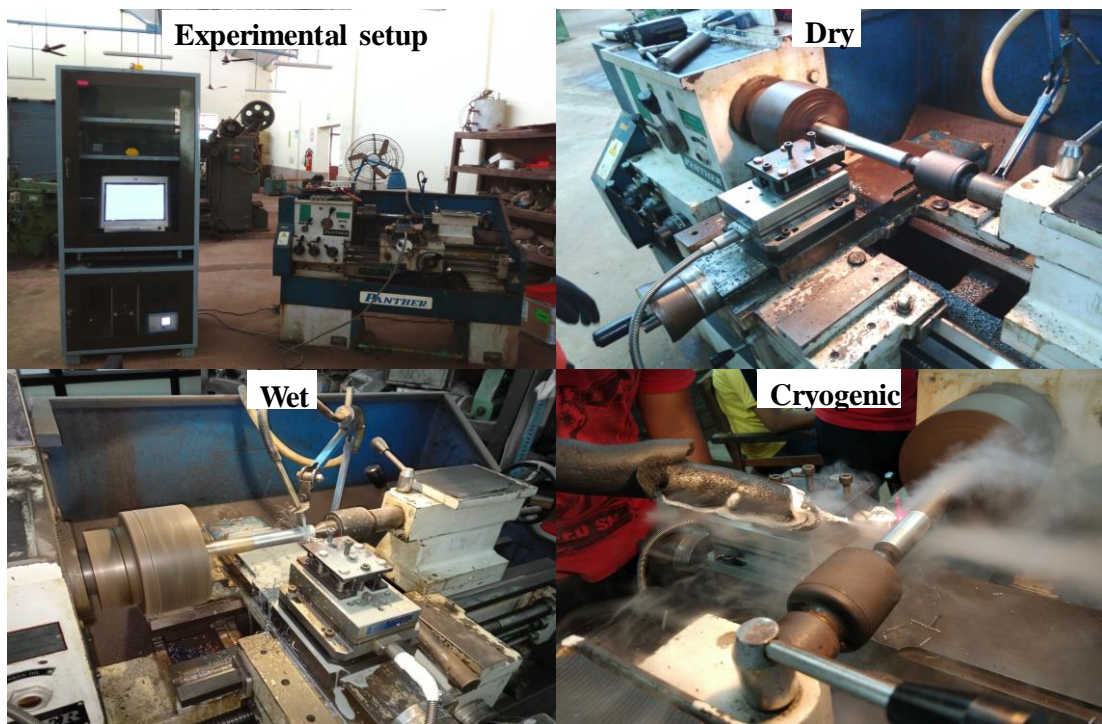


Figure 4.8 Experimental setup during dry, wet and cryogenic condition

Table 4.8 Experimental plan and output responses

| Sl No | a_p | V_c | f | F_z Dry | R_a Dry | T Dry | F_z Wet | R_a Wet | T Wet | F_z Cryo | R_a Cryo | T Cryo |
|-------|-------|-------|-------|-----------|-----------|-------|-----------|-----------|-------|------------|------------|--------|
| 1 | 0.2 | 59 | 0.070 | 85.95 | 3.54 | 39.60 | 79.56 | 3.28 | 35.90 | 71.90 | 2.13 | 34.95 |
| 2 | 0.2 | 59 | 0.093 | 125.90 | 4.27 | 40.12 | 115.60 | 4.02 | 37.90 | 73.70 | 2.75 | 35.15 |
| 3 | 0.2 | 59 | 0.117 | 167.05 | 5.12 | 42.56 | 142.95 | 4.77 | 37.80 | 85.33 | 3.51 | 36.55 |
| 4 | 0.2 | 75 | 0.070 | 66.55 | 3.31 | 55.86 | 89.11 | 3.06 | 39.56 | 66.65 | 1.83 | 34.35 |
| 5 | 0.2 | 75 | 0.093 | 123.05 | 3.88 | 57.98 | 114.87 | 3.56 | 40.78 | 72.36 | 2.39 | 36.15 |
| 6 | 0.2 | 75 | 0.117 | 166.89 | 4.25 | 58.87 | 133.10 | 3.98 | 45.23 | 84.78 | 2.76 | 37.65 |
| 7 | 0.2 | 118 | 0.070 | 65.00 | 3.43 | 62.58 | 85.635 | 3.14 | 55.58 | 65.54 | 1.92 | 37.95 |
| 8 | 0.2 | 118 | 0.093 | 120.20 | 4.21 | 63.84 | 113.98 | 3.96 | 58.63 | 71.89 | 2.71 | 38.25 |
| 9 | 0.2 | 118 | 0.117 | 164.89 | 4.93 | 64.25 | 132.28 | 4.87 | 61.20 | 83.83 | 3.42 | 38.55 |
| 10 | 0.4 | 59 | 0.070 | 144.15 | 4.12 | 40.59 | 110.00 | 3.84 | 41.90 | 106.14 | 2.63 | 34.25 |
| 11 | 0.4 | 59 | 0.093 | 219.35 | 4.28 | 45.26 | 139.75 | 4.08 | 42.87 | 121.50 | 2.77 | 34.45 |
| 12 | 0.4 | 59 | 0.117 | 281.75 | 4.79 | 46.85 | 214.00 | 4.55 | 44.83 | 131.09 | 3.29 | 34.65 |
| 13 | 0.4 | 75 | 0.070 | 142.83 | 3.83 | 60.87 | 109.21 | 3.59 | 58.84 | 97.36 | 2.33 | 36.55 |
| 14 | 0.4 | 75 | 0.093 | 217.69 | 4.02 | 61.89 | 138.91 | 3.81 | 59.90 | 115.09 | 2.52 | 37.25 |
| 15 | 0.4 | 75 | 0.117 | 279.86 | 4.68 | 62.48 | 169.80 | 4.48 | 60.10 | 119.36 | 3.19 | 37.65 |
| 16 | 0.4 | 118 | 0.070 | 115.50 | 3.34 | 66.58 | 90.18 | 3.08 | 65.50 | 87.92 | 1.85 | 38.95 |
| 17 | 0.4 | 118 | 0.093 | 214.69 | 4.12 | 67.56 | 136.93 | 3.89 | 65.69 | 113.69 | 2.61 | 39.65 |
| 18 | 0.4 | 118 | 0.117 | 276.89 | 4.81 | 67.98 | 167.56 | 4.56 | 67.97 | 117.96 | 3.29 | 39.85 |
| 19 | 0.6 | 59 | 0.070 | 198.45 | 4.37 | 42.69 | 122.40 | 4.01 | 40.50 | 125.23 | 2.86 | 34.35 |
| 20 | 0.6 | 59 | 0.093 | 326.25 | 5.17 | 44.85 | 179.30 | 4.92 | 41.87 | 165.65 | 3.67 | 34.85 |
| 21 | 0.6 | 59 | 0.117 | 442.35 | 5.45 | 45.27 | 221.70 | 5.17 | 43.60 | 202.95 | 3.94 | 35.55 |
| 22 | 0.6 | 75 | 0.070 | 195.92 | 4.25 | 56.70 | 120.84 | 4.06 | 52.89 | 124.83 | 2.73 | 36.35 |
| 23 | 0.6 | 75 | 0.093 | 321.45 | 4.59 | 58.50 | 175.35 | 4.39 | 56.88 | 164.15 | 3.07 | 36.65 |
| 24 | 0.6 | 75 | 0.117 | 424.45 | 5.09 | 59.86 | 220.60 | 4.85 | 58.19 | 198.50 | 3.59 | 37.65 |
| 25 | 0.6 | 118 | 0.070 | 193.61 | 3.19 | 75.89 | 118.96 | 2.93 | 72.76 | 122.68 | 1.68 | 40.85 |
| 26 | 0.6 | 118 | 0.093 | 318.25 | 4.05 | 86.23 | 174.63 | 3.74 | 78.96 | 163.79 | 2.54 | 41.65 |
| 27 | 0.6 | 118 | 0.117 | 422.87 | 4.77 | 97.50 | 218.96 | 4.52 | 92.58 | 197.54 | 3.28 | 42.35 |

4.3.1 Analysis of variance (ANOVA)

(a) Cutting force:

During cutting process, cutting forces are exerted by the tool on to higher cutting forces reduce the tool life and the machined surface affected. In this experimental work predictive modelling developed for cutting force by using 2nd order regression equation, to optimize the process parameters.

Table 4.9 ANOVA for tangential cutting force (F_z) during dry condition

| F_z Dry | Sum of Squares | DoF | Mean Square | F-Value | P-value | % Cont |
|-----------|----------------|-----|-------------|---------|----------|--------|
| Model | 2.9970E+05 | 9 | 33295.68 | 626.06 | < 0.0001 | |
| A-f | 1.09E+05 | 1 | 1.09E+05 | 2056.06 | < 0.0001 | 36.36 |
| B- V_c | 544.38 | 1 | 544.38 | 10.24 | 0.0053 | 0.18 |
| C- a_p | 1.67E+05 | 1 | 1.67E+05 | 3140.11 | < 0.0001 | 55.56 |
| Total | 3.01E+05 | 26 | | | | |

Table 4.10 ANOVA for tangential cutting force (F_z) during wet condition

| F_z Wet | Sum of Squares | DoF | Mean Square | F-Value | P-value | % Cont |
|-----------|----------------|-----|-------------|---------|----------|--------|
| Model | 4.5645E+04 | 9 | 5071.65 | 59.89 | < 0.0001 | |
| A-f | 2.55E+04 | 1 | 2.55E+04 | 301.18 | < 0.0001 | 54.17 |
| B- V_c | 415.16 | 1 | 415.16 | 4.9 | 0.0408 | 0.88 |
| C- a_p | 1.61E+04 | 1 | 1.61E+04 | 189.67 | < 0.0001 | 34.11 |
| Total | 4.71E+04 | 26 | | | | |

Table 4.11 ANOVA for tangential cutting force (F_z) during cryogenic condition

| F_z Cryo | Sum of Squares | DoF | Mean Square | F-Value | P-value | % Cont |
|------------|----------------|-----|-------------|---------|----------|--------|
| Model | 4.4625E+04 | 9 | 4958.28 | 123.82 | < 0.0001 | |
| A-f | 6.78E+03 | 1 | 6.78E+03 | 169.28 | < 0.0001 | 14.96 |
| B- V_c | 190.39 | 1 | 190.39 | 4.75 | 0.0436 | 0.42 |
| C- a_p | 3.37E+04 | 1 | 3.37E+04 | 840.79 | < 0.0001 | 74.32 |
| Total | 4.53E+04 | 26 | | | | |

From ANOVA Table 4.9 to Table 4.11 in all cutting environments depth of cut and feed rate influence the cutting force. P-value shows less than 0.05 in all the cases. Cutting speed is less significant as confirmed from ANOVA tables. Cutting force is reduced by increasing the cutting speed, as the contact time between tool and workpiece very less at higher speed. Higher temperature leads to thermal softening of work material and which reduces the cutting force (Chen et al. 2014).

(b) Surface roughness:

Surface finish plays a vital role in manufacturing sector as it is the most important quality characteristics which, influence production rate as well as, machine part. Most of the industries try to achieve better quality of the products with less operating cost and shorten manufacturing time. Surface roughness can be reduced by increasing the cutting speed. This is because of thermal softening of work material, which results in better surface finish. At lower cutting speed, surface roughness was increased because of the formation of built of edge (BUE) on the tool flank face which leads to higher surface roughness. (Pawade et al. 2007). Table 4.12 to Table 4.14, it is shown that, feed rate influences surface roughness and it is confirmed by ANOVA tables. P-value shows less than 0.05 in all cutting environments. Feed rate is the major influencing factor during machining, followed by cutting speed, and depth cut, which have lesser significant. Surface roughness increases with increase in feed rate.

Table 4.12 ANOVA for surface roughness (R_a) during dry condition

| R_a Dry | Sum of Squares | DoF | Mean Square | F-Value | P-value | % Cont |
|-----------|----------------|-----|-------------|---------|----------|--------|
| Model | 9.18 | 9 | 1.02 | 27.56 | < 0.0001 | |
| A-f | 6.34 | 1 | 6.34 | 171.3 | < 0.0001 | 64.63 |
| B- V_c | 1.00 | 1 | 1 | 27.03 | < 0.0001 | 10.19 |
| C- a_p | 0.59 | 1 | 0.59 | 15.93 | 0.0009 | 6.01 |
| Total | 9.81 | 26 | | | | 100 |

Table 4.13 ANOVA for surface roughness (R_a) during wet condition

| R_a Wet | Sum of Squares | DoF | Mean Square | F-Value | P-value | % Cont |
|-----------|----------------|-----|-------------|---------|----------|--------|
| Model | 9.5 | 9 | 1.06 | 27.05 | < 0.0001 | |
| A-f | 6.71 | 1 | 6.71 | 171.95 | < 0.0001 | 66.04 |
| B- V_c | 0.86 | 1 | 0.86 | 22.01 | 0.0002 | 8.46 |
| C- a_p | 0.55 | 1 | 0.55 | 14.19 | 0.0015 | 5.41 |
| Total | 10.16 | 26 | | | | 100 |

In general, increasing feed rate (f) causes helical grooves on the machined surface; which are wider and deeper and leads to high surface roughness value. surface roughness decreases with increase in cutting speed, which is due to increasing temperature at the chip-tool interface, thus softening the work material, because of that workpiece can be easily deformed. High cutting speeds are categorized by the absence

of built-up edge (BUE), because there is no surface degradation due to fragmented chips on the machined surface.(A. Chabbi et al. 2017)

Table 4.14 ANOVA for surface roughness (R_a) during cryogenic condition

| R_a Cryo | Sum of Squares | DoF | Mean Square | F-Value | P-value | % Cont |
|------------|----------------|-----|-------------|---------|----------|--------|
| Model | 8.93 | 9 | 0.99 | 32.57 | < 0.0001 | |
| A-f | 6.15 | 1 | 6.15 | 201.93 | < 0.0001 | 65.15 |
| B- V_c | 1 | 1 | 1 | 32.68 | < 0.0001 | 10.59 |
| C- a_p | 0.57 | 1 | 0.57 | 18.86 | 0.0004 | 6.04 |
| Total | 9.44 | 26 | | | | 100 |

(c) Tool tip temperature:

There are three distinct sources of heat generation in metal cutting. They are a) shear zone b) chip-tool interface c) work-tool interface. Majority of heat is generated at the shear zone and lowest heat is generated at work-tool interface. For successful machining operation, the generated heat is to be dissipated or removed from the machining zone. Heat is carried away by chip (60%), tool (30%) and machined surface (10%). Therefore, it becomes important to estimate the amount of heat generated and also various methods of reducing the heat generated.

In this experimental work, analysis of tool tip temperature has been done with infrared thermal heat gun. Cutting speed increases the tool tip temperature also increases, because of the high friction between tool and the workpiece which leads to higher temperature at the tool tip interface, Moreover, at higher cutting speeds, formation of built up edge (BUE) are reduced, which intern improves the surface finish and reduce the cutting force. But, at higher cutting speed, tool wear is more and it affects the tool life. (Sivaiah and Chakradhar 2018a).

Table 4.15 ANOVA for tool tip temperature (T) during dry condition

| T Dry | Sum of Squares | DoF | Mean Square | F-Value | P-value | % Cont |
|----------|----------------|-----|-------------|---------|----------|--------|
| Model | 4819.4 | 9 | 535.49 | 28.05 | < 0.0001 | |
| A-f | 122.42 | 1 | 122.42 | 6.41 | 0.0215 | 2.38 |
| B- V_c | 3894.64 | 1 | 3894.64 | 203.97 | < 0.0001 | 75.71 |
| C- a_p | 505.9 | 1 | 505.9 | 26.5 | < 0.0001 | 9.83 |
| Total | 5144 | 26 | | | | 100 |

Table 4.16 ANOVA for tool tip temperature (T) during wet condition

| T Wet | Sum of Squares | DoF | Mean Square | F-Value | P-value | % Cont |
|------------------|----------------|-----|-------------|---------|----------|--------|
| Model | 4920.1 | 9 | 546.68 | 30.27 | < 0.0001 | |
| A-f | 149.59 | 1 | 149.59 | 8.28 | 0.0104 | 2.86 |
| B-V _c | 3525.42 | 1 | 3525.42 | 195.22 | < 0.0001 | 67.45 |
| C-a _p | 1015.93 | 1 | 1015.93 | 56.26 | < 0.0001 | 19.44 |
| Total | 5227.1 | 26 | | | | 100 |

Table 4.17 ANOVA for tool tip temperature (T) during cryogenic condition

| T Cryo | Sum of Squares | DoF | Mean Square | F-Value | P-value | % Cont |
|------------------|----------------|-----|-------------|---------|----------|--------|
| Model | 133.82 | 9 | 14.87 | 46.48 | < 0.0001 | |
| A-f | 7.35 | 1 | 7.35 | 22.96 | 0.0002 | 5.28 |
| B-V _c | 104.11 | 1 | 104.11 | 325.41 | < 0.0001 | 74.76 |
| C-a _p | 9.59 | 1 | 9.59 | 29.99 | < 0.0001 | 6.89 |
| Total | 139.26 | 26 | | | | 100 |

Tables ANOVA Table 4.15 to Table 4.17 shows ANOVA results for tool tip temperatures at different cutting conditions. In all cases cutting speed influences the tool tip temperature. P- value shows less than 0.05. Cutting speed and depth of cut are more significant, feed rate is less significant in the model. Increasing the cutting speed, tool tip temperature also increases because of the friction between tool and work material being high at higher cutting speed leads to higher temperature in cutting zone.

4.3.2 Main effects plots

Main effect plot is the graphical representation of each individual influencing factor for output response. Highest slope tends to more significant factor in model and optimal cutting conditions are identified. Figure 4.9 to Figure 4.11 shows the main effects plots for tangential cutting force during dry, wet and cryogenic conditions. Depth of cut shows a highest slope, followed by feed rate, and cutting speed have lesser slope. This is due to supplying of emulsion type of soluble coolant and liquid nitrogen on cutting zone, which leads reduced cutting force. The similar results were by (Jadhav and Jadhav 2014; Sivaiah and Chakradhar 2017b).

Figure 4.12 to Figure 4.14 shows the surface finish during machining at dry, wet and cryogenic condition. Surface roughness is highly influenced by feed rate, followed by

cutting speed and depth of cut. At higher cutting speed and lower feed rate, better surface roughness was achieved at all cutting environments. Figure 4.15 to Figure 4.17 shows the main effects plots for tool tip temperature during machining at dry, wet and cryogenic condition. Cutting temperature is highly influenced by cutting speed, followed by depth of cut and feed rate. Table 4.18 to Table 4.20 depicts optimum conditions of output response under different cutting environments.

Table 4.18 Optimum condition for cutting force (F_z) under different cutting environments

| | a_p (mm) | V_c (m/min) | f (mm/rev) |
|-----------|------------|---------------|--------------|
| Dry | 0.2 | 118 | 0.070 |
| Wet | 0.2 | 118 | 0.070 |
| Cryogenic | 0.2 | 118 | 0.070 |

Table 4.19 Optimum condition for surface roughness (R_a) under different cutting environments

| | a_p (mm) | V_c (m/min) | f (mm/rev) |
|-----------|------------|---------------|--------------|
| Dry | 0.2 | 118 | 0.070 |
| Wet | 0.2 | 118 | 0.070 |
| Cryogenic | 0.2 | 118 | 0.070 |

Table 4.20 Optimum condition for tool tip temperature (T) under different cutting environments

| | a_p (mm) | V_c (m/min) | f (mm/rev) |
|-----------|------------|---------------|--------------|
| Dry | 0.2 | 59 | 0.070 |
| Wet | 0.2 | 59 | 0.070 |
| Cryogenic | 0.2 | 59 | 0.070 |

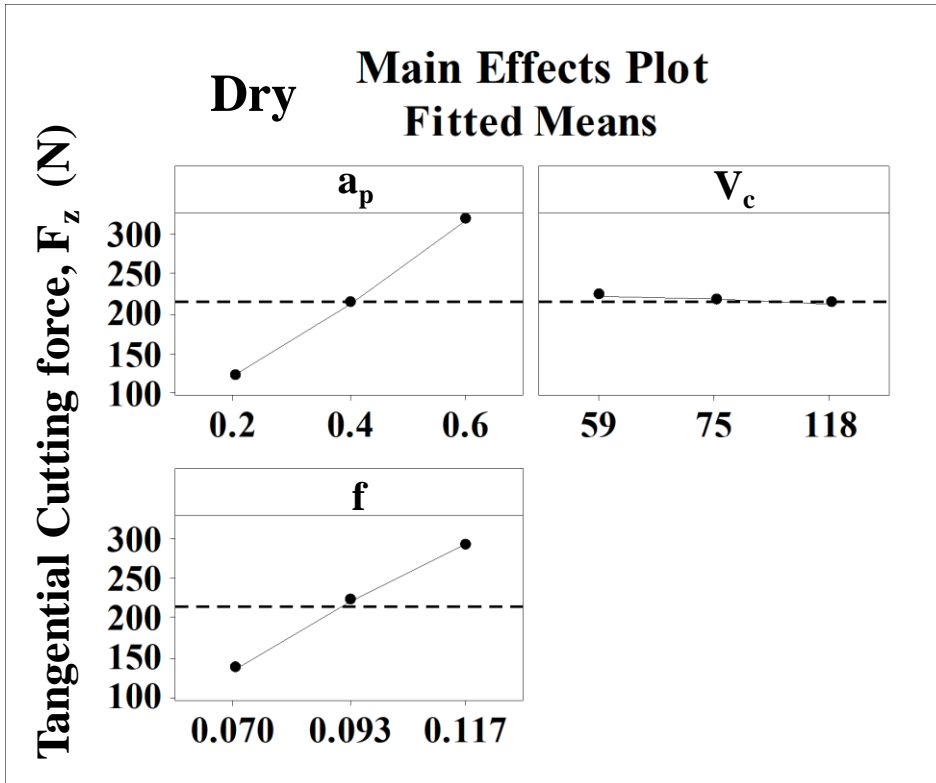


Figure 4.9 Main effects plot for tangential cutting force (F_z) during dry condition

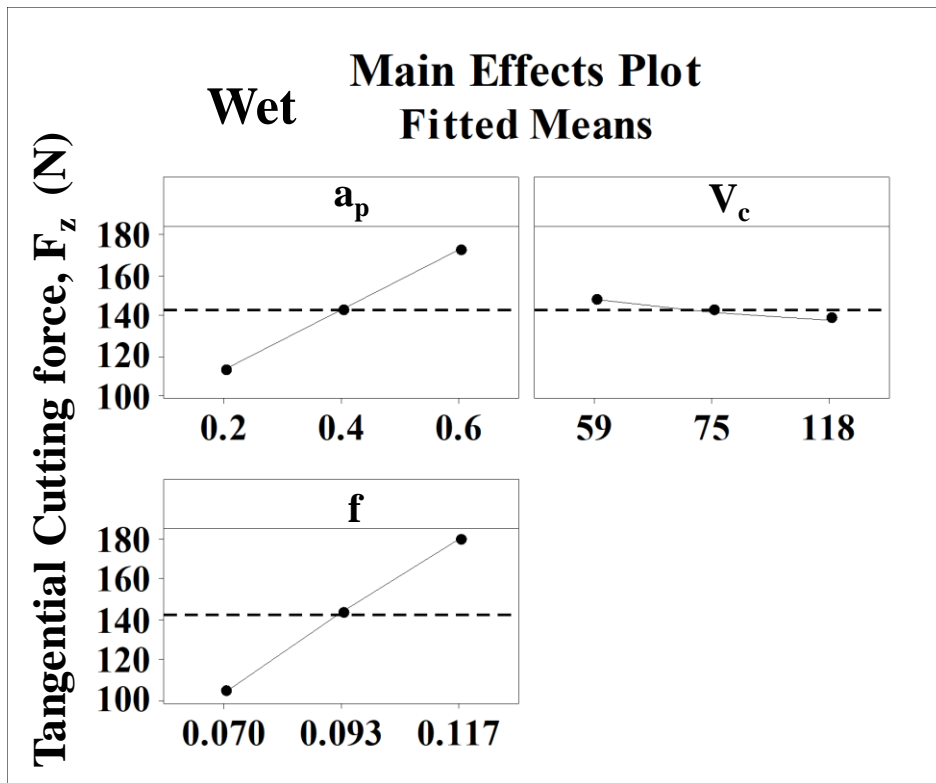


Figure 4.10 Main effects plot for tangential cutting force (F_z) during wet condition

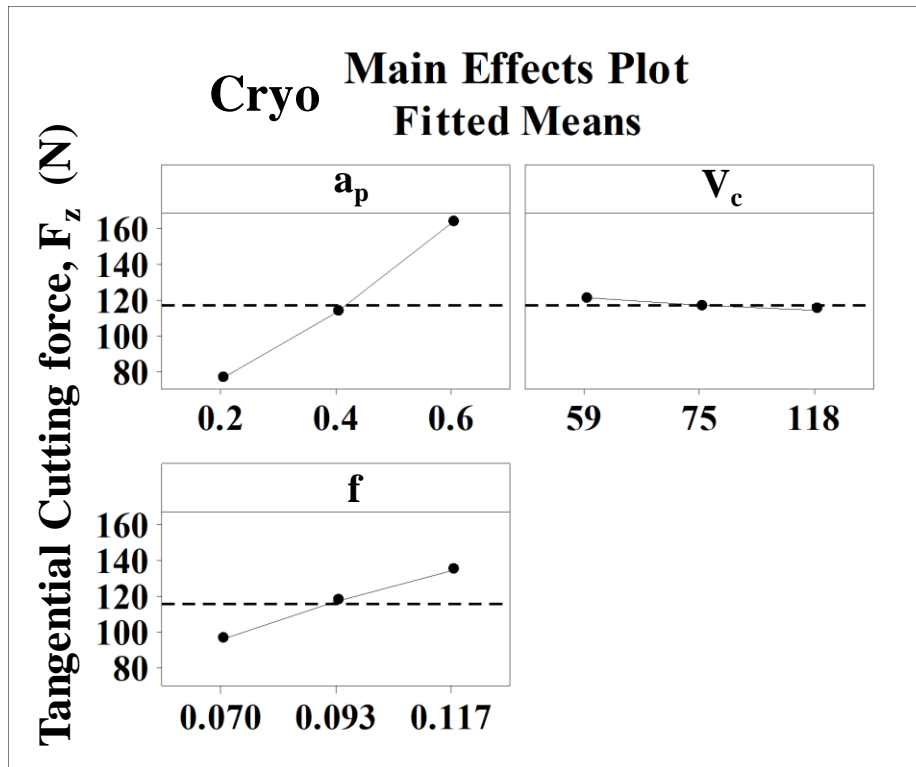


Figure 4.11 Main effects plot for tangential cutting force (F_z) during cryogenic condition

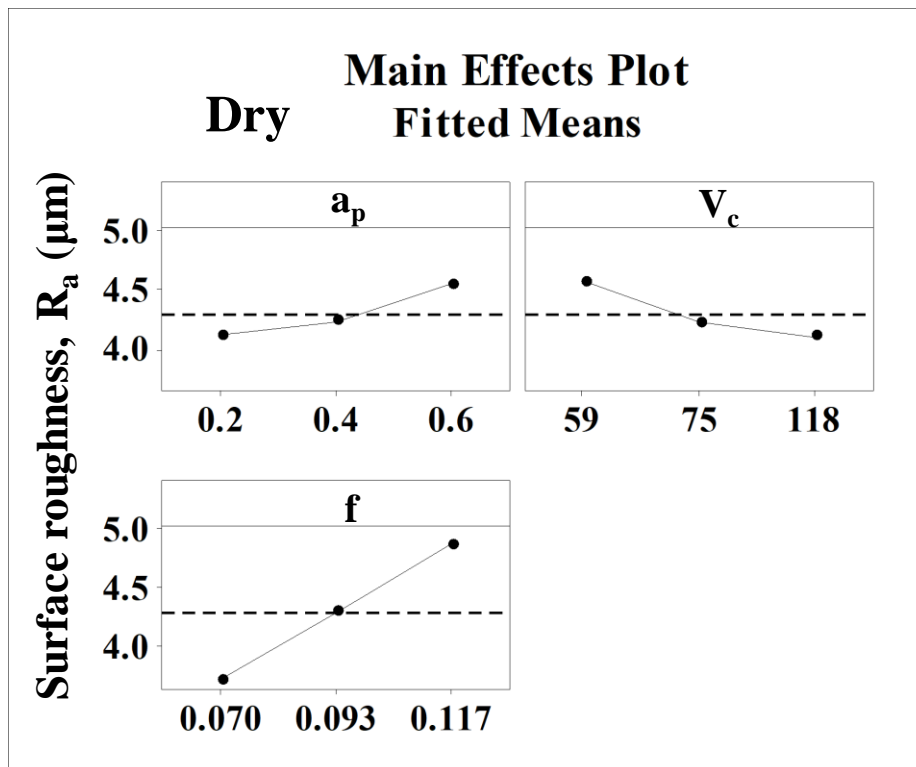


Figure 4.12 Main effects plot for surface roughness (R_a) during dry condition

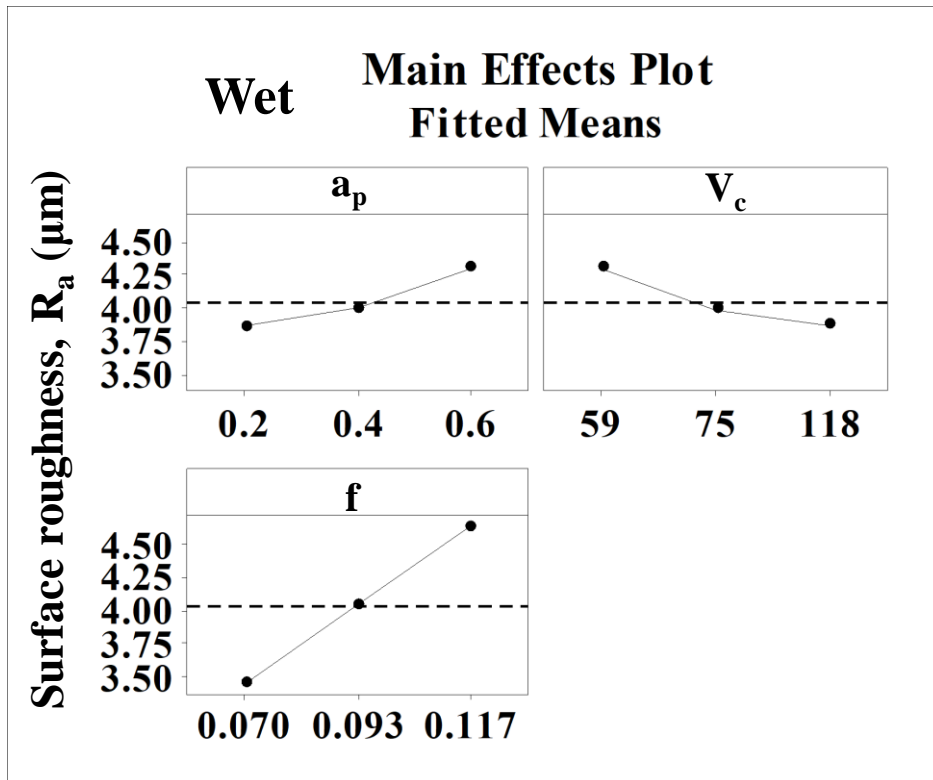


Figure 4.13 Main effects plot for surface roughness (R_a) during wet condition

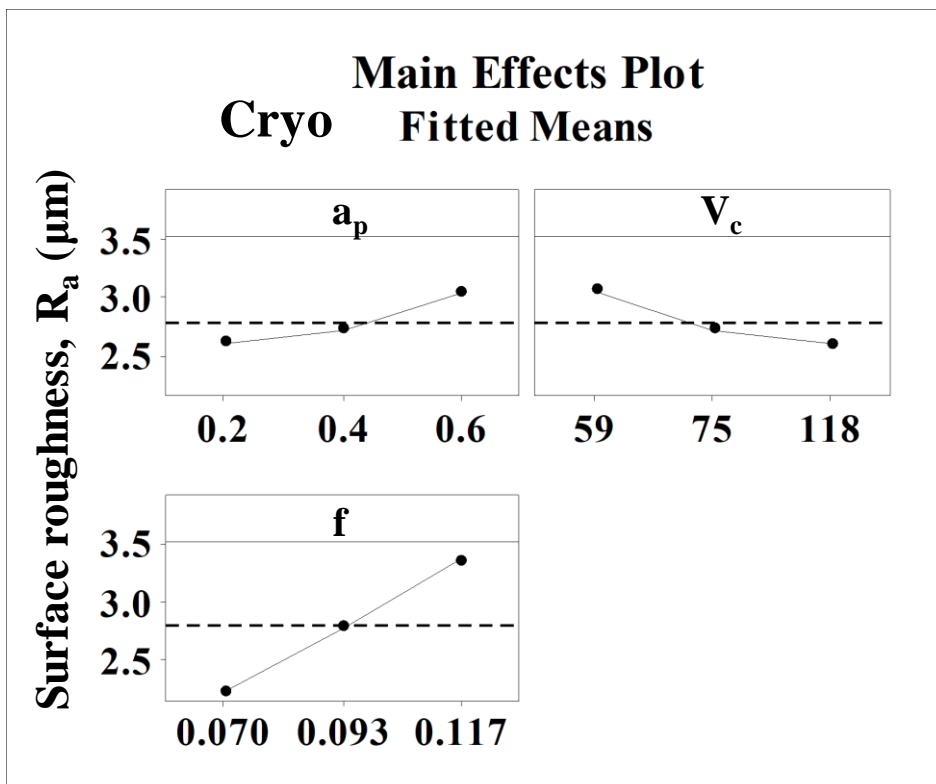


Figure 4.14 Main effects plot for surface roughness (R_a) during cryogenic condition

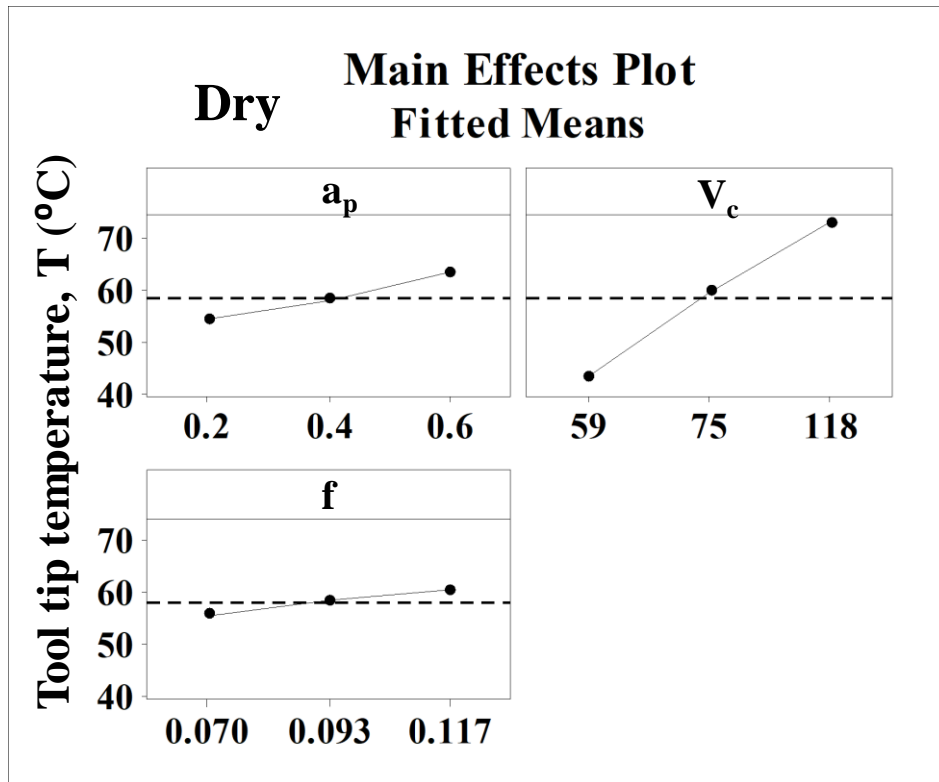


Figure 4.15 Main effects plot for tool tip temperature (T) during dry condition

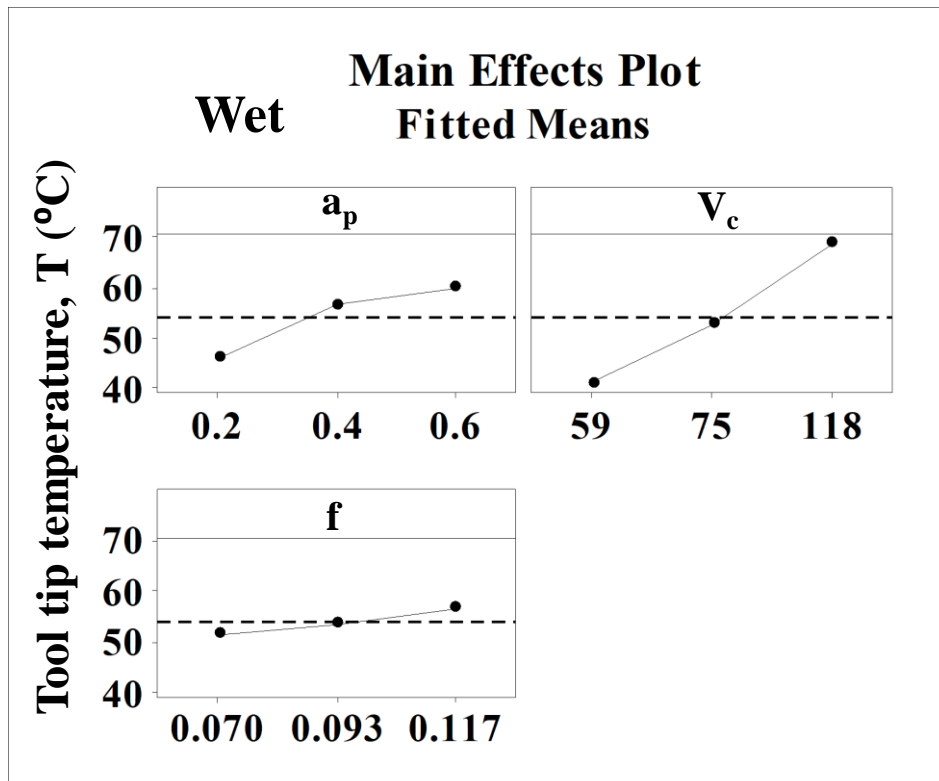


Figure 4.16 Main effects plot for tool tip temperature (T) during wet condition

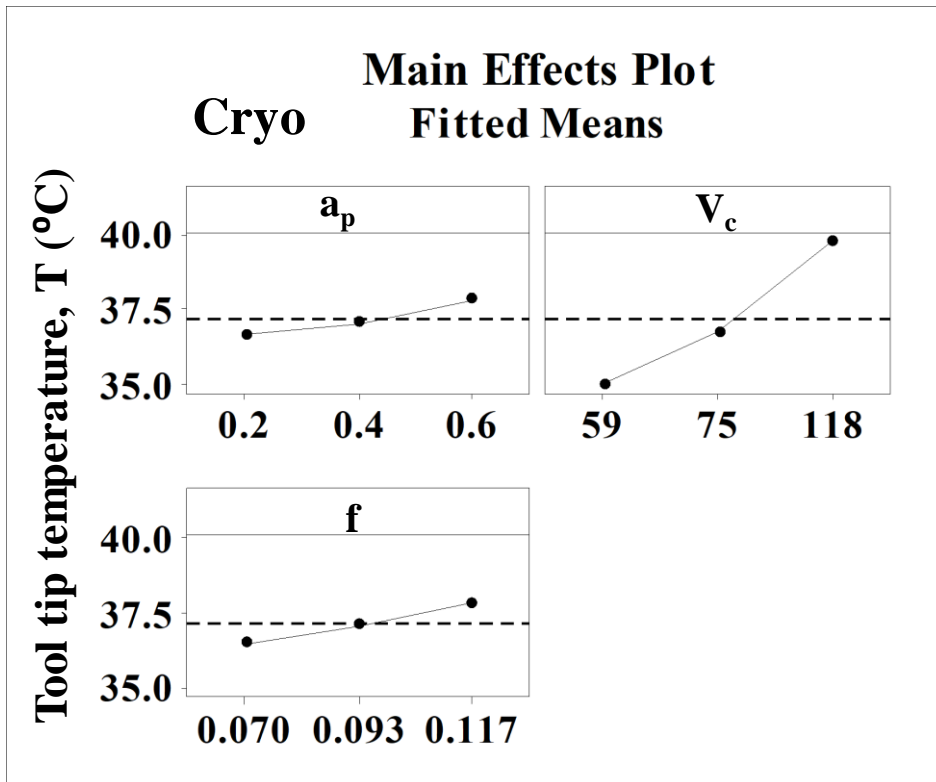


Figure 4.17 Main effects plot for tool tip temperature (T) during cryogenic condition

4.3.3 Normal Probability plots

Normal probability plot is the graphical representation, when analysing data from unreplicated factorial designs, occasionally real high order interactions occur. The use of an error mean square obtained by pooling high order interactions is inappropriate in these cases. A method of analysis attributed to (Cuthbert 1959) provides a simple way to overcome this problem.

Daniel suggests examining a normal probability plot of the estimates the effects. The effects that are negligible are normally distributed, with mean zero and variance σ^2 and will tend to fall along a straight line on this plot, whereas significant effects will have non-zero means and will not lie along the straight line. Thus, the preliminary model will be specified to contain those effects that are apparently non-zero, based on the normal probability plot. The apparently negligible effects are combined as an estimate of error (Montgomery 2012).

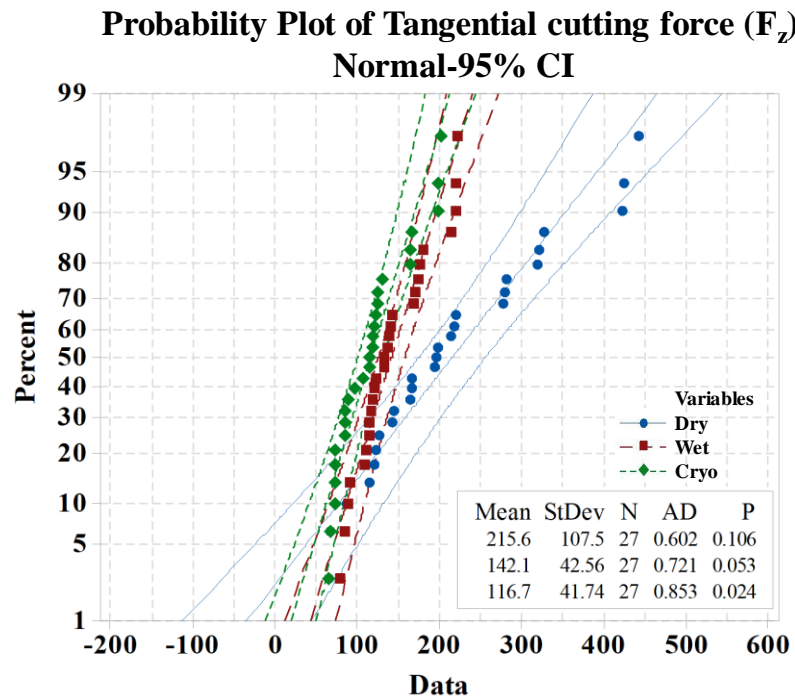


Figure 4.18 Normal probability plot for cutting force (F_z) during dry, wet & cryogenic condition

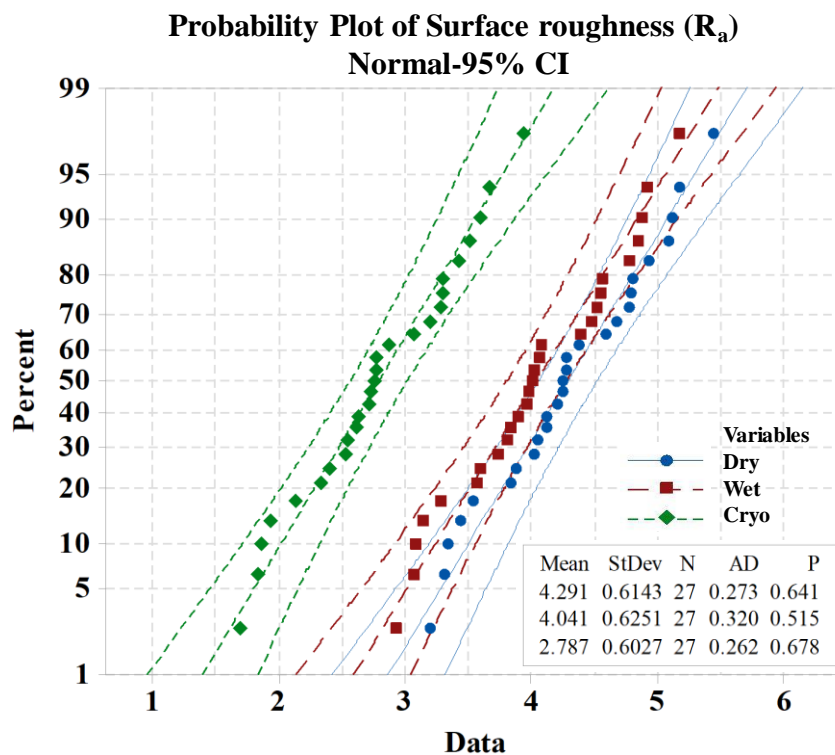


Figure 4.19 Normal probability plot for surface roughness (R_a) during dry, wet & cryogenic condition

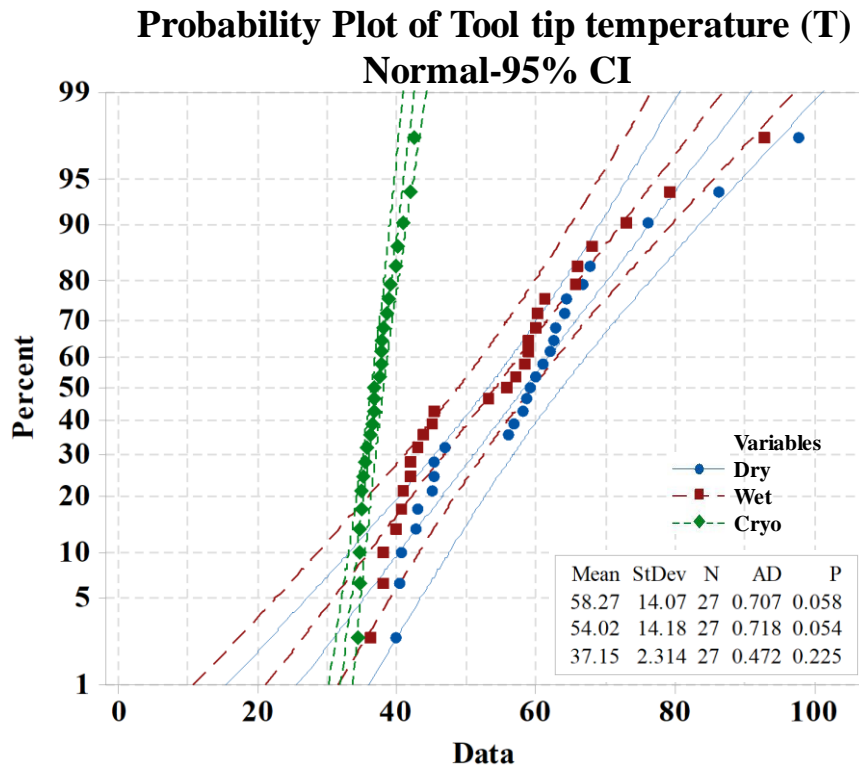


Figure 4.20 Normal probability plot for tool tip temperature (T) during dry, wet & cryogenic condition

Figure 4.18 to Figure 4.20 shows that normal probability plot for cutting force (F_z), surface roughness (R_a) and tool tip temperature (T) during dry, wet and cryogenic condition respectively. This representation is basically a plot of the ordered observations from a sample of data against the corresponding percentage points from the standard normal distribution for the studied output responses.

The diagnostic checking of the models were performed to prove the statistical validity of the models (Das et al. 2015). The model is said to be adequate if the points on the normal probability plots of the residuals should form a straight line. The other way is the plots of the residuals versus the predicted response should be structured less that is they should not contain particular obvious patterns (Sivaiah and Chakradhar 2018b). From the analysis it was observed that, all the points are fall on the straight line which indicates that the model is adequate.

4.3.4 3D surface graphs

3D surface graphs help to identify the interaction effect on output response of cutting force (F_z), surface roughness (R_a) and tool tip temperature (T). Since each model has three variables (a_p , V_c & f), each variable has three levels. Figure 4.21 to Figure 4.23 show the surface response plots for tangential cutting force, surface roughness and tool tip temperature in dry, wet and cryogenic conditions. From 3D response plots, can understand the interaction of input factor influencing the various output responses, keeping the middle level as constant for each factor.

Figure 4.21 (a-c) shows the interaction effect of input parameters on tangential cutting force. Cutting force is mainly influenced by the feed rate and depth of cut, as confirmed by analysis of variance and main effects plots. Experiments are conducted with different cutting environment like dry, wet and cryogenic. From the plots it is observed that cryogenic machining exhibits lower cutting force, as compared to, dry and wet condition.

From Figure 4.22 (a-c) shows the interaction effect of input parameters on surface roughness. Surface roughness is mainly influenced by feed rate and cutting speed. From the plots, it is noticed that higher cutting speed and lower feed rate play a major role in achieving better surface finish. Cryogenic machining gives better surface finish as compared to dry and wet machining.

From Figure 4.23 (a-c) it is observed that tool tip temperature is mainly influenced by cutting speed, as well as, depth of cut. At higher depth of cut and cutting speed leads to higher tool tip temperature. From the 3D plots, it is observed that lower tool tip temperature was obtained using cryogenic machining.

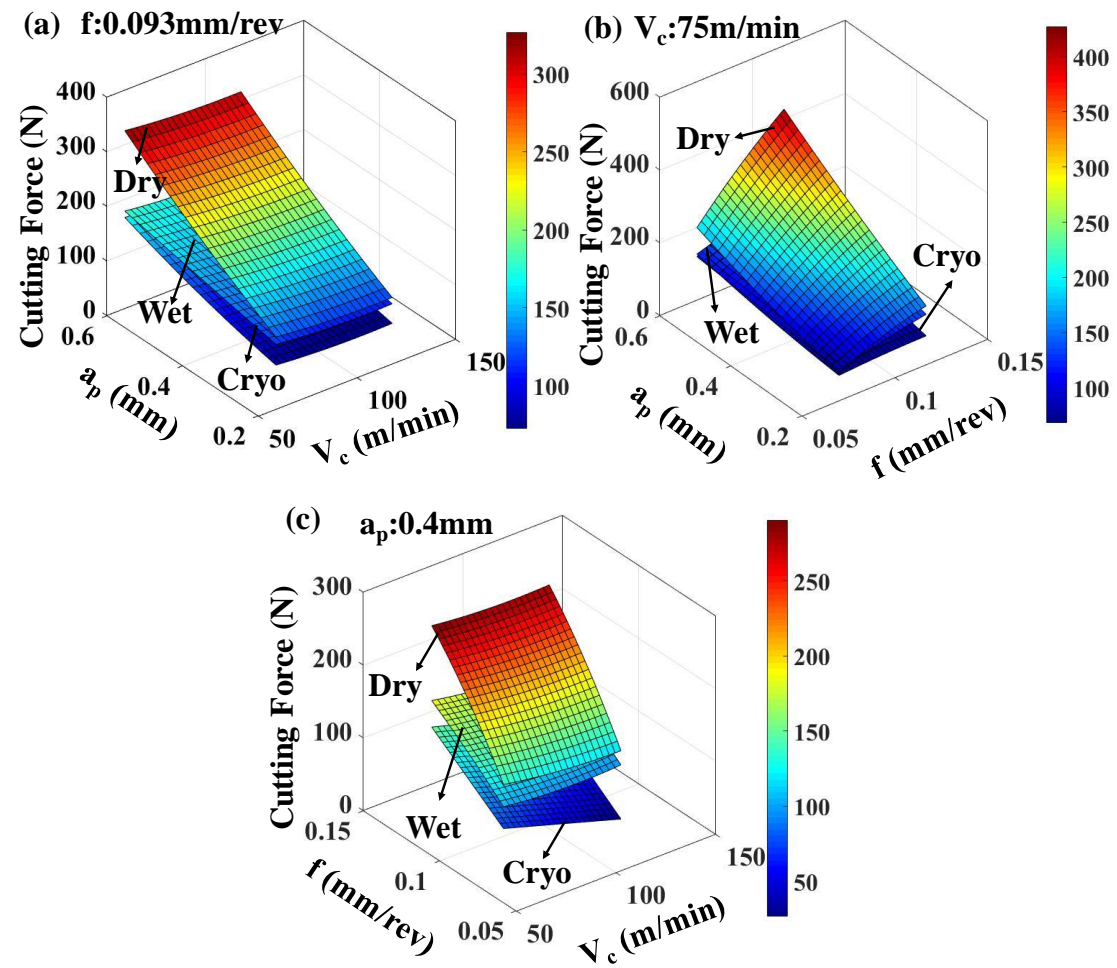


Figure 4.21 (a-c) 3D surface plot for cutting force (F_z) during dry, wet and cryogenic condition

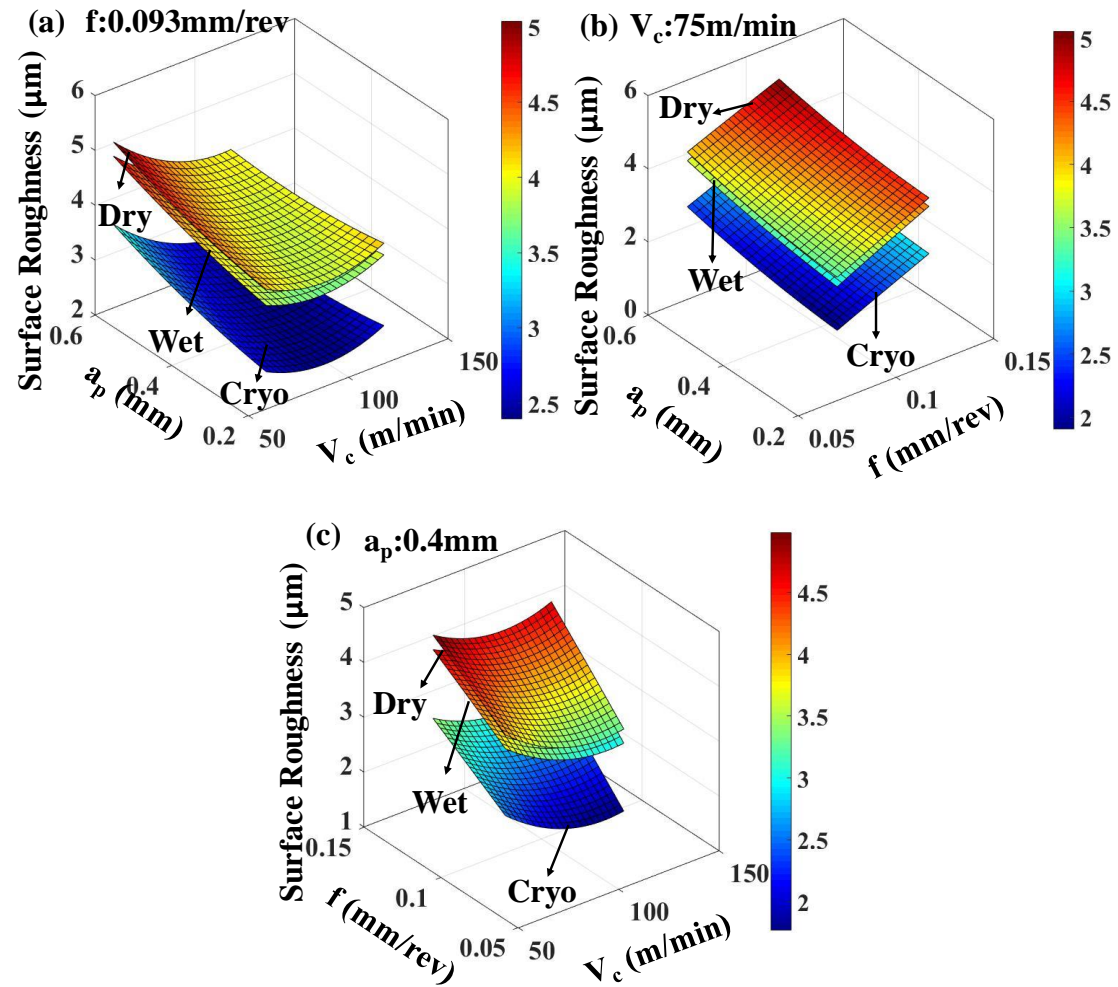


Figure 4.22 (a-c) 3D surface plot for surface roughness (R_a) during dry, wet and cryogenic condition

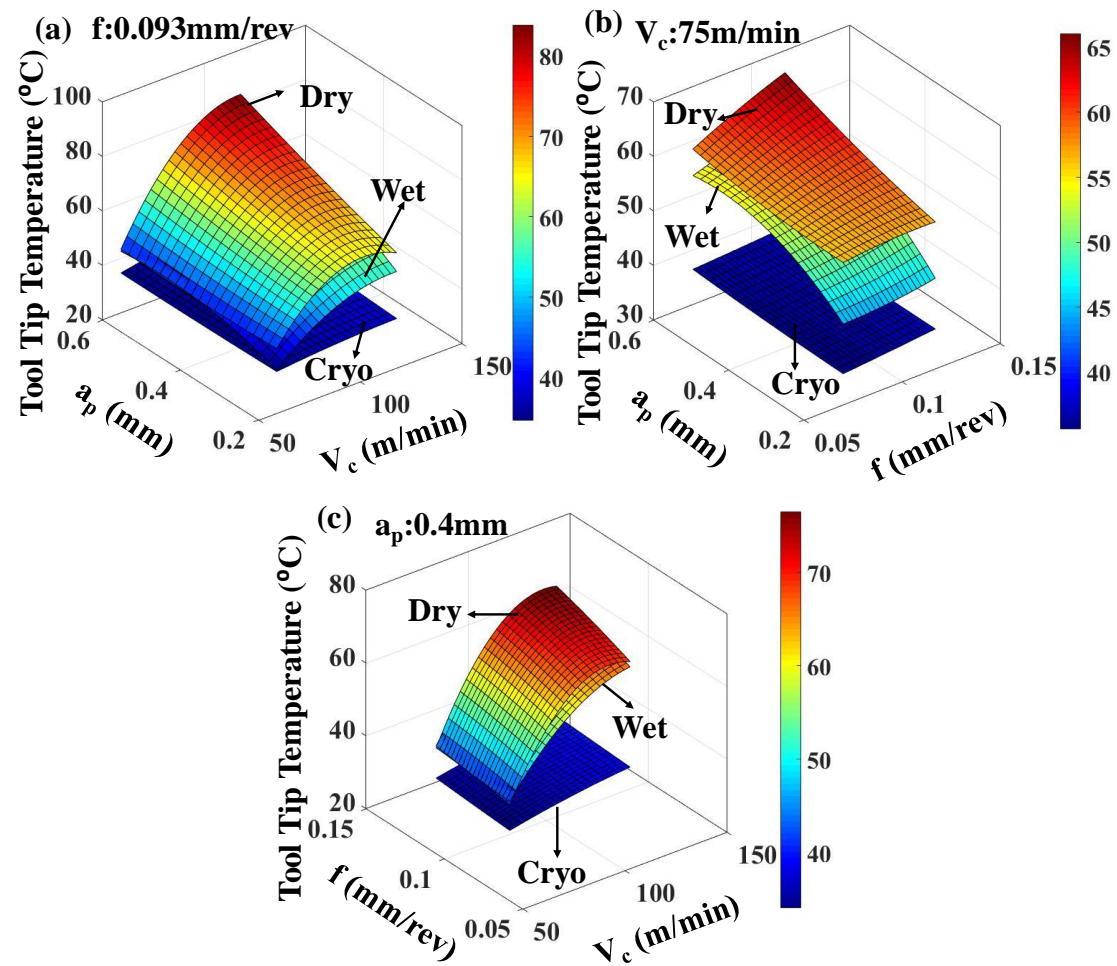


Figure 4.23 (a-c) 3D surface plot tool tip temperature (T) during dry, wet and cryogenic condition

4.3.5 Regression analysis

Regression analysis was performed to obtain the correlation between the input and output response parameters. These models are developed by *Design Expert 10* software. Input cutting parameters and output responses of performance measures, was modelled by the second order quadratic equation. Regression equation is very useful to obtain predicted values, and will be compared with experiment result. Developed mathematical model has been tested through ANOVA, and the coefficient of determination R^2 value is estimated. If these R^2 values are 100% then, the obtained model is adequate, and is the desirable results. it can be calculated and approaching by equation 4.1 The regression equations for various cutting forces, surface roughness and tool tip temperature at different cutting conditions like dry, wet and cryogenic conditions are given in equations 4.2 to 4.10.

$$R^2 = \frac{\text{Model sum of squares}}{\text{Total sum of squares}} \quad 4.1$$

Regression equation for Cutting force during dry, wet and cryogenic condition

$$F_z(Dry) = \left(\begin{array}{l} (-59.3) - (362.9 \times a_p) - (1.225 \times V_c) + (3263 \times f) - \\ (0.024 \times a_p \times V_c) + (7448 \times a_p \times f) + (3.47 \times V_c \times f) + \\ (199.5 \times a_p^2) + (0.00413 \times V_c^2) - (16998 \times f^2) \end{array} \right) \quad 4.2$$

$$R^2=87.33\%$$

$$F_z(Wet) = \left(\begin{array}{l} (6.2) - (92.2 \times a_p) - (0.68 \times V_c) + (1780 \times f) - \\ (0.048 \times a_p \times V_c) + (2570 \times a_p \times f) - (3.43 \times V_c \times f) + \\ (9.9 \times a_p^2) + (0.00486 \times V_c^2) - (4688 \times f^2) \end{array} \right) \quad 4.3$$

$$R^2=96.80\%$$

$$F_z(LN_2) = \left(\begin{array}{l} (100.3) - (206.3 \times a_p) - (0.9 \times V_c) + (286 \times f) - \\ (0.005 \times a_p \times V_c) + (3123 \times a_p \times f) + (0.98 \times V_c \times f) - \\ (168.2 \times a_p^2) + (0.00396 \times V_c^2) - (4185 \times f^2) \end{array} \right) \quad 4.4$$

$$R^2=92.67\%$$

Regression equation for surface roughness during dry wet and cryogenic condition

$$R_a(Dry) = \left(\begin{array}{l} (4.51) + (3.37 \times a_p) - (0.0671 \times V_c) + (15.8 \times f) - \\ (0.04160 \times a_p \times V_c) - (9.3 \times a_p \times f) + (0.1816 \times V_c \times f) + \\ (2.62 \times a_p^2) + (0.000332 \times V_c^2) - (13 \times f^2) \end{array} \right) \quad 4.5$$

$$R^2=87.07\%$$

$$R_a(Wet) = \left(\begin{array}{l} (3.75) + (4.28 \times a_p) - (0.0602 \times V_c) + (16.2 \times f) - \\ (0.04546 \times a_p \times V_c) - (10.7 \times a_p \times f) + (0.2126 \times V_c \times f) + \\ (2.04 \times a_p^2) + (0.000289 \times V_c^2) - (23 \times f^2) \end{array} \right) \quad 4.6$$

$$R^2=97.21\%$$

$$R_a(LN_2) = \left(\begin{array}{l} (3.35) + (3.00 \times a_p) - (0.0669 \times V_c) + (10.5 \times f) - \\ (0.04135 \times a_p \times V_c) - (4.8 \times a_p \times f) + (0.1996 \times V_c \times f) + \\ (2.53 \times a_p^2) + (0.000321 \times V_c^2) - (5 \times f^2) \end{array} \right) \quad 4.7$$

$$R^2=95.54\%$$

Regression equation for tool tip temperature during dry wet and cryogenic condition

$$T(Dry) = \left(\begin{array}{l} -(32.6) - (101.8 \times a_p) + (2.061 \times V_c) - (66 \times f) + \\ (0.922 \times a_p \times V_c) + (349 \times a_p \times f) + (1.81 \times V_c \times f) - \\ (18.1 \times a_p^2) - (0.01186 \times V_c^2) - (646 \times f^2) \end{array} \right) \quad 4.8$$

$$R^2=97.12\%$$

$$T(Wet) = \left(\begin{array}{l} -(6.1) + (21.3 \times a_p) + (1.015 \times V_c) - (330 \times f) + \\ (0.717 \times a_p \times V_c) + (267 \times a_p \times f) + (2.45 \times V_c \times f) - \\ (89.4 \times a_p^2) - (0.00597 \times V_c^2) + (699 \times f^2) \end{array} \right) \quad 4.9$$

$$R^2=92.74\%$$

$$T(LN_2) = \left(\begin{array}{l} (26.94) - (12.06 \times a_p) + (0.1336 \times V_c) + (36.1 \times f) + \\ (0.1649 \times a_p \times V_c) - (26.6 \times a_p \times f) - (0.113 \times V_c \times f) + \\ (4.58 \times a_p^2) - (0.000607 \times V_c^2) + (65 \times f^2) \end{array} \right) \quad 4.10$$

$$R^2=96.09\%$$

4.3.6 Machined surface analysis

Machined surface, was analyzed by scanning electron microscope. Average surface roughness (R_a) value was considered for analysis. From the experimental work, different cutting environments namely dry, wet and cryogenic condition was employed for conducting the experiments. Turning experiments are conducted at various conditions and are listed below.

- (i) $V_c=118$ m/min; $f= 0.093$ mm/rev and $a_p=0.4$ mm
- (ii) $V_c=59$ m/min; $f= 0.093$ mm/rev and $a_p=0.4$ mm
- (iii) $V_c=75$ m/min; $f= 0.070$ mm/rev and $a_p=0.4$ mm
- (iv) $V_c=75$ m/min; $f= 0.117$ mm/rev and $a_p=0.4$ mm

Condition (i) SEM micrograph is shown in Figure 4.24 (a-c) at higher cutting speed, in dry condition, microchips are adhered, burrs are formed with side flow of materials. In wet machining, burrs are eliminated and side flow of material is absent. Whereas in cryogenic machining, surface defects are much reduced, with good surface finish. This is because of thermal softening of workpiece as the friction and contact between the tool and workpiece are less. Further, increased cutting velocity tends to better surface finish. Surface roughness values, as measured by Talysurf roughness tester, and is estimated as $4.12\mu\text{m}$, $3.89\mu\text{m}$ and $2.61\mu\text{m}$ for dry, wet and cryogenic machining respectively.

Condition (ii) SEM image shows in Figure 4.25 (a-c) the presence of large number of microchips and microparticles are being adhered on the workpiece surface machined at dry condition. During machining at wet condition, formation of chips is reduced. During Cryogenic machining microchips are completely absent and present a defect free surface which is much smoother when compared to dry and wet machining. At lower cutting speeds, large quantity of materials moves on to the edge of the tool, thereby leading to high surface roughness. surface roughness values at dry, wet and cryogenic condition were found to be $4.28\mu\text{m}$, $4.08\mu\text{m}$ and $2.77\mu\text{m}$ respectively.

Condition (iii) SEM images shown in Figure 4.26 (a-c) and samples containing less pits, less adhered micro particle, minimal microchips and less feed marks which leads

to minimum surface roughness. R_a value are measured by Talysurf roughness tester was found to be $3.83 \mu\text{m}$, $3.59 \mu\text{m}$ and $2.33 \mu\text{m}$ for dry, wet and cryogenic respectively.

Condition (iv) At higher feed rates, impressions of the tool marks are seen on the machined surface, which results in large roughness and is seen from SEM images (Figure 4.27 (a-c)). Surface roughness values for dry, wet and cryogenic machining are $4.68 \mu\text{m}$, $4.48 \mu\text{m}$ and $3.19 \mu\text{m}$ respectively. In dry machining adhered microparticles and microchips leads to higher surface roughness values. This is because of the formation of helical furrows formed by tool movement which are deeper and wider (Bensouilah et al. 2016). In cryogenic machining liquid nitrogen (LN_2) was sprayed at the machined zone, i.e. at the tool – work piece interface led to the reduced temperature and less debris formation hence, better surface finish. From the SEM images, it is clearly shown that more surface defects like grooves, debris, side flow, and adhered micro particles were identified in dry and wet machining conditions and fewer surface defects was observed during cryogenic conditions, because of reduced material plasticity at cryogenic machining conditions (Bordin et al. 2017).

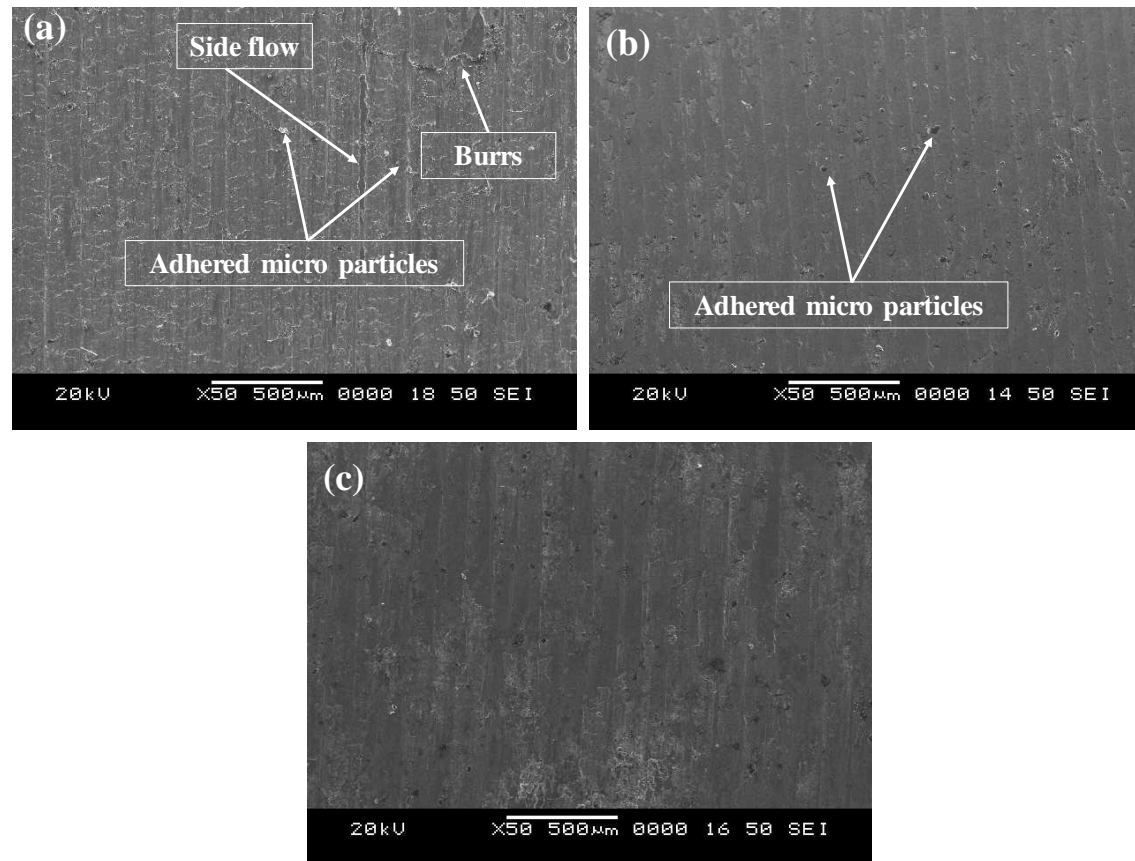


Figure 4.24 (a-c) SEM micrographs of machined surface at higher cutting speed (118 m/min) at different cutting environments (a) Dry (b) Wet & (c) Cryogenic condition

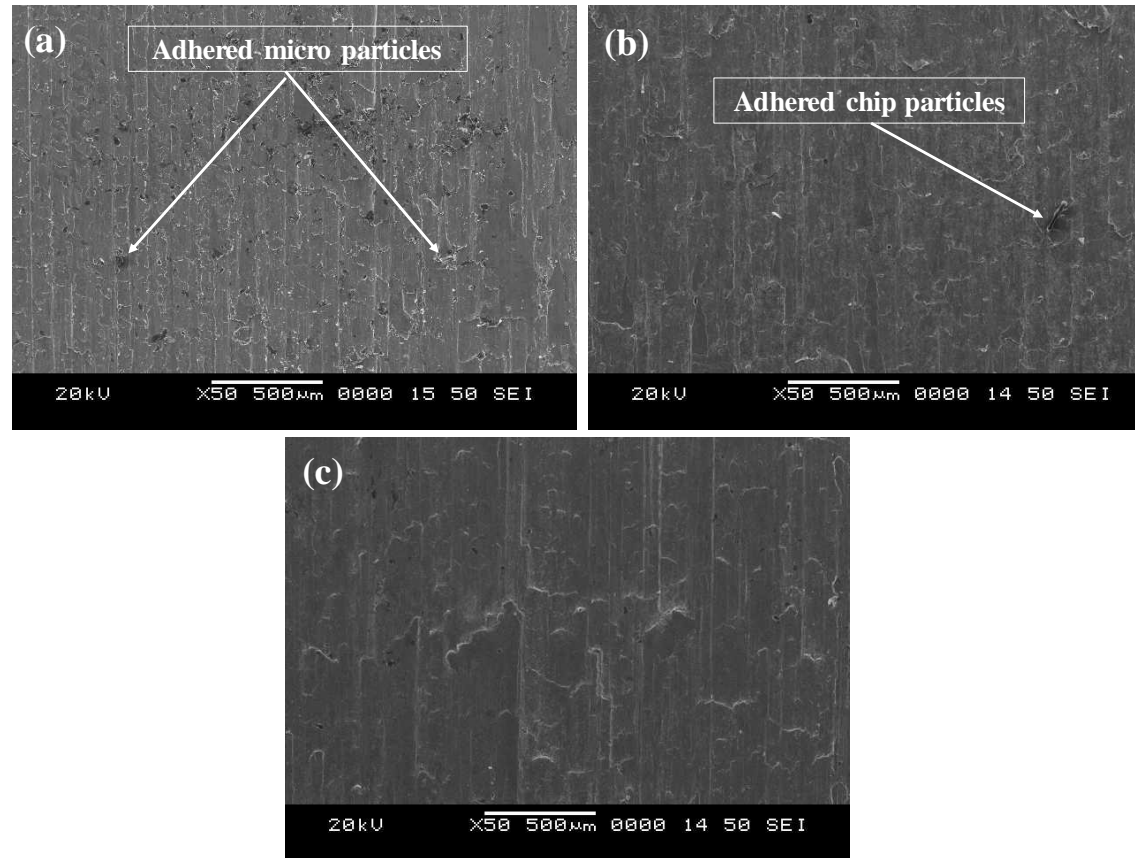


Figure 4.25 SEM micrographs of machined surface at lower cutting speed (59 m/min) at different cutting environments (a) Dry (b) Wet & (c) Cryogenic condition

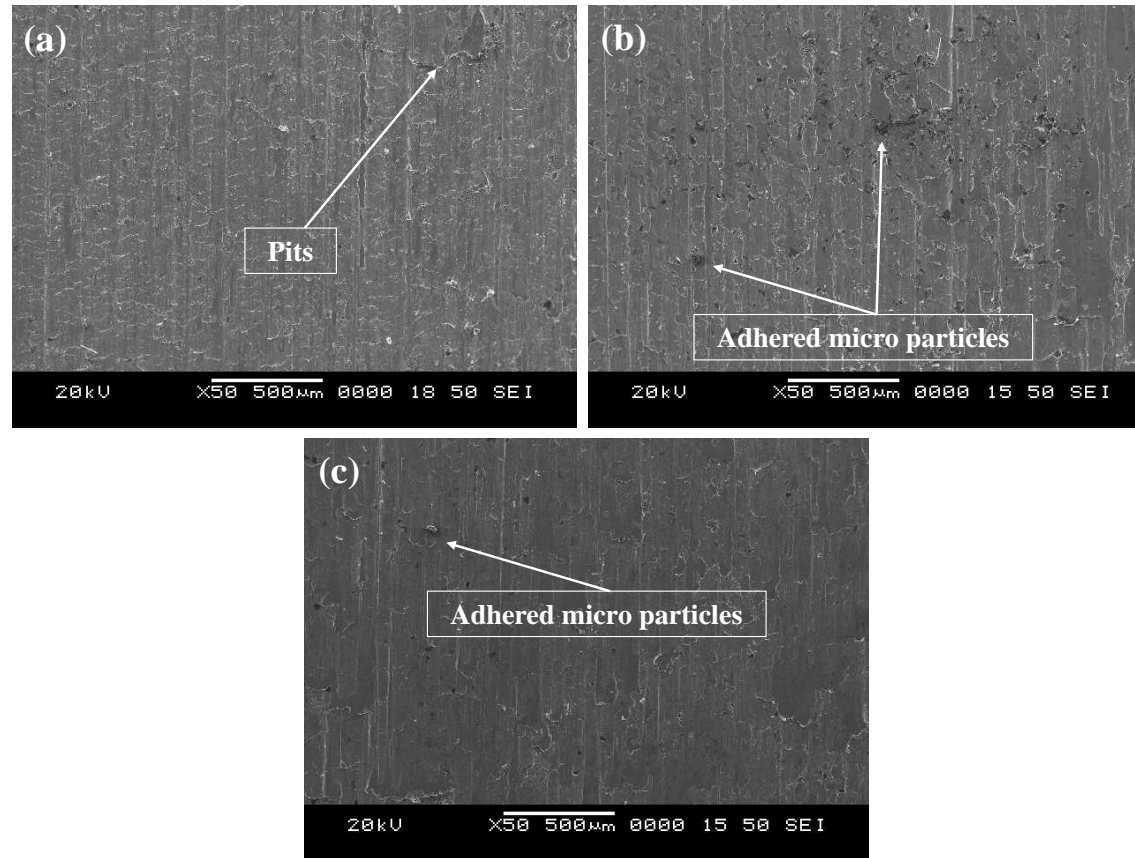


Figure 4.26 SEM micrographs of machined surface at lower feed rate (0.070 mm/rev) at different cutting environments (a) Dry (b) Wet & (c) Cryogenic condition

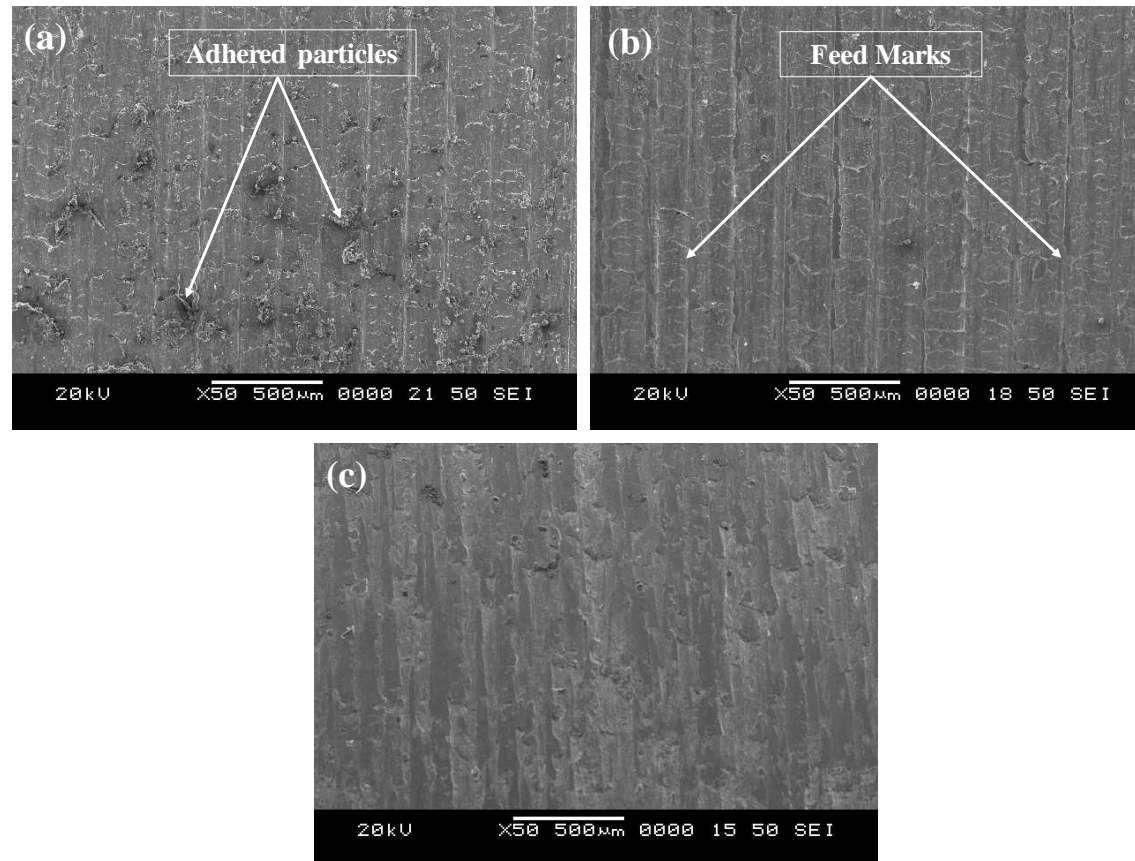


Figure 4.27 SEM micrographs of machined surface at higher feed rate (0.117 mm/rev) at different cutting environments (a) Dry (b) Wet & (c) Cryogenic condition

4.3.7 Machined surface topography

Machined surface topography as observed under confocal microscope are shown in Figure 4.28 and Figure 4.29. At low feed rate ($f=0.070\text{mm/rev}$, $V_c=75\text{m/min}$ & $a_p=0.4\text{mm}$) cryogenic machining produce lower surface peaks which compared to dry and wet machining. Figure 4.28 (a-c) during dry machining the waviness was very high due to side flow of chips at high temperature. In wet machining, waviness reduced slightly due to present of coolant during machining. At higher feed rate ($f=0.117\text{mm/rev}$, $V_c=75\text{m/min}$ & $a_p=0.4\text{mm}$) feed marks are very clear in dry, wet, and cryogenic condition and is shown in Figure 4.29 (a-c). Surface defects maximum during dry machining and is shown in Figure 4.29 (a). Higher feed rate forms helical furrows which are wider and deeper. At higher feed rate, machined compromises of surface adhered micro particles, microchips and more side flow of materials which forms high surface roughness.

Figure 4.30 and Figure 4.31 show the confocal images of machined surface at varying cutting speed in different cutting environments. At lower cutting speed ($V_c=59\text{ m/min}$, $f=0.093\text{mm/rev}$, & $a_p=0.4\text{mm}$), surface roughness is very high due to the presence of built up edge on cutting tool which affects the machined surface. This is because of very high contact time between tool and workpiece. During cryogenic machining, surface peak intensity is comparatively lower than dry and wet conditions, as observed from Figure 4.30 (a-c). At higher cutting speed ($V_c=118\text{ m/min}$, $f=0.093\text{mm/rev}$, & $a_p=0.4\text{mm}$), surface roughness is reduced, due to thermal softening of workpiece material and reduction in friction between tool and workpiece leads to better surface finish. During cryogenic machining very few surface defects as shown in Figure 4.31 (a-c). Better surface roughness values are obtained with cryogenic machining and it can improve the product performance, compared to other cutting environments.

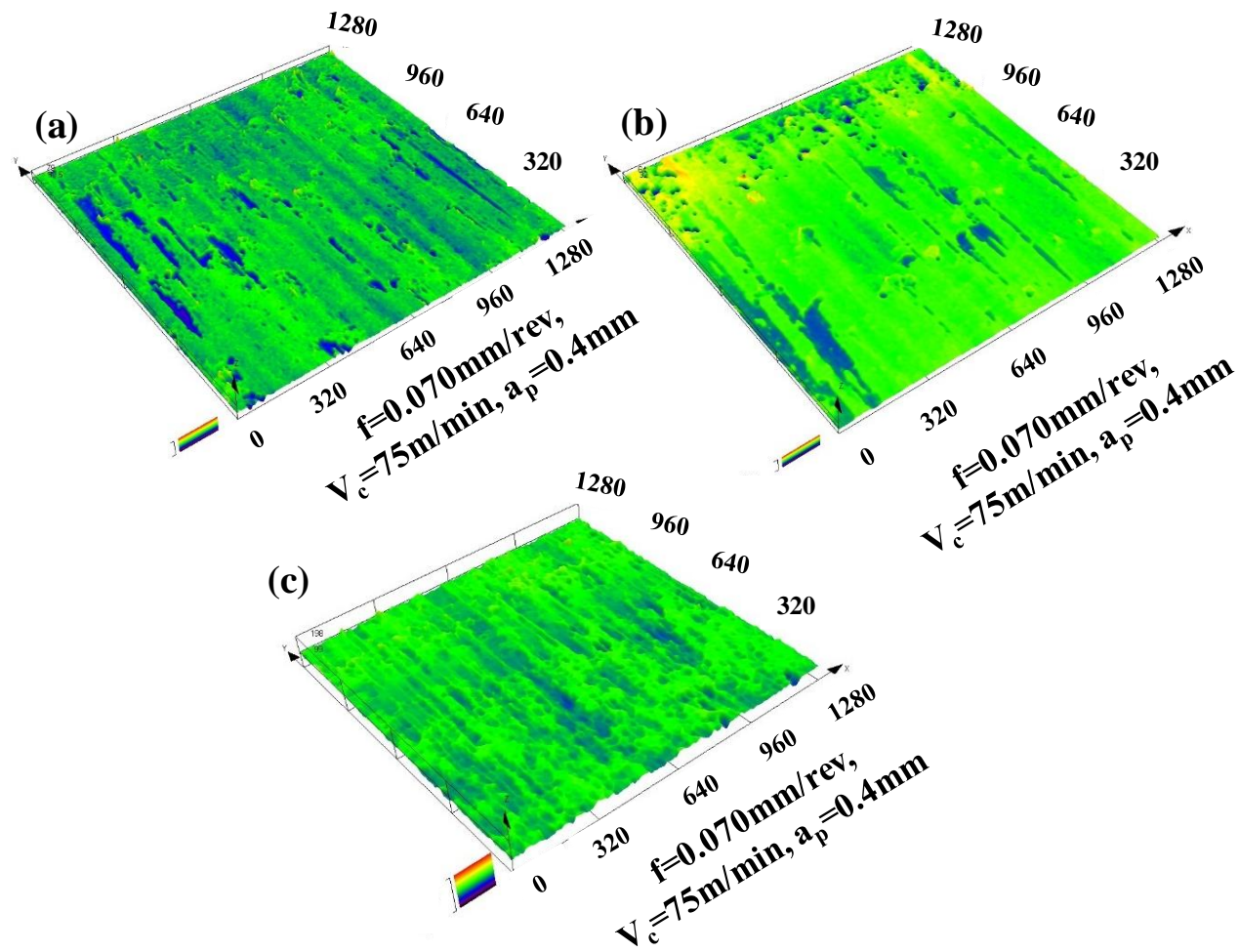


Figure 4.28 Surface topography at lower feed rate under different cutting environments (a) Dry (b) Wet & (c) Cryogenic condition

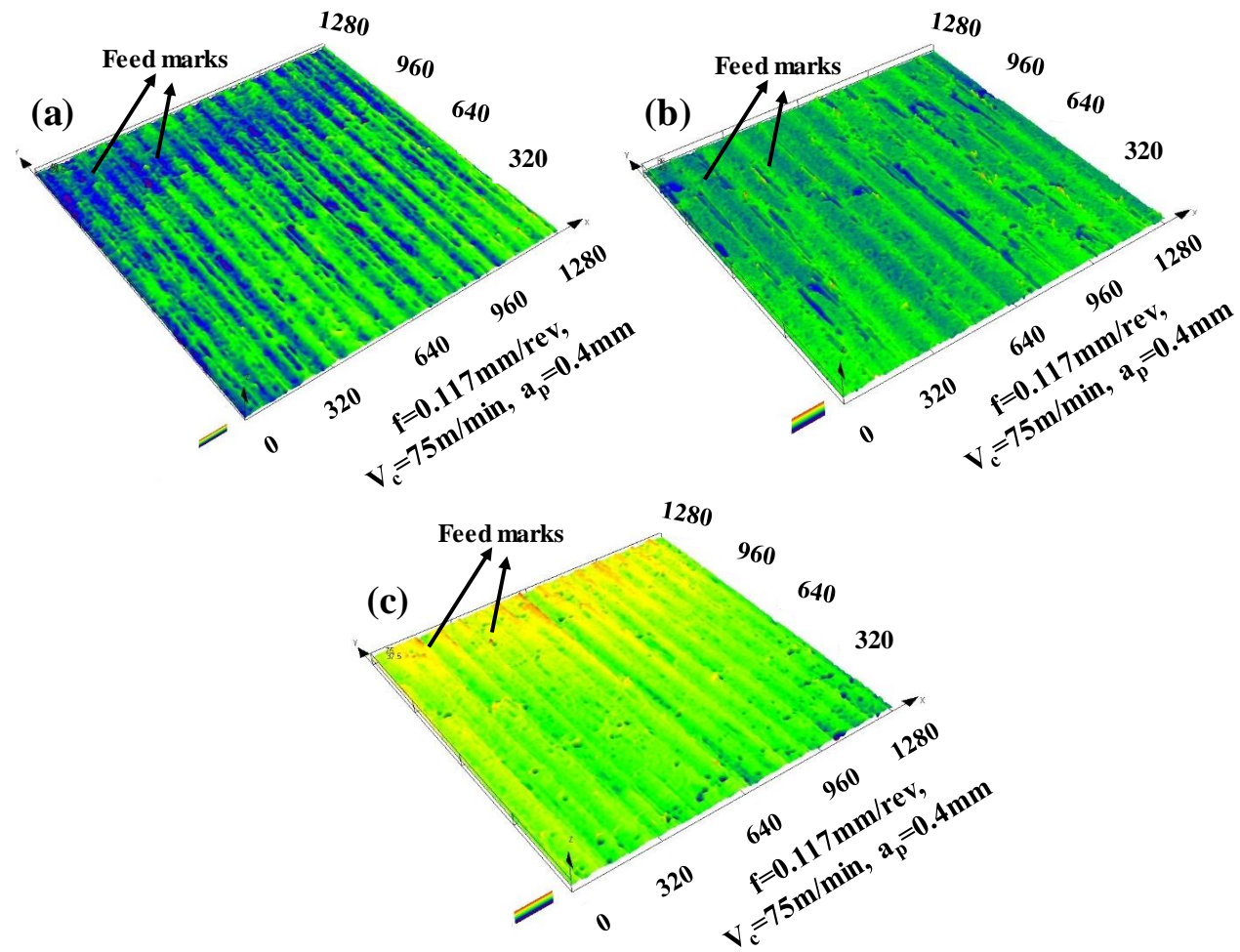


Figure 4.29 Surface topography at higher feed rate under different cutting environments (a) Dry (b) Wet & (c) Cryogenic condition

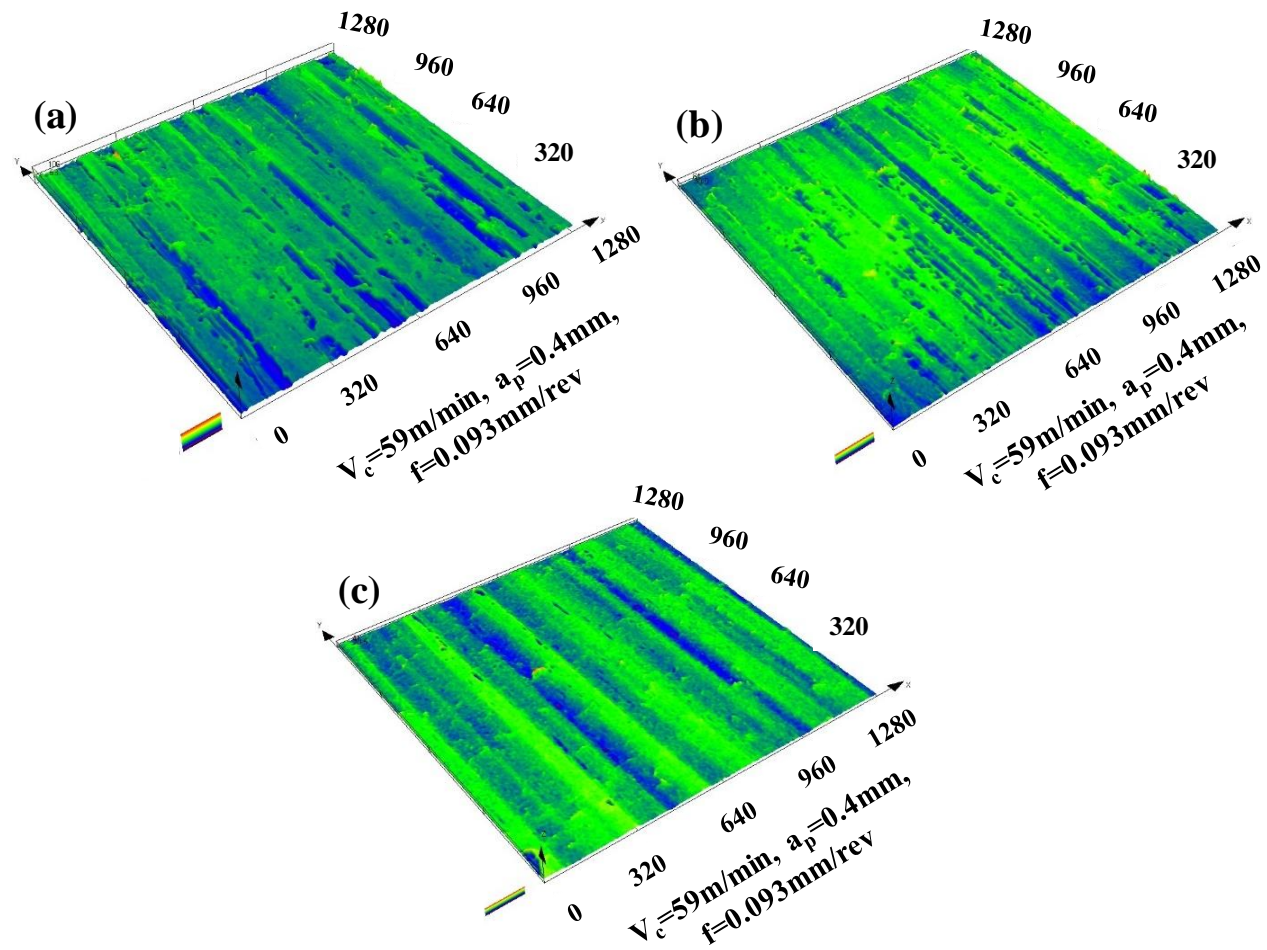


Figure 4.30 Surface topography at lower cutting speed under different cutting environments (a) Dry (b) Wet & (c) Cryogenic condition

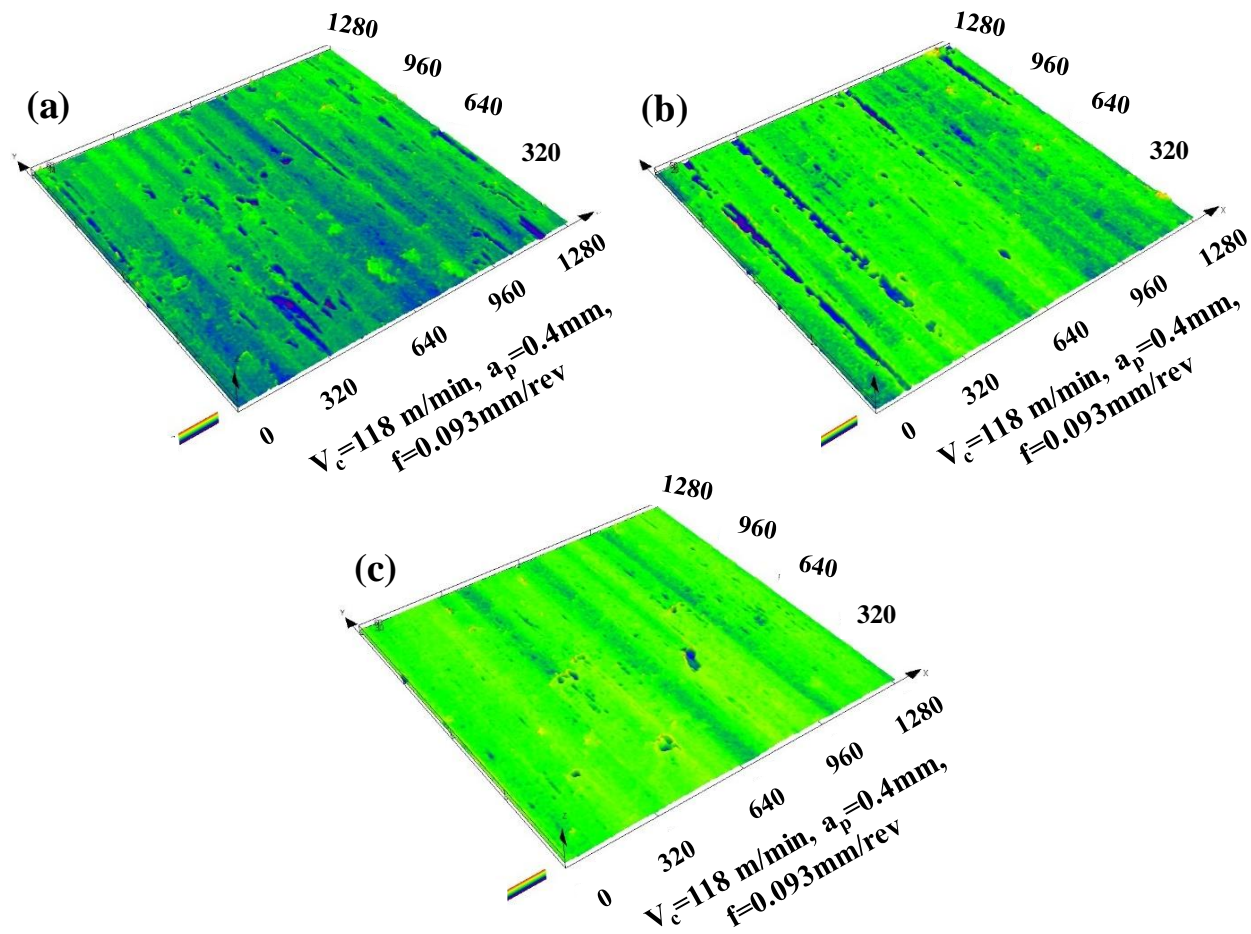


Figure 4.31 Surface topography at higher cutting speed under different cutting environments (a) Dry (b) Wet & (c) Cryogenic condition

4.3.8 Chip morphology

During machining material is removed from the bulk material in the form of chip. New surface will appear on the bulk material. Formation of chips helps to control machining condition, turning costs, surface finish and tool life, which often lead to better process and increased productivity. From the Figure 4.32 to Figure 4.37 show the SEM images of chips produced at different cutting parameters at various cutting condition of dry, wet and cryogenic conditions. Figure 4.32 shows the chips at lower cutting speed ($V_c=59$ m/min, $f=0.093$ mm/rev and $a_p=0.4$ mm) all the cutting environments. At lower cutting velocity, chips are broken, irregular shapes and short. This is due to severe abrasive and rubbing action.

From Figure 4.32 (a), during dry condition, chips are in the form of broken and irregular shape, thick long ribbon. which creates problem to machining operation as well as the operator. Whereas, in wet machining, chips are in the form of discontinuous spiral shape. Chip diameter is quite larger in wet machining, as observed from Figure 4.32 (b). Similarly, in cryogenic machining chips are in the form of helical or tabular shape, with metallic color, spiral with small diameters and is shown in Figure 4.32 (c).

Figure 4.33 (a) shows the chip morphology. At a higher cutting speed ($V_c=118$ m/min, $f=0.093$ m/min and $a_p=0.4$ mm). Chips in the form of long ribbon with bluish color and saw tooth. These kinds of chips are unfavorable for machining, which affects the machined surface. Whereas, in wet machining, chips are in the form of a very long ribbon type and continuous having gray color as observed from Figure 4.33 (b). Similarly, in cryogenic machining, chips are in the form of long thin discontinuous chips as shown in Figure 4.33 (c). This type of chip is the most favorable condition. This is because of the presence of liquid nitrogen (LN_2) at the machining zone, which leads to a lower temperature at cutting zone, causing a drop in the plasticity, as well as, breakability during chip formation and improve the chip flow control. During dry condition, extraction of chips becomes difficult because of jamming while machining and causes scratches on the machined surface, resulting in poor surface. In addition, side flow of material is increased during dry condition Whereas, very less side flow of material occurs during wet and cryogenic conditions and chips are easily extracted from the workpiece, due to application of coolant and LN_2 in the cutting zone.

From the Figure 4.34 and Figure 4.35 it was observed that varying feed rate effects on chips. At low feed rate ($f= 0.070$ mm/rev, $V_c=75$ m/min and $a_p=0.4$ mm) during dry machining chips are in the form of spiral shape bluish color. Whereas, wet and cryogenic condition chips in the form of close spring shape having metallic color, which are favorable chips, easily extracted from the workpiece. At high feed rate ($f=0.117$ mm/rev, 75 m/min and 0.4 mm) chips are in the form of elongated spiral shape during dry conditions, chips obtained with blueish color and chipping of side flow of material are more. Whereas wet and cryogenic condition chips are in the form of metallic color, which are favorable for machining. Feed rate increase from 0.070 mm/rev to 0.117 mm/rev in dry and wet condition side chipping is more compare to cryogenic machining.

Figure 4.36 and Figure 4.37 shows the SEM images of chips produced at depth of cut of 0.2 mm and 0.6 mm respectively at different cutting conditions. With increase in depth of cut chip thickness increases because of in rate of deformation. At low depth of cut ($a_p=0.2$ mm $f= 0.093$ mm/rev, $V_c=75$ m/min), under three different cutting environments, chips are in the form of spiral shape, long continuous thin ribbon type and having thickness of 186 μm , 123 μm and 98.7 μm for dry, wet and cryogenic respectively, diameter of the spirals formed are more in dry and wet machining. Whereas in cryogenic machining diameter is small. At higher depth of cut ($a_p=0.6$ mm $f= 0.093$ mm/rev, $V_c=75$ m/min) under three different cutting environments, chips are in the form of elongated spiral shape, helical with large diameter and having thickness of 455 μm , 376 μm and 225 μm for dry, wet and cryogenic respectively. Chip thickness was reduced during cryogenic machining.

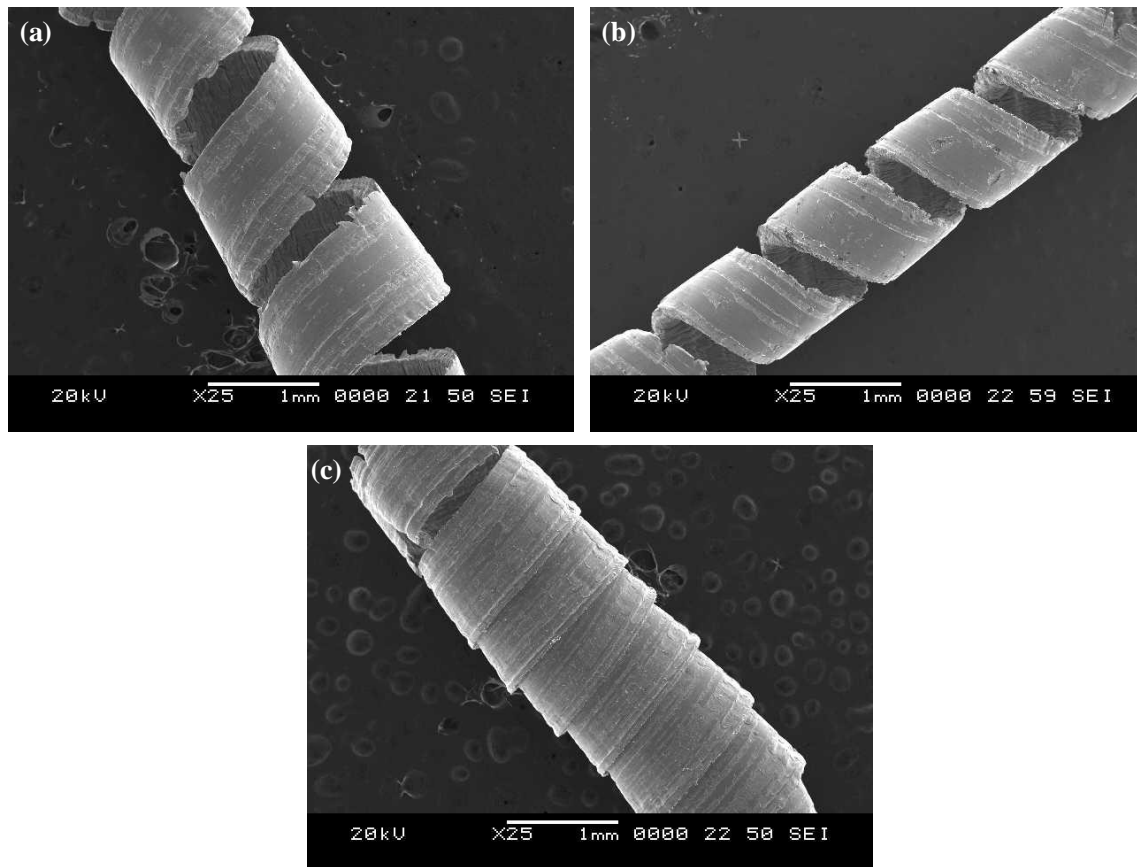


Figure 4.32 SEM images of chips at $V_c=59$ m/min, $f=0093$ mm/rev & $a_p=0.4$ mm (a) dry (b) wet & (c) cryogenic condition

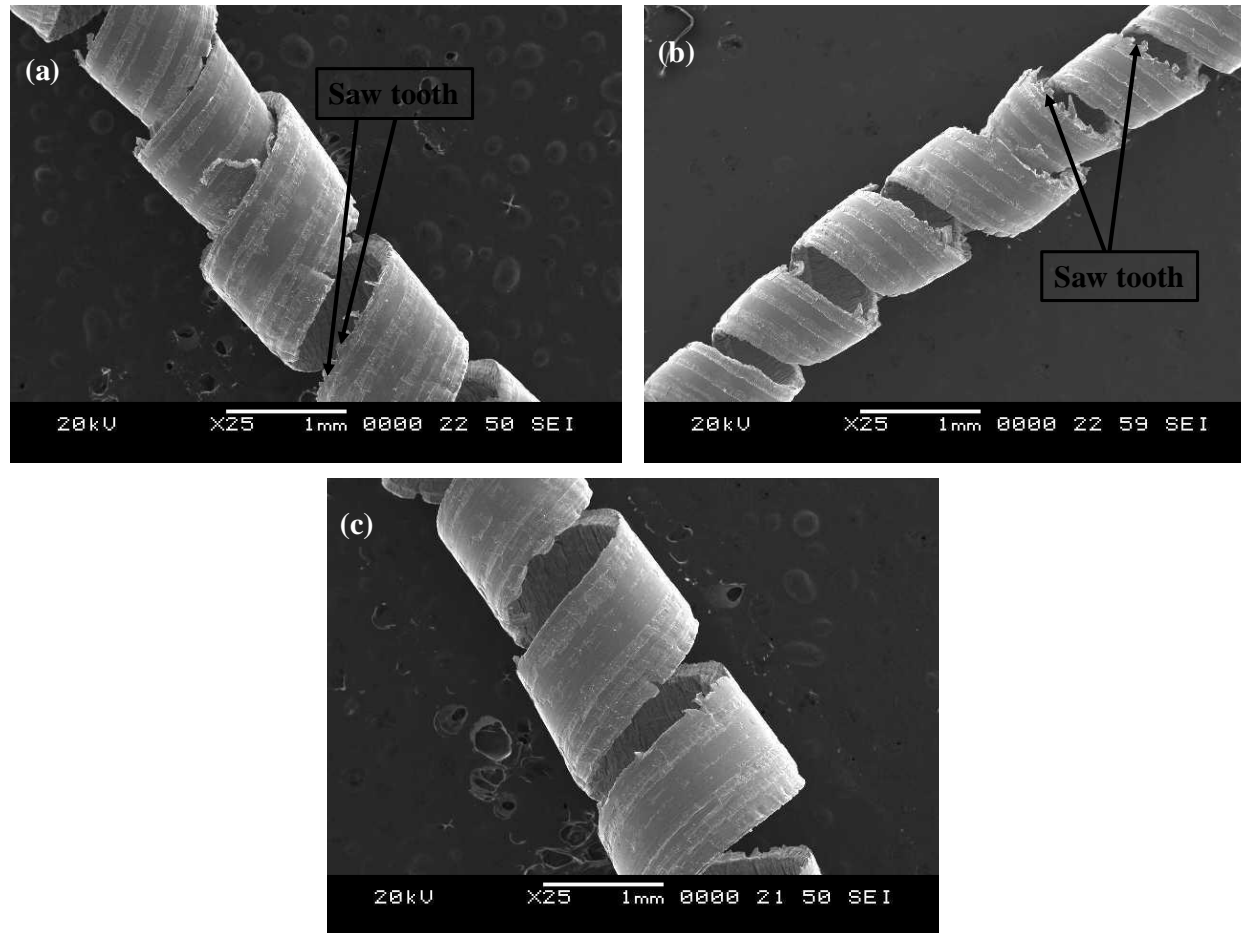


Figure 4.33 SEM images of chips at $V_c=118$ m/min, $f=0093$ mm/rev & $a_p=0.4$ mm (a) dry (b) wet & (c) cryogenic condition

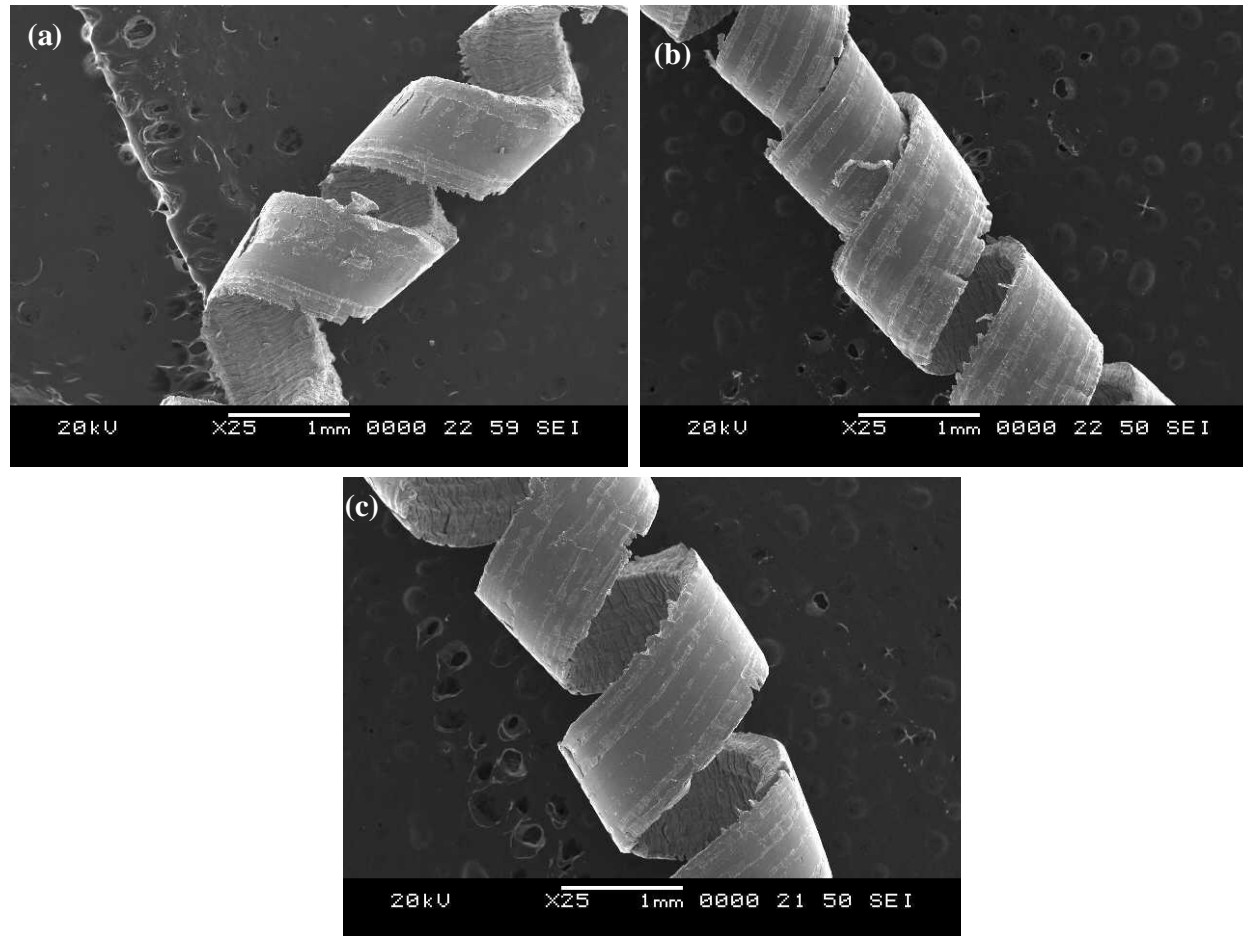


Figure 4.34 SEM images of chips at $f=0.070$ mm/rev, $V_c=59$ m/min & $a_p=0.4$ mm (a) dry (b) wet & (c) cryogenic condition

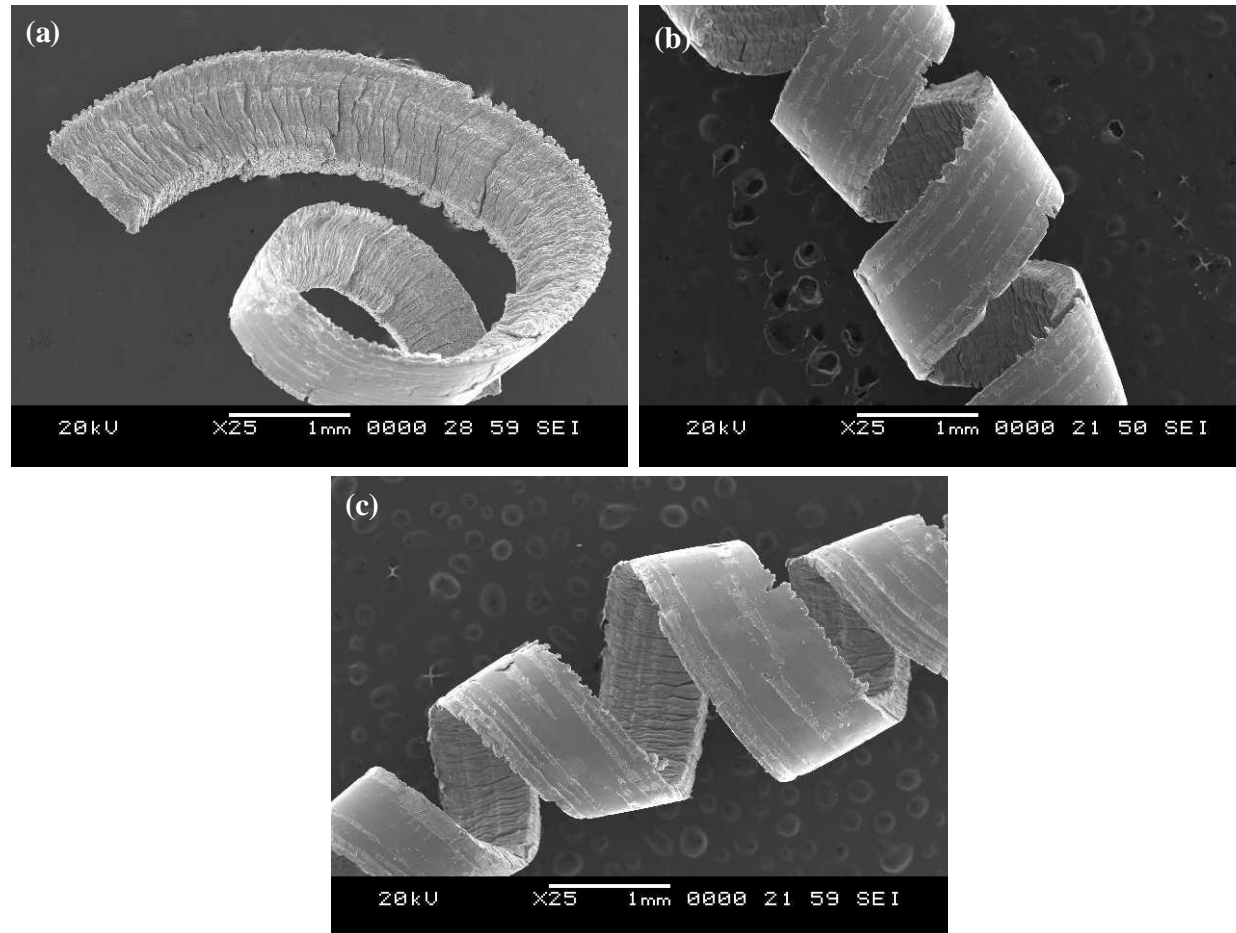


Figure 4.35 SEM images of chips at $f=0.117$ mm/rev, $V_c=59$ m/min & $a_p=0.4$ mm (a) dry (b) wet & (c) cryogenic condition

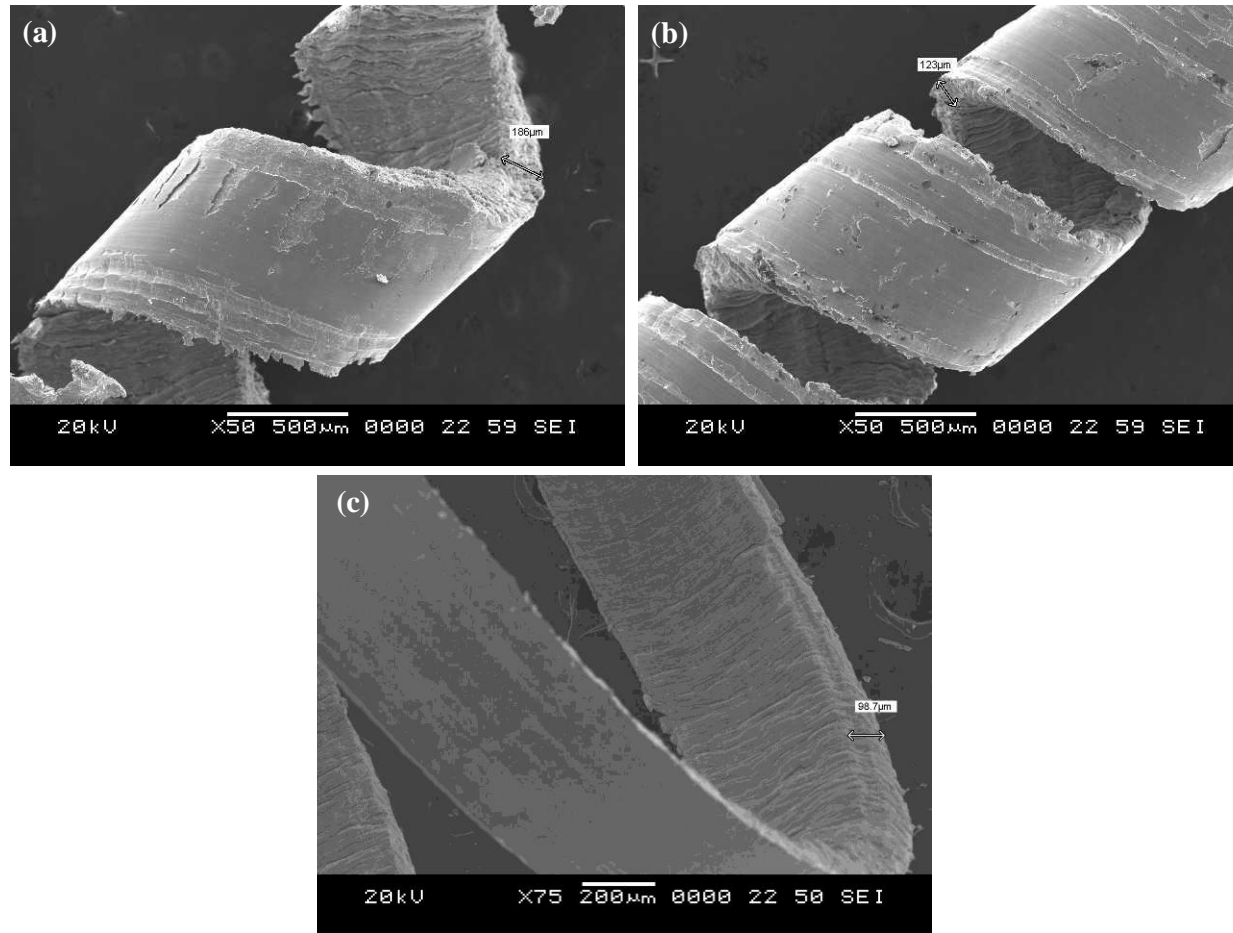


Figure 4.36 SEM images of chips at $a_p=0.2$ mm, $f=0.093$ mm/rev & $V_c=75$ m/min (a) dry (b) wet & (c) cryogenic condition

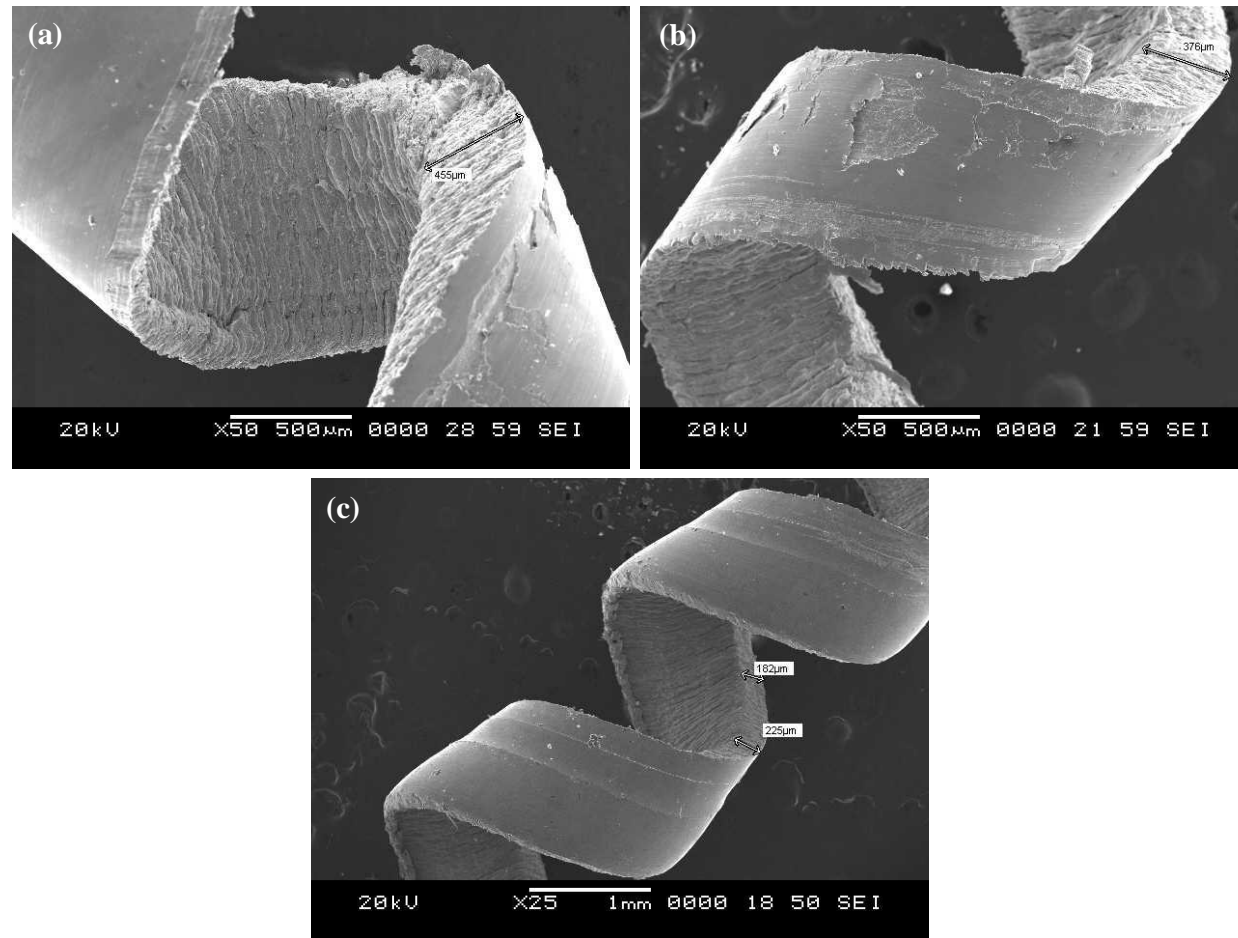


Figure 4.37 SEM images of chips at $a_p=0.6$ mm, $f=0.093$ mm/rev & $V_c=75$ m/min (a) dry (b) wet & (c) cryogenic condition

From the analysis, it is observed that cryogenic machining gives better performance. This is because of the high pressure of LN₂ impinging the cutting zone, which leads to reduced temperature and also less adhesion of chip residuals, side flow of material is minimum in cryogenic machining, due to action LN₂. Whereas in dry machining, obtained chips are unfavorable than at different machining environments due to high cutting temperatures. Among all the machining environments cryogenic exhibits better performance, resulting in superior cooling effect, easy extraction of chips from workpiece material and avoid jamming of chips while machining. In addition, cryogenic machining involves no chip cleaning cost, no health hazards and easy disposal of chips.

4.3.9 Tool wear analysis

Tool wear describes the gradual failure of cutting tools due to regular operation. There are mainly two types of wear occurred during machining a) Flank wear b) Crater wear. Flank wear occurs on the flank face of the single point cutting tool. During cutting, the portion of the tool in contact with the machined workpiece erodes. Crater wear occurs on the rake face of the tool, which is in contact with chips, this erodes the rake face. Flank wear was identified, during the turning process of EN47 spring steel with coated cutting tool insert during dry, wet and cryogenic condition. In dry machining, no coolant was supplied at the machining zone and in wet machining, emulsion type cutting fluid was used and which was obtained by mixing the water with soluble oil in 1:20 ratio. In cryogenic machining liquid nitrogen (LN₂) are used conduct the experiments (Coelho et al. 2007; Davoodi and Eskandari 2015).

Experiments are conducted based on L₂₇ FFD optimization technique. The desirability approach is used to obtained optimum cutting condition for multi output responses and these conditions are considered for tool wear analysis. In such cases machining time was varied from 5 min to 20 min, at 5 min interval, using a new cutting edge for tool wear analysis for every experiment. Tool wear at different cutting conditions was measured by confocal microscope. Figure 4.38 to Figure 4.40 shows the tool wear at varying machining time for dry, wet and cryogenic conditions. The different machining times considered are 5, 10, 15 & 20min. Tool wear are found for dry condition are 95.42, 177.33, 297.57 & 310.63 μm respectively; for wet condition 61.23, 70.67,

115.76 & 144.72 μm respectively; for cryogenic condition 44.57, 52.72, 61.23 & 73.33 μm respectively.

Tool wear is minimum in cryogenic machining at all machining times this is due to less tool tip temperature, and less distortion of cutting edge during turning process. From the experimental work it is observed that the flank wear reduction in cryogenic machining was 53.29% and 27.21%, respectively compared to dry and wet condition at low cutting time. Similarly, at higher cutting time tool wear reduction in cryogenic machining was 76.40% and 49.32%, respectively compared to dry and wet condition. Overall, relationship between tool wear and machining time is shown in Figure 4.41. From the analysis it was observed that cryogenic machining is highly influencing the tool wear. This is due to efficient penetration of liquid nitrogen between tool and workpiece material resulting in reduced friction and reduced temperature.

Formation of microgrooves, notch wear and adhesive wear were observed from the confocal images as shown in Figure 4.38 during dry machining. Similarly, Figure 4.39 shows that, built of edge, edge chipping and abrasive marks forms during wet machining are observed. Figure 4.40 at cryogenic machining only abrasion wear is occurred, because of spraying of liquid nitrogen at cutting zone which reduces the sticking of workpiece to the cutting edge, resulting the absence of built up edge (BUE), microgrooves and notch wear, which leads an improved tool life. The major wear mechanism observed in cryogenic machining was abrasion wear. Control of abrasion and adhesion wear is done by spraying of liquid nitrogen (LN_2). It provides lower friction and reduced tool tip temperature. While in wet machining, abrasion wear, adhesive wear and built up edge are formed. In dry machining microgrooves, edge chipping and notch wear are found during machining.

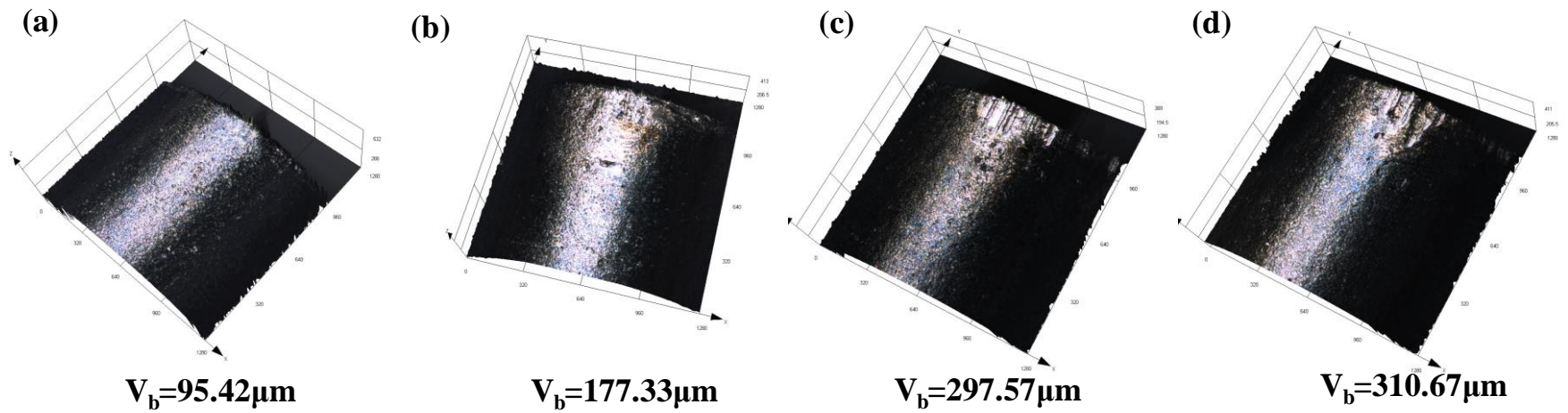
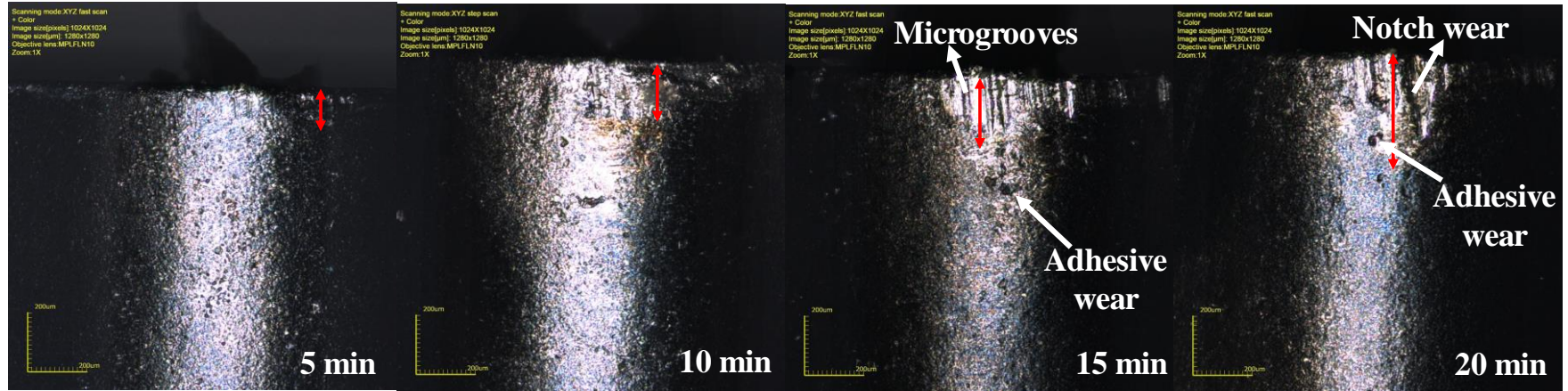


Figure 4.38 Tool wear analysis during dry condition

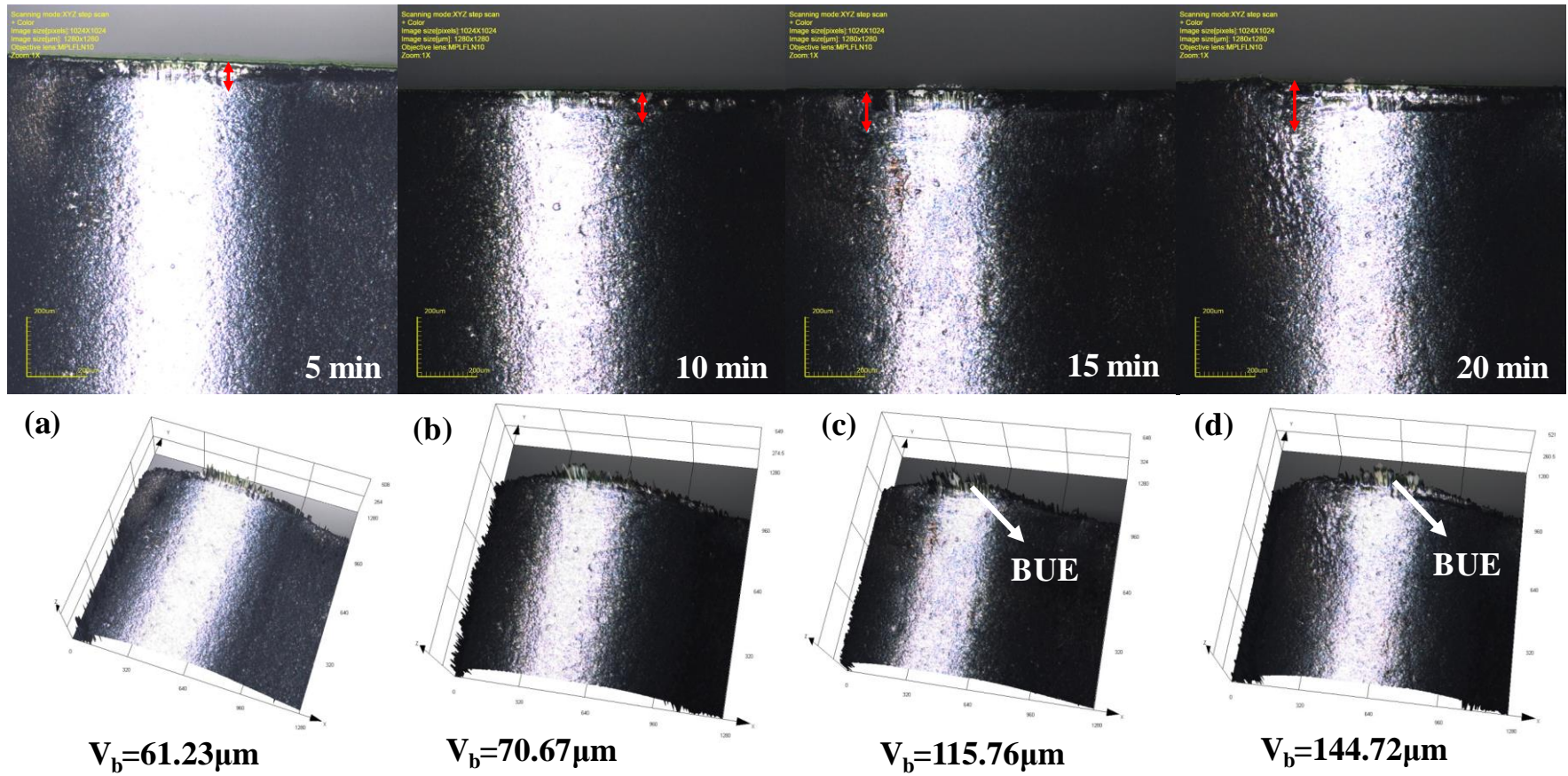


Figure 4.39 Tool wear analysis during wet condition

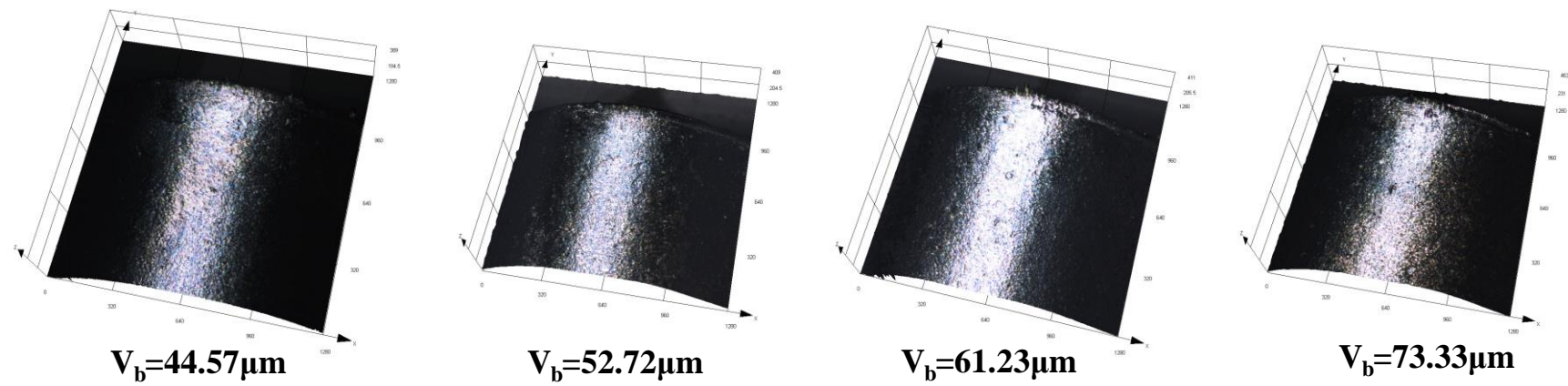
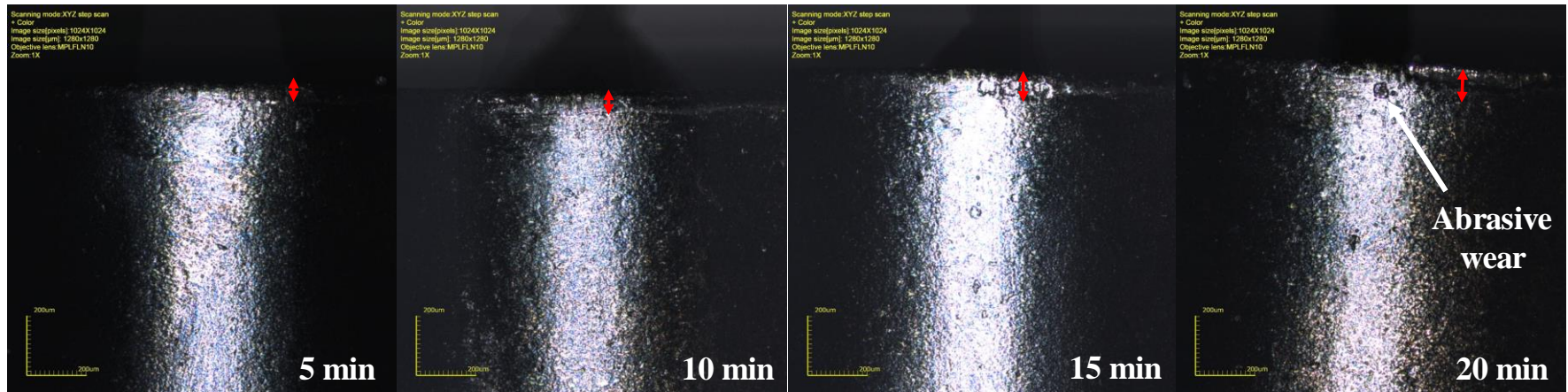


Figure 4.40 Tool wear analysis during cryogenic condition

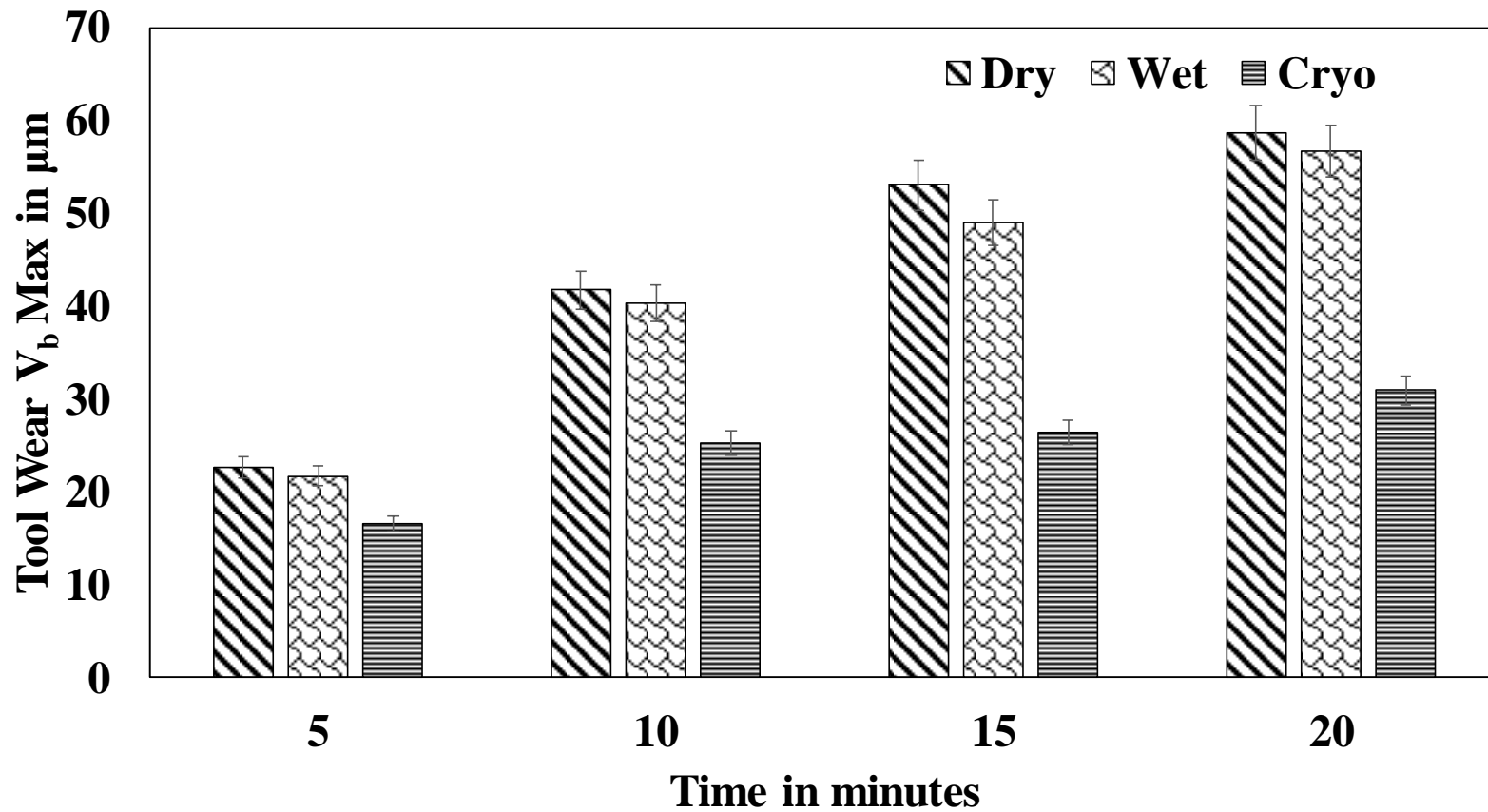


Figure 4.41 Variation of tool wear with machining time for different conditions of machining

4.4 Multi objective optimization using DA and PSO technique

(a) Desirability approach (DA)

Desirability approach was proposed by Harrington and popularized by Derringer and Suich. DA is an optimization technique, widely used in industry, to optimize two or more responses. Desirability function optimization has been employed for all the responses in the machining study. During optimization process it is required to find out the optimal values of cutting parameters, to minimize the values of cutting force, surface roughness and tool tip temperature, under different cutting environments such as dry, wet and cryogenic. Optimization of multi objective responses was done by desirability approach.

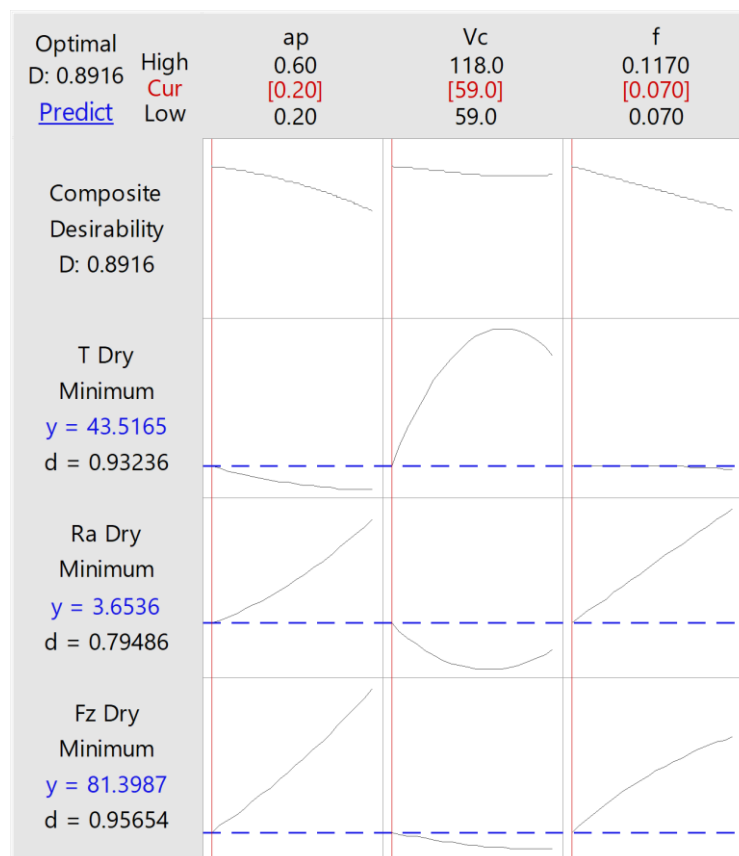


Figure 4.42 Desirability plot for cutting force, surface roughness and tool tip temperature during dry condition

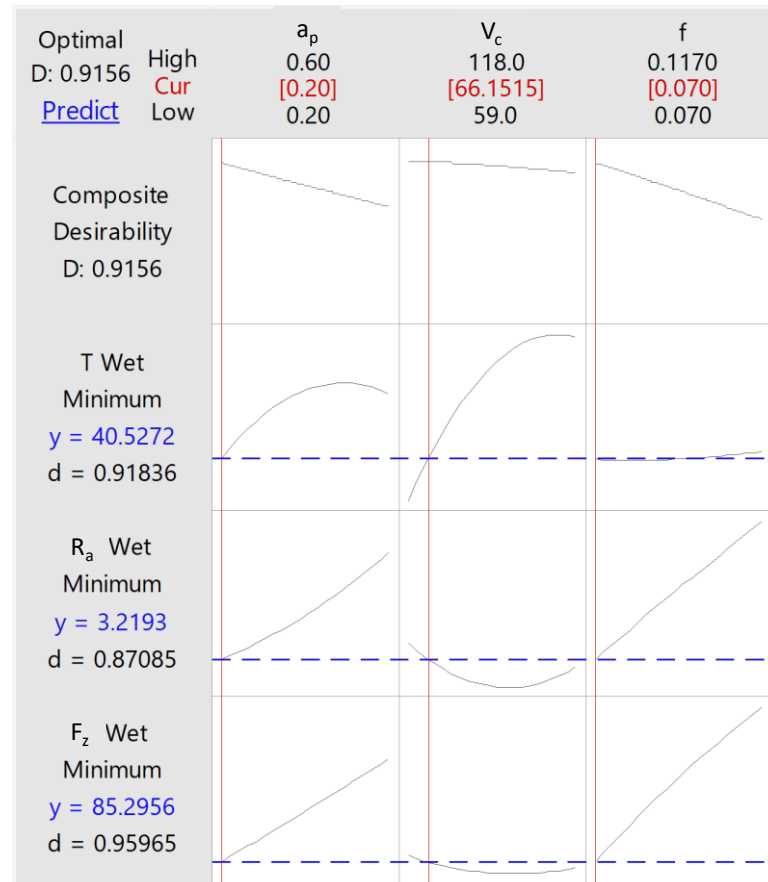


Figure 4.43 Desirability plot for cutting force, surface roughness and tool tip temperature during wet condition

Figure 4.42 to Figure 4.44 shows the desirability plot for cutting force, surface roughness and tool tip temperature with various cutting environment namely dry, wet and cryogenic conditions. From DA technique, optimum conditions of combined output responses as well as optimum value for each output response is obtained and is shown in Table 4.21.

Table 4.21 Optimum conditions by desirability approach

| | V_c | f | a_p | F_z | R_a | T | Desirability Value |
|------|---------|------|-------|---------|--------|---------|--------------------|
| Dry | 59 | 0.07 | 0.2 | 81.3987 | 3.6536 | 43.5165 | 0.8916 |
| Wet | 66.1515 | 0.07 | 0.2 | 85.2956 | 3.2193 | 40.5272 | 0.9156 |
| Cryo | 69.7273 | 0.07 | 0.2 | 70.178 | 1.9801 | 35.2923 | 0.9005 |

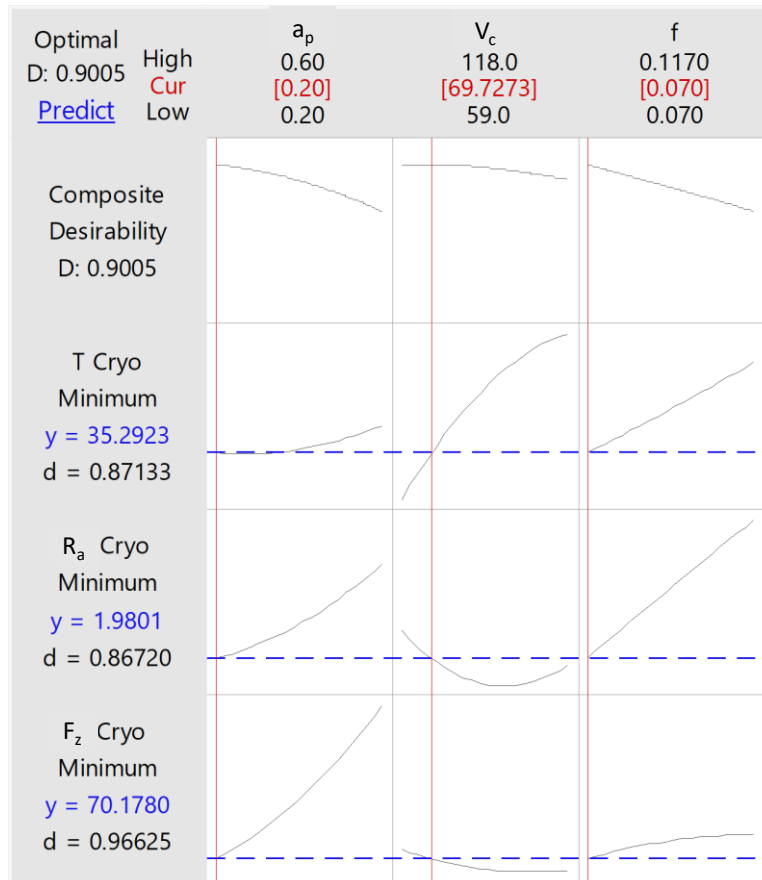


Figure 4.44 Desirability plot for cutting force, surface roughness and tool tip temperature during cryogenic condition

(b) Multi objective particle swarm optimization (MOPSO)

Particle swarm optimization (PSO) technique is used to obtaining a multi objective response. In the present work, multi objective optimization is imposed on the cutting parameters (speed, feed and depth of cut) to optimize output parameters (cutting force, surface roughness and tool tip temperature). Particle swarm optimization uses MATLAB codes for minimizing the output responses. Experiments are planned, based on design of experiments (DOE) a full factorial design (FFD) orthogonal array (OA) are employed. The parameters of MOPSO are represented in Table 4.22 and the working conditions for the MOPSO model are illustrated in Figure 4.45.

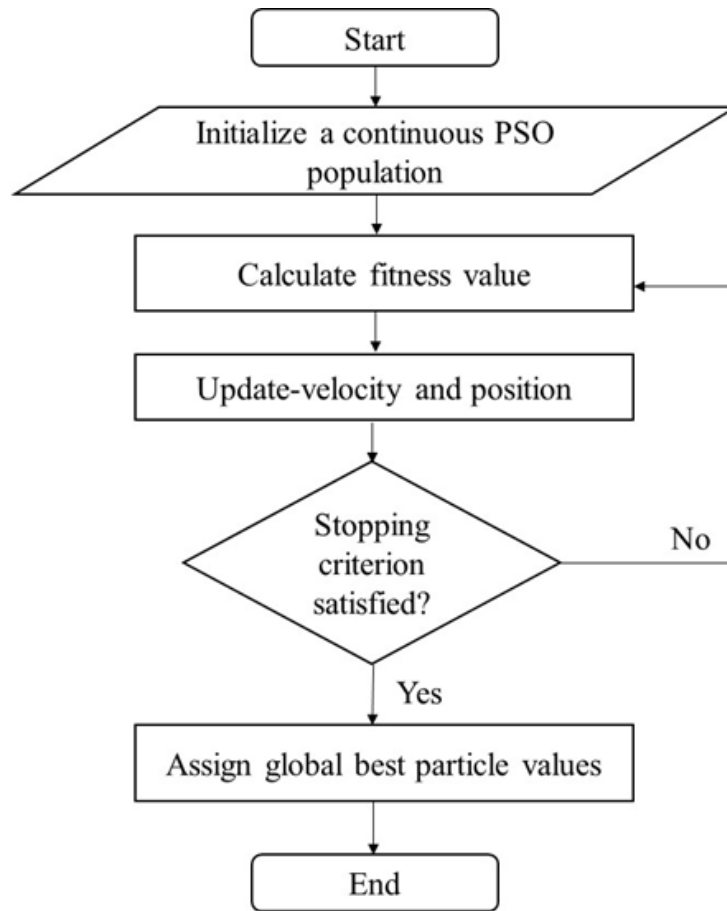


Figure 4.45 Principle of the particle swarm optimization

Table 4.22 Parameters of MOPSO

| | |
|--------------------------------|-----------------|
| Number of parameters (m) | 3 |
| Number of iterations (i) | 1000 |
| Number of particles (n) | 100 |
| Lower bounds of variables (LB) | [59 0.070 0.2] |
| Upper bounds of variables (UB) | [118 0.117 0.4] |

2nd order regression equations are developed form statistical technique, and the same regression equations are used for PSO and corresponding PSO codes are developed from MATLAB software for minimization problem. Optimized cutting conditions and corresponding values of output response under dry, wet and cryogenic condition are depicted in Table 4.23. Multi objective optimization of optimal values are observed from convergence plots as shown in Figure 4.46 (a-c) under different cutting environments.

Table 4.23 Optimum condition by PSO technique

| | V_c | f | a_p | F_z | R_a | T | Optimum Value |
|------|---------|------|-------|---------|--------|---------|---------------|
| Dry | 118 | 0.07 | 0.2 | 66.1189 | 3.4241 | 59.6338 | 63.4500 |
| Wet | 81.0368 | 0.07 | 0.2 | 82.0368 | 3.0477 | 47.2132 | 70.9801 |
| Cryo | 103.651 | 0.07 | 0.2 | 65.2688 | 1.7990 | 37.1093 | 56.9649 |

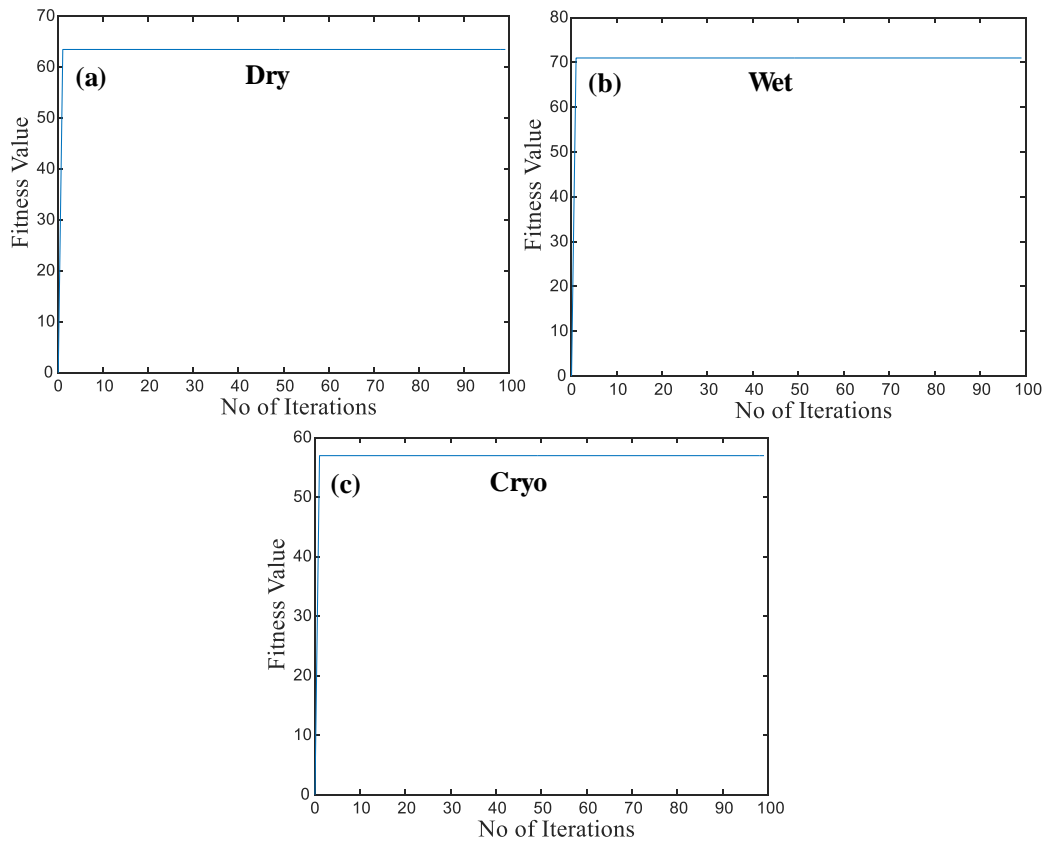


Figure 4.46 MOPSO Convergence graph

4.5 Artificial Neural Networks (ANNs)

ANN is an information handling and demonstrating strategy that emerged in quest for scientific displaying of the learning procedure, which was motivated by the human brain. ANN is particularly helpful in grouping and capacity guess issues, more often when not decided, for example, neural processing, requires various neurons, to be associated together into a neural system. Neurons are arranged in the form of layers. Every neuron inside the system is typically a straightforward preparing unit, which takes at least, one source of info and produces a yield. At every neuron, each info has a related weight, which changes the quantity. The neuron essentially includes each one of the sources of information and computes an output yield to be passed on.

In the present work, ANN is developed using MATLAB software with neural network tool box, the most suitable activation function, and the best training algorithm. Figure 4.47 represents three input parameters such as cutting speed, feed rate, depth of cut and ten hidden layer and one output layer are present in the network. Table 4.24 depicts ANN training parameters.

Table 4.24 ANN training parameters

| ANN Training parameters | |
|----------------------------|-------------------------------|
| Network Type | Feed forward back propagation |
| Training function | TRAINLM |
| Adoption learning function | LEARNGDM |
| Performance function | MSE |
| Number of layers | 2 |
| Number of neurons | 10 |
| Transfer function | LOGSIG |
| Epochs | 1000 |
| Max fail | 600 |

Figure 4.48 to Figure 4.56 shows the regression plot for tangential cutting force, surface roughness and tool tip temperature during dry, wet and cryogenic condition respectively. Feed forward back propagation method was used to train the network, in order to reduce the Mean square error (MSE) between experimental value and predicted

results. By adjusting the synaptic weight connections, the error is reduced. The R^2 -value of the training, testing and validating data should be near to 1 or 100% then trained model are adequate. From the ANN model, predicted values are obtained, and these predicted values are compared with regression model and experimental value.

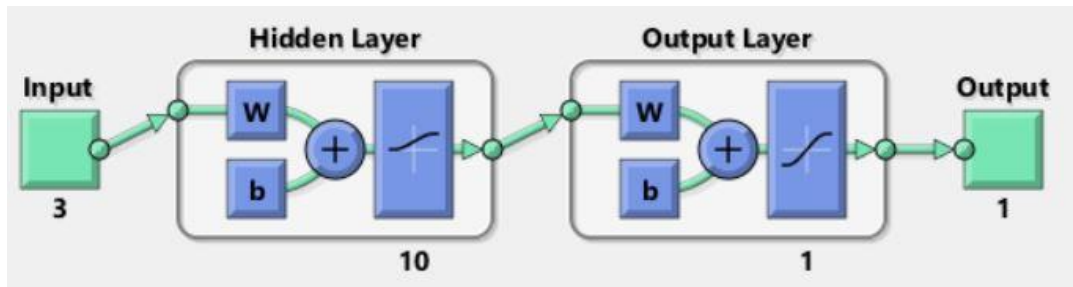


Figure 4.47 Artificial Neural Network

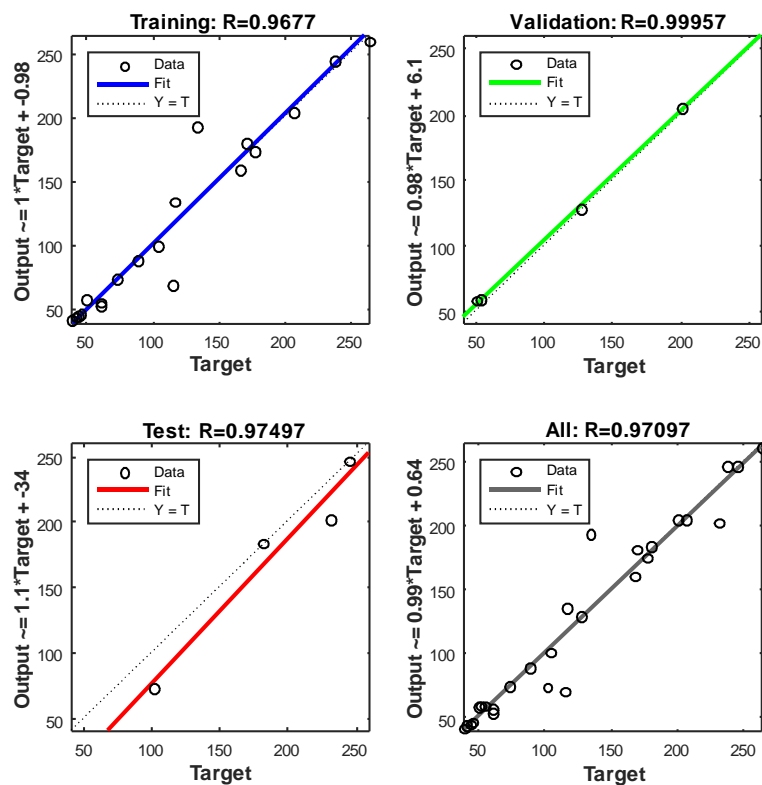


Figure 4.48 ANN Regression plots for cutting force during dry condition

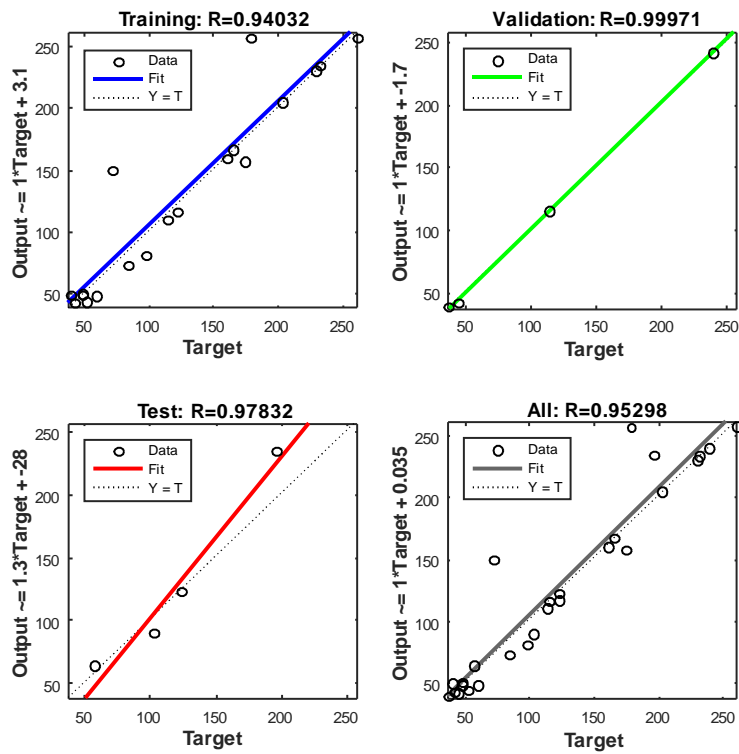


Figure 4.49 ANN Regression plots for cutting force during wet condition

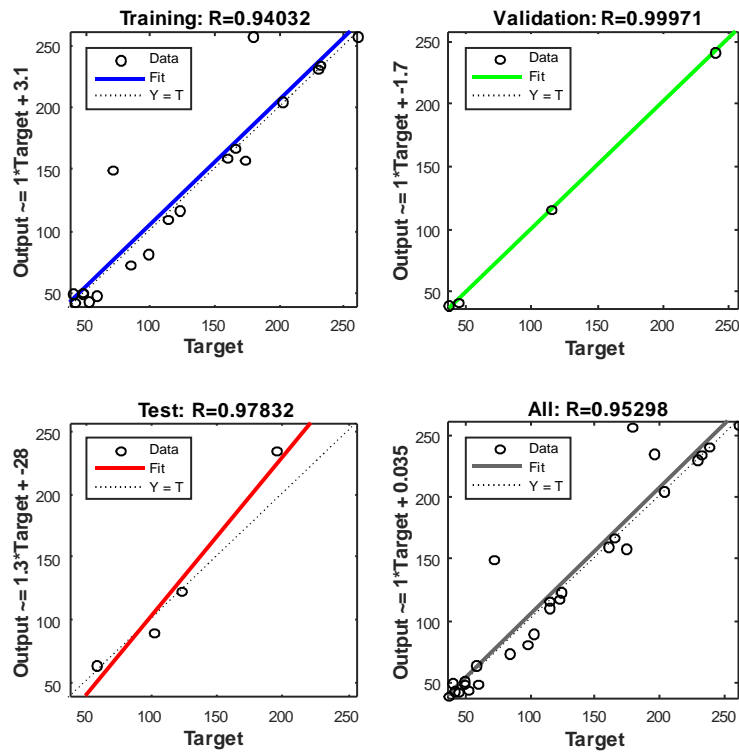


Figure 4.50 ANN Regression plots for cutting force during cryogenic condition

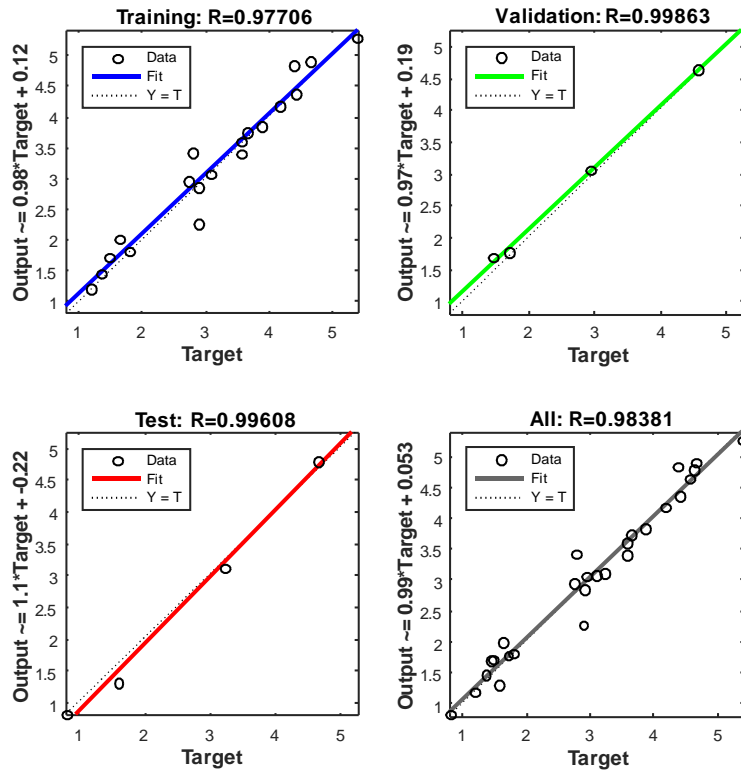


Figure 4.51 ANN Regression plots for surface roughness during dry condition

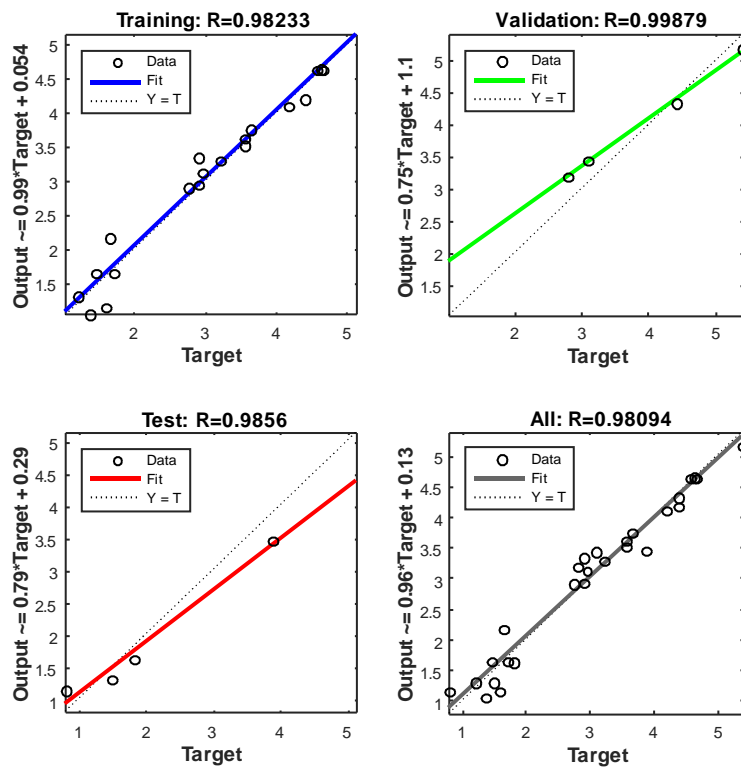


Figure 4.52 ANN Regression plots for surface roughness during wet condition

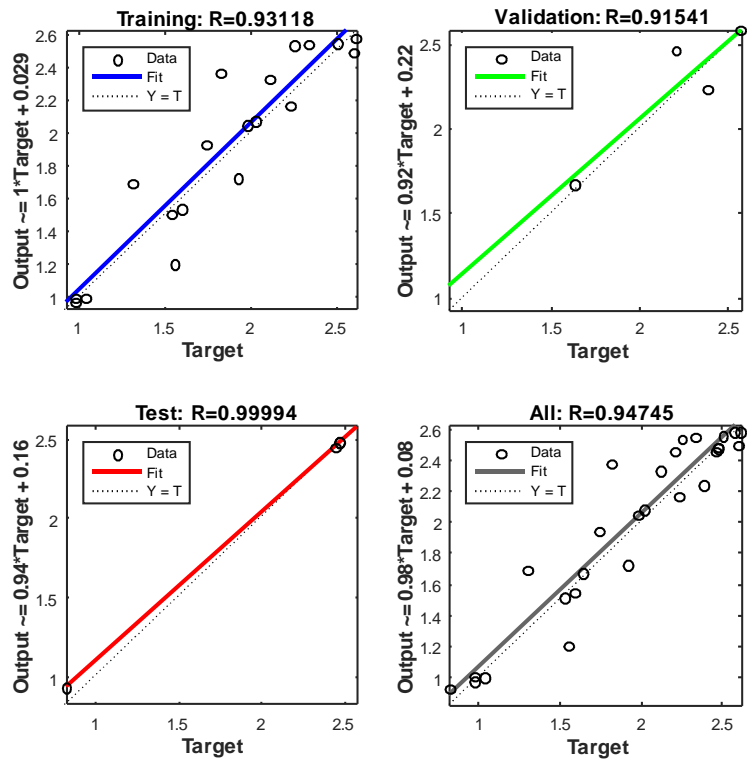


Figure 4.53 ANN Regression plots for surface roughness during cryogenic condition

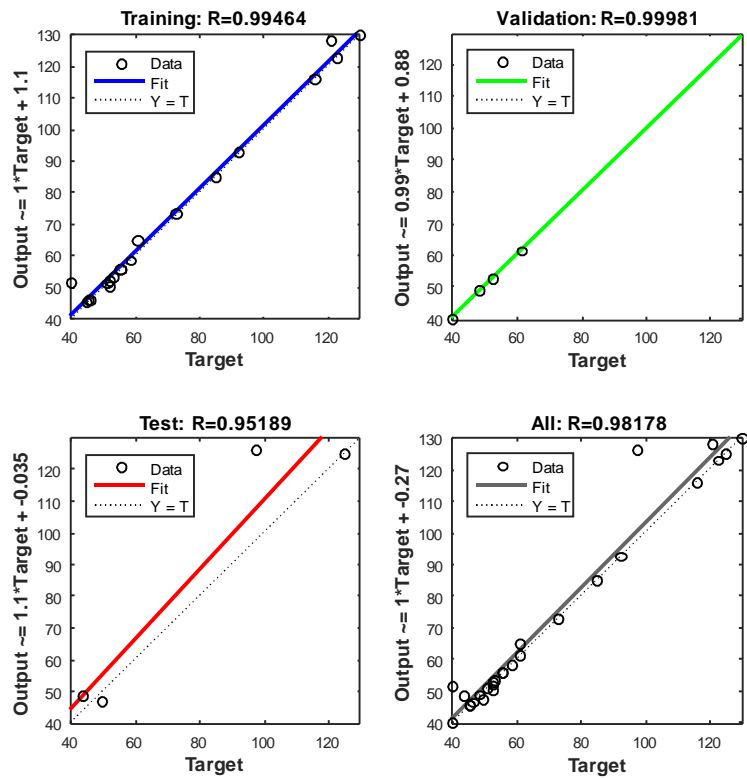


Figure 4.54 ANN Regression plots for tool tip temperature during dry condition

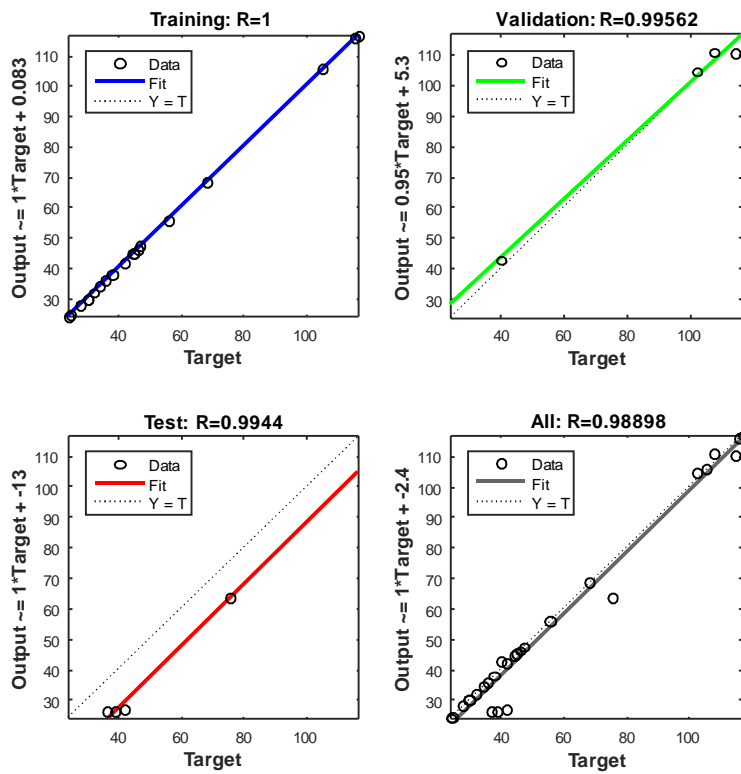


Figure 4.55 ANN Regression plots for tool tip temperature during wet condition

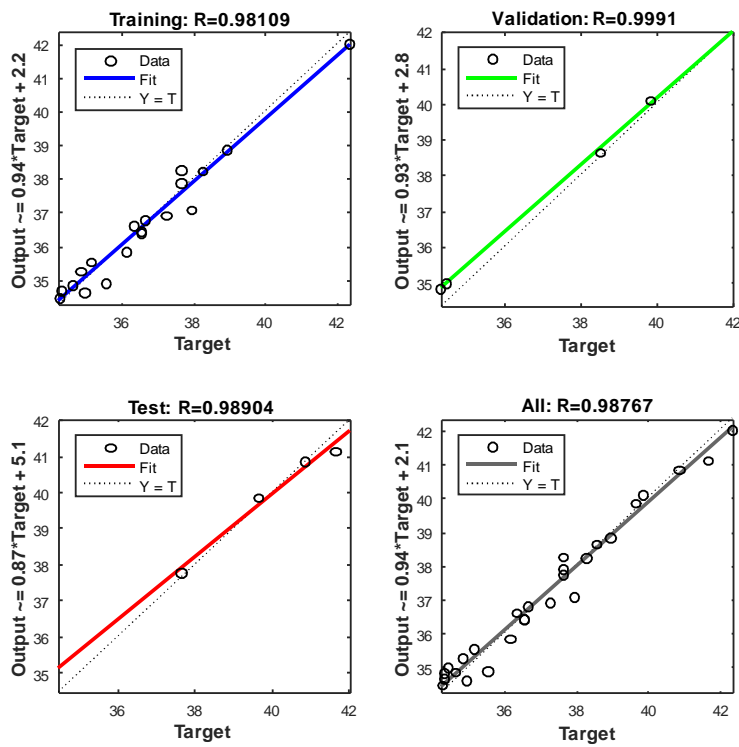


Figure 4.56 ANN Regression plots for tool tip temperature during cryogenic condition

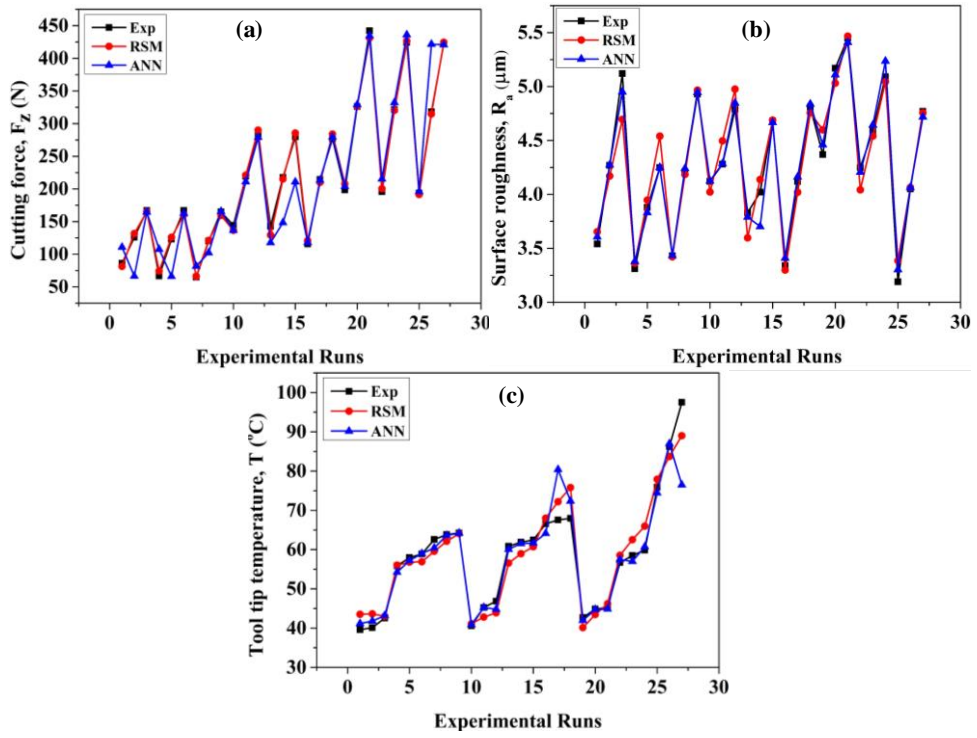


Figure 4.57 (a-c) Experimental versus predicted values for cutting force, surface roughness and tool tip temperature during dry condition

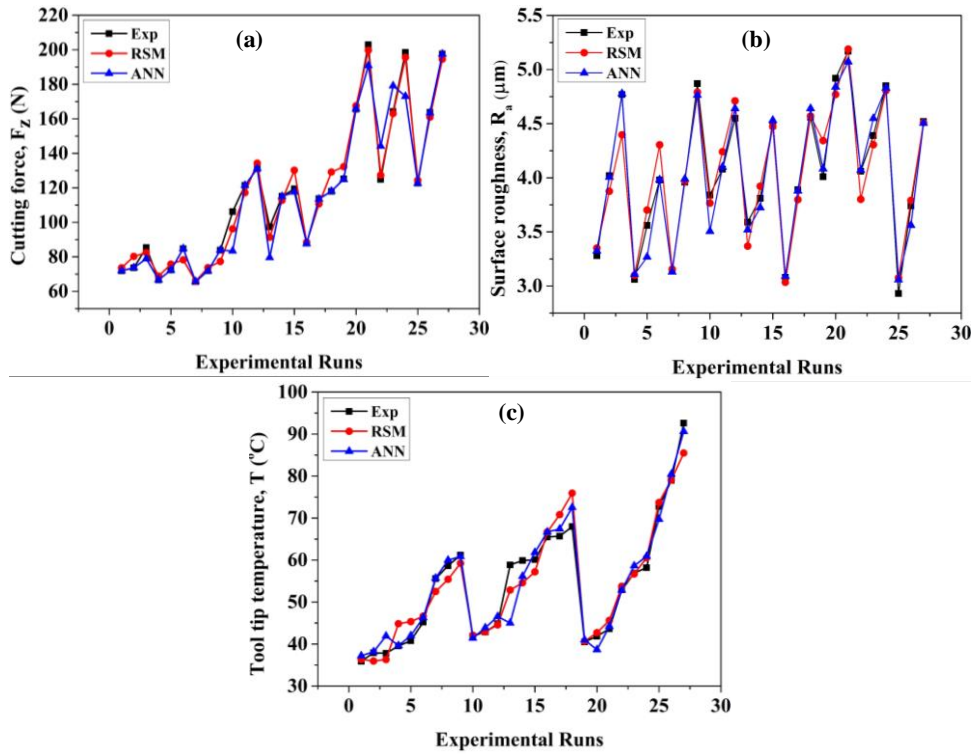


Figure 4.58 (a-c) Experimental versus predicted for cutting force, surface roughness and tool tip temperature during wet condition

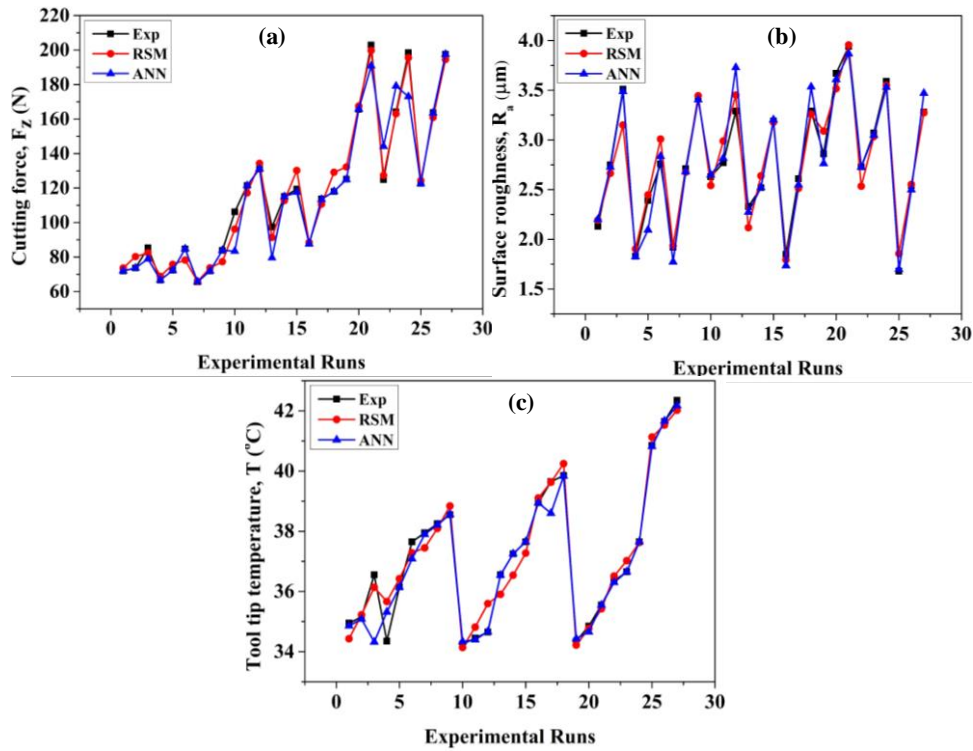


Figure 4.59 (a-c) Experimental versus predicted for cutting force, surface roughness and tool tip temperature during cryogenic condition

Figure 4.57 to Figure 4.59 shows the experimental and predicted values of ANN and RSM of cutting force, surface roughness and tool tip temperature, at dry, wet and cryogenic condition. From the graphs, it is noticed that trained and predicted results are in good agreement with the experimental data.

4.6 Validation

In order to validate the model, nine new cutting conditions are select randomly which are available on the lathe machine but does not belongs to previous cutting conditions. Regression model and ANN models are arranged with new cutting conditions as shown in Table 4.25. Error percentage was ANN trained network and RSM models was calculated by equation 4.11.

$$\% Error = \left| \frac{y_e - y_p}{y_e} \right| \times 100 \quad 4.11$$

Where y_e is the experimental value and y_p is the predicted value

Table 4.25 New cutting condition for validation

| SI No | a_p | V_c | f |
|-------|-------|-------|-------|
| 1 | 0.3 | 59 | 0.078 |
| 2 | 0.3 | 75 | 0.087 |
| 3 | 0.3 | 118 | 0.100 |
| 4 | 0.5 | 59 | 0.087 |
| 5 | 0.5 | 75 | 0.100 |
| 6 | 0.5 | 118 | 0.078 |
| 7 | 0.6 | 59 | 0.100 |
| 8 | 0.6 | 75 | 0.078 |
| 9 | 0.6 | 118 | 0.087 |

Table 4.26 to Table 4.31 shows the percentage errors are comparing experimental values with RSM model and ANN trained network, during different cutting environments such as dry, wet and cryogenic respectively. From the analysis it is observed that % error is not exceeding 10% while comparing experimental values with RSM and ANN model.

Table 4.26 Error percentage of output response during experimental vs RSM under dry condition

| SI No | F _z Dry | | | R _a Dry | | | T Dry | | |
|-------|--------------------|--------|---------|--------------------|------|---------|-------|-------|---------|
| | Exp | RSM | % Error | Exp | RSM | % Error | Exp | RSM | % Error |
| 1 | 136.89 | 132.46 | 3.23 | 3.77 | 3.99 | 5.71 | 43.89 | 42.52 | 3.11 |
| 2 | 148.45 | 152.42 | 2.67 | 3.73 | 3.87 | 3.77 | 62.59 | 57.35 | 8.37 |
| 3 | 194.52 | 181.92 | 6.48 | 4.32 | 4.30 | 0.49 | 71.82 | 67.87 | 5.51 |
| 4 | 255.85 | 246.99 | 3.46 | 4.56 | 4.62 | 1.33 | 45.26 | 42.37 | 6.39 |
| 5 | 310.19 | 293.62 | 5.34 | 4.39 | 4.47 | 1.79 | 56.89 | 61.40 | 7.92 |
| 6 | 181.96 | 193.09 | 6.12 | 3.42 | 3.56 | 4.10 | 68.48 | 74.60 | 8.93 |
| 7 | 375.15 | 359.05 | 4.29 | 5.20 | 5.16 | 0.77 | 42.84 | 44.34 | 3.50 |
| 8 | 232.49 | 244.19 | 5.03 | 4.29 | 4.22 | 1.70 | 65.42 | 60.01 | 8.27 |
| 9 | 291.75 | 284.37 | 2.53 | 3.72 | 3.89 | 4.51 | 75.59 | 82.26 | 8.83 |

Table 4.27 Error percentage of output response during experimental vs ANN under dry condition

| SI No | F _z Dry | | | R _a Dry | | | T Dry | | |
|-------|--------------------|--------|---------|--------------------|------|---------|-------|-------|---------|
| | Exp | ANN | % Error | Exp | ANN | % Error | Exp | ANN | % Error |
| 1 | 136.89 | 138.82 | 1.41 | 3.77 | 3.71 | 1.47 | 43.89 | 40.92 | 6.77 |
| 2 | 148.45 | 140.29 | 5.50 | 3.73 | 3.55 | 4.80 | 62.59 | 60.28 | 3.69 |
| 3 | 194.52 | 188.32 | 3.19 | 4.32 | 4.40 | 1.90 | 71.82 | 72.89 | 1.49 |
| 4 | 255.85 | 272.23 | 6.40 | 4.56 | 4.62 | 1.32 | 45.26 | 47.43 | 4.80 |
| 5 | 310.19 | 304.74 | 1.76 | 4.39 | 4.11 | 6.37 | 56.89 | 51.24 | 9.94 |
| 6 | 181.96 | 188.29 | 3.48 | 3.42 | 3.57 | 4.37 | 68.48 | 72.51 | 5.88 |
| 7 | 375.15 | 368.29 | 1.83 | 5.20 | 5.24 | 0.81 | 42.84 | 40.56 | 5.31 |
| 8 | 232.49 | 238.96 | 2.78 | 4.29 | 4.35 | 1.34 | 65.42 | 68.29 | 4.39 |
| 9 | 291.75 | 299.63 | 2.70 | 3.72 | 3.79 | 1.92 | 75.59 | 79.58 | 5.28 |

Table 4.28 Error percentage of output response during experimental vs RSM under wet condition

| Sl No | F _z Wet | | | R _a Wet | | | T Wet | | |
|-------|--------------------|--------|---------|--------------------|------|---------|-------|-------|---------|
| | Exp | RSM | % Error | Exp | RSM | % Error | Exp | RSM | % Error |
| 1 | 102.59 | 109.84 | 7.07 | 3.58 | 3.71 | 3.74 | 39.56 | 40.10 | 1.38 |
| 2 | 109.56 | 118.50 | 8.16 | 3.36 | 3.64 | 8.41 | 46.59 | 50.49 | 8.37 |
| 3 | 144.59 | 132.51 | 8.35 | 4.11 | 4.10 | 0.30 | 60.28 | 65.23 | 8.22 |
| 4 | 148.56 | 151.31 | 1.85 | 4.37 | 4.37 | 0.01 | 45.45 | 43.26 | 4.83 |
| 5 | 185.74 | 170.75 | 8.07 | 4.31 | 4.25 | 1.41 | 60.16 | 57.38 | 4.62 |
| 6 | 115.69 | 125.76 | 8.71 | 3.39 | 3.29 | 2.83 | 73.59 | 72.66 | 1.26 |
| 7 | 193.47 | 194.42 | 0.49 | 4.93 | 4.89 | 0.72 | 40.84 | 43.48 | 6.46 |
| 8 | 135.59 | 138.89 | 2.44 | 4.13 | 3.98 | 3.65 | 53.18 | 54.67 | 2.80 |
| 9 | 145.89 | 156.40 | 7.21 | 3.38 | 3.61 | 6.69 | 78.54 | 77.61 | 1.18 |

Table 4.29 Error percentage of output response during experimental vs ANN under wet condition

| Sl No | F _z Wet | | | R _a Wet | | | T Wet | | |
|-------|--------------------|--------|---------|--------------------|------|---------|-------|-------|---------|
| | Exp | ANN | % Error | Exp | ANN | % Error | Exp | ANN | % Error |
| 1 | 102.59 | 105.69 | 3.02 | 3.58 | 3.41 | 4.65 | 39.56 | 37.24 | 5.85 |
| 2 | 109.56 | 114.56 | 4.56 | 3.36 | 3.23 | 3.76 | 46.59 | 43.05 | 7.59 |
| 3 | 144.59 | 148.69 | 2.84 | 4.11 | 4.22 | 2.67 | 60.28 | 62.36 | 3.45 |
| 4 | 148.56 | 150.62 | 1.38 | 4.37 | 4.39 | 0.54 | 45.45 | 48.49 | 6.70 |
| 5 | 185.74 | 185.29 | 0.24 | 4.31 | 4.39 | 1.79 | 60.16 | 60.21 | 0.08 |
| 6 | 115.69 | 117.51 | 1.57 | 3.39 | 3.13 | 7.64 | 73.59 | 75.52 | 2.62 |
| 7 | 193.47 | 192.69 | 0.40 | 4.93 | 4.95 | 0.33 | 40.84 | 38.80 | 4.99 |
| 8 | 135.59 | 133.54 | 1.51 | 4.13 | 4.28 | 3.69 | 53.18 | 54.54 | 2.57 |
| 9 | 145.89 | 144.72 | 0.80 | 3.38 | 3.24 | 3.99 | 78.54 | 79.49 | 1.21 |

Table 4.30 Error percentage of output response during experimental vs RSM under cryogenic condition

| Sl No | F _z Cryogenic | | | R _a Cryogenic | | | T Cryogenic | | |
|-------|--------------------------|--------|---------|--------------------------|------|---------|-------------|-------|---------|
| | Exp | RSM | % Error | Exp | RSM | % Error | Exp | RSM | % Error |
| 1 | 85.56 | 88.54 | 3.49 | 2.63 | 2.50 | 4.86 | 34.55 | 34.49 | 0.18 |
| 2 | 87.45 | 89.27 | 2.09 | 2.25 | 2.38 | 5.73 | 36.98 | 36.25 | 1.98 |
| 3 | 92.58 | 94.23 | 1.78 | 2.91 | 2.79 | 4.11 | 38.83 | 39.01 | 0.46 |
| 4 | 130.36 | 133.78 | 2.62 | 2.98 | 3.11 | 4.49 | 34.5 | 34.58 | 0.23 |
| 5 | 148.57 | 143.98 | 3.09 | 3.01 | 2.97 | 1.47 | 36.95 | 36.92 | 0.08 |
| 6 | 113.49 | 115.41 | 1.70 | 2.15 | 2.05 | 4.84 | 41.56 | 40.22 | 3.21 |
| 7 | 182.49 | 177.44 | 2.77 | 3.56 | 3.64 | 2.38 | 34.85 | 34.95 | 0.30 |
| 8 | 147.75 | 140.29 | 5.05 | 2.77 | 2.71 | 2.22 | 36.88 | 36.68 | 0.54 |
| 9 | 142.51 | 151.84 | 6.55 | 2.25 | 2.37 | 5.36 | 40.76 | 41.42 | 1.62 |

Table 4.31 Error percentage of output response during experimental vs ANN under cryogenic condition

| Sl No | F _z Cryogenic | | | R _a Cryogenic | | | T Cryogenic | | |
|-------|--------------------------|--------|---------|--------------------------|------|---------|-------------|-------|---------|
| | Exp | ANN | % Error | Exp | ANN | % Error | Exp | ANN | % Error |
| 1 | 85.56 | 80.95 | 5.39 | 2.63 | 2.71 | 2.91 | 34.55 | 34.69 | 0.39 |
| 2 | 87.45 | 86.22 | 1.41 | 2.25 | 2.19 | 2.86 | 36.98 | 37.21 | 0.63 |
| 3 | 92.58 | 90.53 | 2.22 | 2.91 | 3.10 | 6.36 | 38.83 | 38.52 | 0.80 |
| 4 | 130.36 | 127.99 | 1.82 | 2.98 | 2.90 | 2.82 | 34.5 | 34.49 | 0.02 |
| 5 | 148.57 | 150.64 | -1.39 | 3.01 | 3.10 | 3.08 | 36.95 | 37.98 | 2.79 |
| 6 | 113.49 | 111.34 | 1.90 | 2.15 | 2.20 | 2.33 | 41.56 | 39.10 | 5.93 |
| 7 | 182.49 | 188.33 | -3.20 | 3.56 | 3.74 | 4.94 | 34.85 | 34.81 | 0.12 |
| 8 | 147.75 | 152.83 | -3.44 | 2.77 | 2.83 | 2.23 | 36.88 | 36.92 | 0.11 |
| 9 | 142.51 | 138.49 | 2.82 | 2.25 | 2.04 | 9.51 | 40.76 | 40.71 | 0.13 |

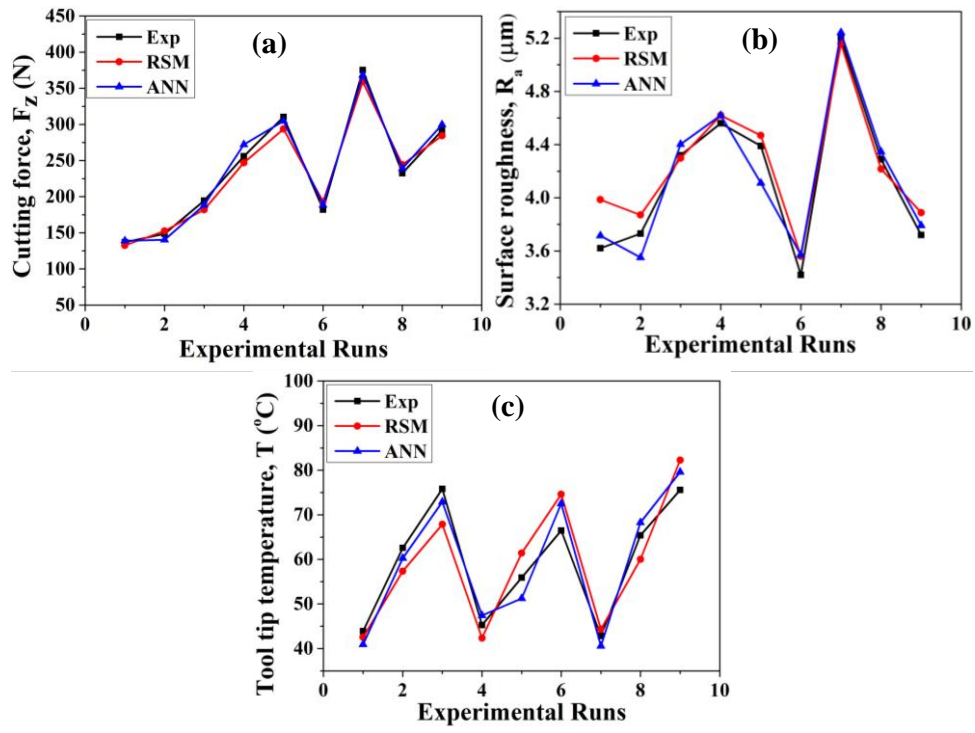


Figure 4.60 (a-c) Validation for cutting force, surface roughness and tool tip temperature during dry condition

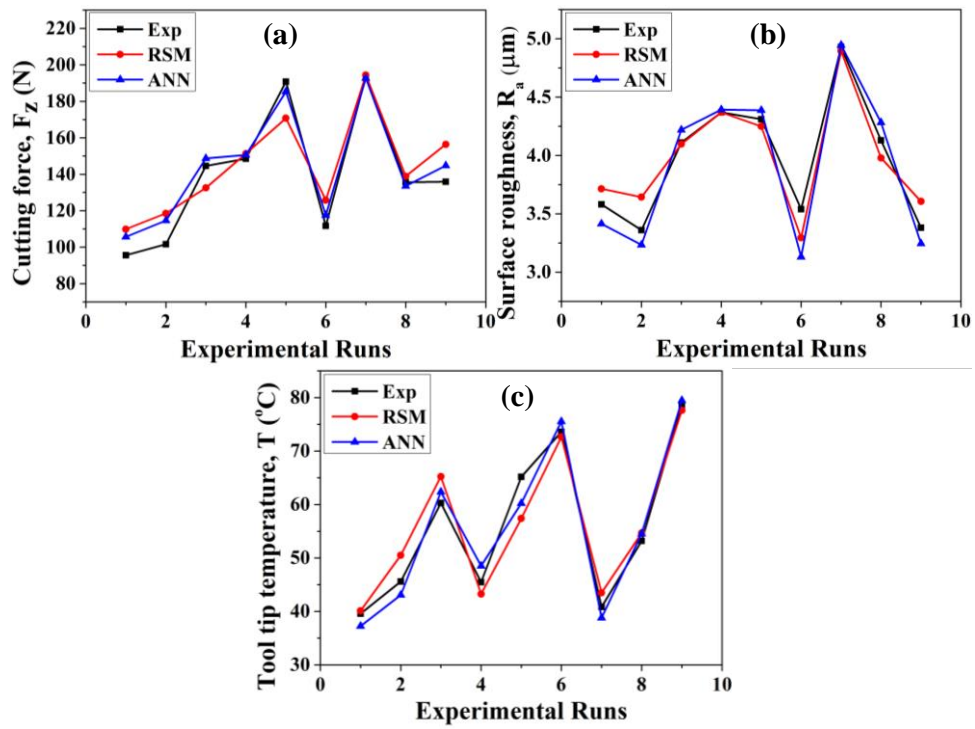


Figure 4.61 (a-c) Validation for cutting force, surface roughness and tool tip temperature during wet condition

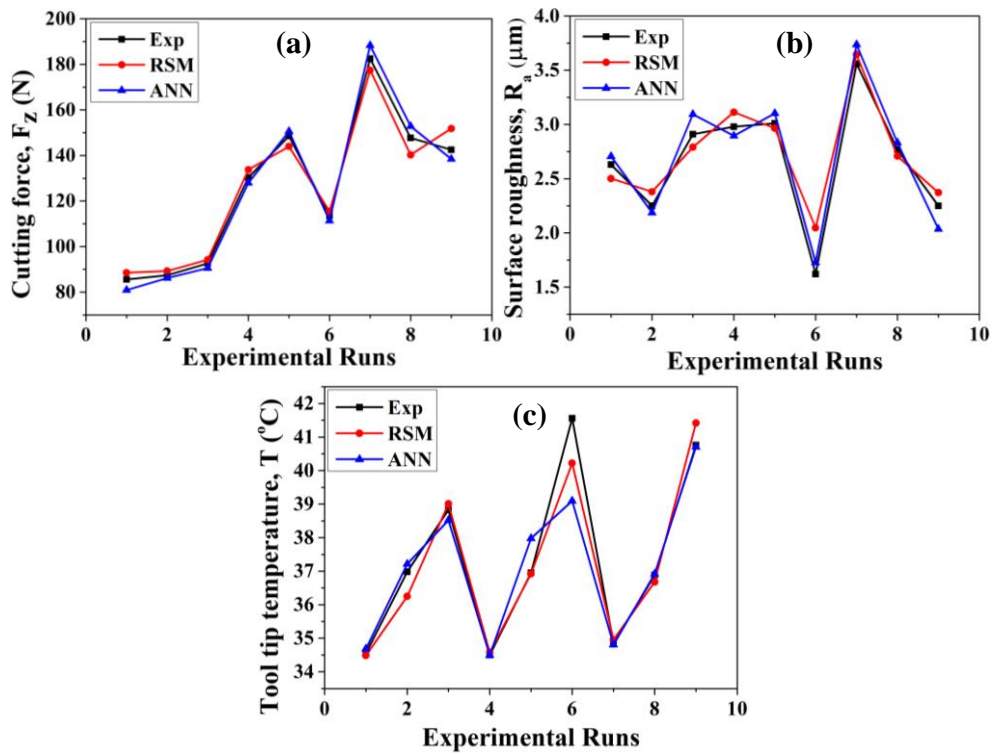


Figure 4.62 (a-c) Validation for cutting force, surface roughness and tool tip temperature during cryogenic condition.

From Figure 4.60 to Figure 4.62, it is observed that validations have been performed with various cutting conditions. From validations, it is observed that developed regression model and ANN trained network are well in agreement with experimental results.

CHAPTER 5

5 CONCLUSIONS

- The present work are to machine EN47 spring steel on a lathe machine using tungsten carbide cutting tool insert of different nose radii 0.4, 0.8 and 1.2mm using various optimization techniques.
- One factor at a time approach (OFAT) was used to identify machinability factor on EN47 spring steel. Result revealed that, in all the cases, tool insert with 0.8mm nose radius exhibits nominal performance.
- Optimization technique was employed to know the machinability characteristics of EN47 spring steel with coated tungsten carbide tool insert of 0.8mm nose radius at different cutting environment such as dry, wet and liquid nitrogen and obtaining the optimum cutting conditions for cutting forces (F_z), the surface roughness (R_a), tool tip temperature (T). Chip morphology, surface integrity with varying cutting speed and feed rate. Tool wear analysis was done with different cutting environment. Obtained results are correlated with Particle Swarm Optimization (PSO) and Artificial Neural Network (ANN). From the above discussion of results the following conclusions are written:
 - From the ANOVA results, cutting force (F_z) was influenced by the depth of cut (a_p) and feed rate (f), surface roughness was influenced by feed rate and cutting speed and tool tip temperature was influenced by cutting speed and depth of cut for all cutting environments.
 - From the main effect plots, it is observed that individual factor like cutting force (F_z), surface roughness (R_a) and tool tip temperature (T) are influenced by depth of cut and feed rate, feed rate and cutting speed, cutting speed and depth of cut respectively, and it was confirmed with ANOVA table.
 - From the experimental analysis, 2nd order regression model has been developed, by investigating using residual analysis, where all residual points closely fall on the straight line, as it confirmed by normal probability plots.

- From the response surface plot, interaction effect of most significant factor is observed.
 - For cutting force (F_z), depth of cut and feed rate are influencing factor.
 - For surface roughness (R_a), feed rate and cutting speed are influencing factor.
 - For tool tip temperature (T), cutting speed and depth of cut are influencing factor.
- From the Regression analysis, it was observed that the predicted values are much closer to the actual values.
- Analysis of machined surface and chip morphology indicate the effect of varying feed rate and cutting speed.
 - Surface roughness, at higher cutting speed during cryogenic machining, was improved by 36.82% and 33.16% as compared to dry and wet machining respectively.
 - Surface roughness, at lower cutting speed during cryogenic machining, was improved by 35.28% and 32.10% as compared to dry and wet machining respectively.
 - Surface roughness, at lower feed rate during cryogenic machining, was improved by 39.16% and 35.10% as compared to dry and wet machining respectively.
 - Surface roughness, at higher feed rate during cryogenic machining, was improved by 31.84% and 28.79% as compared to dry and wet machining respectively.
- Machined surface analysis, showed the appearance of surface defects such as feed marks, pits, adhered micro particle, adhered chip particle side flows and saw tooth of chips. These defects are predominant in dry condition and very less in cryogenic machining.

- Machined surface topography was done by different cutting environment to identify the surface waviness of machined surface. From the analysis, it is observed that cryogenic machining gives the best surface finish.
- In the tool wear analysis have been to identify the failure of cutting-edge features, such as micro grooving, notch wear, adhesive, and abrasive wear and built up edge are observed in dry condition while wet and cryogenic condition tool wear was minimum.
- Multi-objective optimization was done by composite Desirability Approach (DA) and Particle Swarm Optimization (PSO) and are compared with each other, for all conditions. Desirable value of (89.16, 91.56 and 90.05) and (63.45, 70.98 and 56.96) under dry, wet and cryogenic condition with respect to DA and PSO. These values are approaching each other, which proves the adequacy of the developed model.
- Artificial Neural Network is used to improve determination of coefficient (R^2) for the output performances such as cutting force, surface roughness and tool tip temperature.

SCOPE OF FUTURE WORK

Machinability studies of EN47 spring steel have been performed under different cutting environments like dry, wet and cryogenic condition. Still, there is a scope for future work on machinability studies of spring steel they are follows.

- Machinability studies along with cutting tool vibration analysis.
- Detailed study of chip morphology.
- Detailed study of tool wear mechanisms during machining.

REFERENCES

- Abbas, A. T., Hamza, K., Aly, M. F., and Al-bahkali, E. A. (2016). "Multiobjective optimization of turning cutting parameters for j-steel material." *Advances in Materials Science and Engineering*.
- Aruna, M., and Dhanalaksmi, V. (2012). "Design Optimization of Cutting Parameters when Turning Inconel 718 with Cermet Inserts." *World Academy of Science, Engineering and Technology*, 61, 952–955.
- Azizi, M. W., Belhadi, S., Yallese, M. A., Mabrouki, T., and Rigal, J. F. (2012). "Surface roughness and cutting forces modeling for optimization of machining condition in finish hard turning of AISI 52100 steel." *Journal of Mechanical Science and Technology*, 26(12), 4105–4114.
- Bensouilah, H., Aouici, H., Meddour, I., Yallese, M. A., Mabrouki, T., and Girardin, F. (2016). "Performance of coated and uncoated mixed ceramic tools in hard turning process." *Measurement*, Elsevier Ltd, 82, 1–18.
- Bharathi Raja, S., and Baskar, N. (2011). "Particle swarm optimization technique for determining optimal machining parameters of different work piece materials in turning operation." *International Journal of Advanced Manufacturing Technology*, 54(5–8), 445–463.
- Bordin, A., Sartori, S., Bruschi, S., and Ghiotti, A. (2017). "Experimental investigation on the feasibility of dry and cryogenic machining as sustainable strategies when turning Ti6Al4V produced by Additive Manufacturing." *Journal of Cleaner Production*, Elsevier Ltd, 142, 4142–4151.
- Chabbi, Amel, Yallese, M. A., Meddour, I., Nouioua, M., Mabrouki, T., and Girardin, F. (2017). "Predictive modeling and multi-response optimization of technological parameters in turning of Polyoxymethylene polymer (POM C) using RSM and desirability function." *Measurement: Journal of the International Measurement Confederation*, Elsevier Ltd, 95, 99–115.
- Chabbi, A., Yallese, M. A., Nouioua, M., Meddour, I., Mabrouki, T., and Girardin, F. (2017). "Modeling and optimization of turning process parameters during the cutting of polymer (POM C) based on RSM, ANN, and DF methods." *International Journal of Advanced Manufacturing Technology*, The International Journal of Advanced Manufacturing Technology, 91(5–8), 2267–2290.

- Chen, T., Li, S., Han, B., and Liu, G. (2014). "Study on cutting force and surface microtopography of hard turning of GCr15 steel." *International Journal of Advanced Manufacturing Technology*, 72(9–12), 1639–1645.
- Chinchanikar, S., and Choudhury, S. K. (2013). "Effect of work material hardness and cutting parameters on performance of coated carbide tool when turning hardened steel: An optimization approach." *Measurement: Journal of the International Measurement Confederation*, 46(4), 1572–1584.
- Chou, Y. K., and Song, H. (2004a). "Tool nose radius effects on finish hard turning." *Journal of Materials Processing Technology*, 148(2), 259–268.
- Chou, Y. K., and Song, H. (2004b). "Tool nose radius effects on finish hard turning." *Journal of Materials Processing Technology*, 148(2), 259–268.
- Choudhuri, K., Goyal, S., and Chakraborti, P. (2014). "Optimization of Multi-Objective Problem By Taguchi Approach and Utility Concept When Turning Aluminium 6061." (August), 14–20.
- Ciurana, J., Arias, G., and Ozel, T. (2009). "Neural network modeling and particle swarm optimization (PSO) of process parameters in pulsed laser micromachining of hardened AISI H13 steel." *Materials and Manufacturing Processes*, 24(3), 358–368.
- Coelho, R. T., Ng, E. G., and Elbestawi, M. A. (2007). "Tool wear when turning hardened AISI 4340 with coated PCBN tools using finishing cutting conditions." *International Journal of Machine Tools and Manufacture*, 47(2), 263–272.
- Cuthbert, D. (1959). *Use of Half-Normal Plots in Interpreting Factorial Two-level Experiments. Technometrics*, Technometrics.
- Das, S. R., Dhupal, D., and Kumar, A. (2015). "Experimental investigation into machinability of hardened AISI 4140 steel using TiN coated ceramic tool." *Measurement: Journal of the International Measurement Confederation*, Elsevier Ltd, 62, 108–126.
- Davim, J. P., Gaitonde, V. N., and Karnik, S. R. (2008). "Investigations into the effect of cutting conditions on surface roughness in turning of free machining steel by ANN models." *Journal of Materials Processing Technology*, 205(1–3), 16–23.
- Davoodi, B., and Eskandari, B. (2015). "Tool wear mechanisms and multi-response optimization of tool life and volume of material removed in turning of N-155 iron-nickel-base superalloy using RSM." *Measurement: Journal of the International Measurement Confederation*, Elsevier Ltd, 68, 286–294.

- Elbah, M., Yallese, M. A., Aouici, H., Mabrouki, T., and Rigal, J. F. (2013). "Comparative assessment of wiper and conventional ceramic tools on surface roughness in hard turning AISI 4140 steel." *Measurement: Journal of the International Measurement Confederation*, Elsevier Ltd, 46(9), 3041–3056.
- Evans, C., and Bryan, J. B. (1991). "Cryogenic Diamond Turning of Stainless Steel." *CIRP Annals - Manufacturing Technology*, 40(1), 571–575.
- Gaitonde, V. N., and Karnik, S. R. (2012). "Minimizing burr size in drilling using artificial neural network (ANN)-particle swarm optimization (PSO) approach." *Journal of Intelligent Manufacturing*, 23(5), 1783–1793.
- Gaitonde, V. N., Karnik, S. R., Figueira, L., and Paulo Davim, J. (2009). "Machinability investigations in hard turning of AISI D2 cold work tool steel with conventional and wiper ceramic inserts." *International Journal of Refractory Metals and Hard Materials*, Elsevier Ltd, 27(4), 754–763.
- Gosai, M., and Bhavsar, S. N. (2016). "Experimental Study on Temperature Measurement in Turning Operation of Hardened Steel (EN36)." *Procedia Technology*, Elsevier B.V., 23, 311–318.
- Gupta, M., and Kumar, S. (2015). "Investigation of surface roughness and MRR for turning of UD-GFRP using PCA and Taguchi method." *Engineering Science and Technology, an International Journal*, Elsevier Ltd, 18(1), 70–81.
- El Hakim, M. A., Shalaby, M. A., Veldhuis, S. C., and Dosbaeva, G. K. (2015). "Effect of secondary hardening on cutting forces, cutting temperature, and tool wear in hard turning of high alloy tool steels." *Measurement: Journal of the International Measurement Confederation*, Elsevier Ltd, 65, 233–238.
- Hanafi, I., Cabrera, F. M., Dimane, F., and Manzanares, J. T. (2016). "Application of Particle Swarm Optimization for Optimizing the Process Parameters in Turning of PEEK CF30 Composites." *Procedia Technology*, Elsevier B.V., 22(October 2015), 195–202.
- Hanief, M., Wani, M. F., and Charoo, M. S. (2017). "Modeling and prediction of cutting forces during the turning of red brass (C23000) using ANN and regression analysis." *Engineering Science and Technology, an International Journal*, Karabuk University, 20(3), 1220–1226.

- Hong, S., and Ding, Y. (2001). "Cooling Approach and Cutting Temperature in Cryogenic Machining of Ti-6 Al-4V." *International journal of machine tool and manufacture*, 41, 1417–1437.
- Hua, Y., and Liu, Z. (2018). "Effects of cutting parameters and tool nose radius on surface roughness and work hardening during dry turning Inconel 718." *The International Journal of Advanced Manufacturing Technology*.
- Jadhav, J. S., and Jadhav, B. R. (2014). "Experimental study of Effect of Cutting Parameters on Cutting Force in Turning Process." *International Journal of Innovative Research in Advanced Engineering*, 1(6), 240–248.
- Jawaid, A., Che-Haron, C. H., and Abdullah, A. (1999). "Tool wear characteristics in turning of titanium alloy Ti-6246." *Journal of Materials Processing Technology*, 92–93, 329–334.
- Jewlikar, A. D., Joshi, V. V., and Borse, S. (2015). "HPT Process Parameter Optimization in Dry Turning of Bohler K110 Steel." *Materials Today: Proceedings*, Elsevier Ltd., 2(4–5), 2414–2422.
- Kaladhar, M., Subbaiah, K. V., Srinivasa Rao, C., and Narayana Rao, K. (2011). "Application of Taguchi approach and utility concept in solving the multi-objective problem when turning AISI 202 austenitic stainless steel." *Journal of Engineering Science and Technology Review*, 4(1), 55–61.
- Kamble, P. D., Waghmare, A. C., Askhedkar, R. D., and Sahare, S. B. (2015). "Multi Objective Optimization of Turning AISI 4340 Steel Considering Spindle Vibration Using Taguchi- Fuzzy Inference System." *Materials Today: Proceedings*, Elsevier Ltd., 2(4–5), 3318–3326.
- Kant, G., and Sangwan, K. S. (2015). "Predictive modelling and optimization of machining parameters to minimize surface roughness using artificial neural network coupled with genetic algorithm." *Procedia CIRP*, Elsevier B.V., 31, 453–458.
- Kaynak, Y. (2014). "Evaluation of machining performance in cryogenic machining of Inconel 718 and comparison with dry and MQL machining." *International Journal of Advanced Manufacturing Technology*, 72(5–8), 919–933.
- Kishore, D. S. C., Rao, K. P., and Mahamani, A. (2014). "Effects of PCD and Uncoated Tungsten Carbide Inserts in Turning of In-situ Al6061-TiC Metal Matrix Composite." *Procedia Materials Science*, 5, 1574–1583.

- Kosaraju, S., and Chandraker, S. (2015). "Taguchi analysis on cutting force and surface roughness in turning MDN350 steel." *Materials Today: Proceedings*, Elsevier Ltd., 2(4–5), 3388–3393.
- Kumar, R., and Chauhan, S. (2015). "Study on surface roughness measurement for turning of Al 7075/10/SiCp and Al 7075 hybrid composites by using response surface methodology (RSM) and artificial neural networking (ANN)." *Measurement: Journal of the International Measurement Confederation*, Elsevier Ltd, 65, 166–180.
- Lalbondre, R., Krishna, P., and Mohankumar, G. C. (2013). "Machinability studies of low alloy steels by face turning method: An experimental investigation." *Procedia Engineering*, Elsevier B.V., 64, 632–641.
- Mahamani, A. (2014). "Influence of Process Parameters on Cutting Force and Surface Roughness During Turning of AA2219-TiB₂/ZrB₂ In-situ Metal Matrix Composites." *Procedia Materials Science*, Elsevier B.V., 6(Icmpc), 1178–1186.
- Malghan, R. L., Rao, K. M. C., Shettigar, A. K., Rao, S. S., and D'Souza, R. J. (2016). "Application of particle swarm optimization and response surface methodology for machining parameters optimization of aluminium matrix composites in milling operation." *Journal of the Brazilian Society of Mechanical Sciences and Engineering*, Springer Berlin Heidelberg.
- Meddour, I., Yallese, M. A., Bensouilah, H., Khellaf, A., and Elbah, M. (2018). "Prediction of surface roughness and cutting forces using RSM, ANN, and NSGA-II in finish turning of AISI 4140 hardened steel with mixed ceramic tool." *International Journal of Advanced Manufacturing Technology*, The International Journal of Advanced Manufacturing Technology, 1–19.
- Mia, M., and Dhar, N. R. (2016). "Response surface and neural network based predictive models of cutting temperature in hard turning." *Journal of Advanced Research*, Cairo University, 7(6), 1035–1044.
- Mohanty, C. P., Mahapatra, S. S., and Singh, M. R. (2016). "A particle swarm approach for multi-objective optimization of electrical discharge machining process." *Journal of Intelligent Manufacturing*, Springer US, 27(6), 1171–1190.
- Montgomery, D. C. (2012). *Design and Analysis of Experiments. Design*.
- Muthukrishnan, N., and Davim, J. P. (2009). "Optimization of machining parameters of Al/SiC-MMC with ANOVA and ANN analysis." *Journal of Materials Processing Technology*, 209(1), 225–232.

- Nikam, K. G., and Kadam, S. S. (2016). "Influence of insert geometry and cutting parameters on surface roughness of 080M40 Steel in turning process." 4(4), 1–6.
- Nithyanandam, J., LalDas, S., and Palanikumar, K. (2014). "Surface Roughness Analysis in Turning of Titanium Alloy by Nanocoated Carbide Insert." *Procedia Materials Science*, 5, 2159–2168.
- Okokpujie, I. P., Ohunakin, O. S., Bolu, C. A., and Okokpujie, K. O. (2018). "Data in Brief Experimental data-set for prediction of tool wear during turning of Al-1061 alloy by high speed steel cutting tools." *Data in Brief*, Elsevier Inc., 18, 1–8.
- Palanisamy, D., Senthil, P., and Senthilkumar, V. (2016). "The effect of aging on machinability of 15Cr-5Ni precipitation hardened stainless steel." *Archives of Civil and Mechanical Engineering*, Politechnika Wrocławska, 16(1), 53–63.
- Parida, A. K., and Maity, K. (2017). "Effect of nose radius on forces, and process parameters in hot machining of Inconel 718 using finite element analysis." *Engineering Science and Technology, an International Journal*, Karabuk University, 20(2), 687–693.
- Pawade, R. S., Joshi, S. S., Brahmanekar, P. K., and Rahman, M. (2007). "An investigation of cutting forces and surface damage in high-speed turning of Inconel 718." *Journal of Materials Processing Technology*, 192–193, 139–146.
- Pugazhenthil, A., Kanagaraj, I. D. G., and Raja, J. D. (2018). "Predicting the effect of machining parameters on turning characteristics of AA7075 / TiB₂ in situ aluminum matrix composites using empirical relationships." 2.
- Richelsen, A. B. (1994). "Materials Processing Technology." 45, 149–154.
- Sahu, S., and Choudhury, B. B. (2015). "Optimization of Surface Roughness Using Taguchi Methodology & Prediction of Tool Wear in Hard Turning Tools." *Materials Today: Proceedings*, Elsevier Ltd., 2(4–5), 2615–2623.
- Satyanarayana, B., Janardhana, G. R., and Rao, D. H. (2013). "Optimized high speed turning on Inconel 718 using Taguchi method based Grey relational analysis." 20(August), 269–275.
- Sayeed Ahmed, G. M., Quadri, S. S. H., and Mohiuddin, M. S. (2015). "Optimization of Feed and Radial Force in Turning Process by using Taguchi Design Approach." *Materials Today: Proceedings*, Elsevier Ltd., 2(4–5), 3277–3285.

- Sharman, A. R. C., Hughes, J. I., and Ridgway, K. (2015). "The effect of tool nose radius on surface integrity and residual stresses when turning Inconel 718" *Journal of Materials Processing Technology*, Elsevier B.V., 216, 123–132.
- Shihab, S. K., Khan, Z. A., Mohammad, A., and Siddiqueed, A. N. (2014). "RSM based Study of Cutting Temperature During Hard Turning with Multilayer Coated Carbide Insert." *Procedia Materials Science*, Elsevier B.V., 6(ICMPC), 1233–1242.
- Siddesh Kumar, N. G., Shiva Shankar, G. S., Basavarajappa, S., and Suresh, R. (2017). "Some studies on mechanical and machining characteristics of Al2219/n-B 4 C/MoS 2 nano-hybrid metal matrix composites." *Measurement*, Elsevier Ltd, 107, 1–11.
- Sivaiah, P., and Chakradhar, D. (2017a). "Machinability studies on 17-4 PH stainless steel under cryogenic cooling environment." *Materials and Manufacturing Processes*, 6914(June), 1–14.
- Sivaiah, P., and Chakradhar, D. (2017b). "Comparative evaluations of machining performance during turning of 17-4 PH stainless steel under cryogenic and wet machining conditions." *Machining Science and Technology*, Taylor & Francis, 0344, 1–16.
- Sivaiah, P., and Chakradhar, D. (2018a). "Effect of cryogenic coolant on turning performance characteristics during machining of 17-4 PH stainless steel: A comparison with MQL, wet, dry machining." *CIRP Journal of Manufacturing Science and Technology*, CIRP, 21, 86–96.
- Sivaiah, P., and Chakradhar, D. (2018b). "Analysis and Modeling of Cryogenic Turning Operation Using Response Surface Methodology." *Silicon*, 10(6), 2751–2768.
- SreeramaReddy, T. V., Sornakumar, T., VenkataramaReddy, M., and Venkatram, R. (2009). "Machinability of C45 steel with deep cryogenic treated tungsten carbide cutting tool inserts." *International Journal of Refractory Metals and Hard Materials*, Elsevier Ltd, 27(1), 181–185.
- Suresh, R., Basavarajappa, S., Gaitonde, V. N., and Samuel, G. L. (2012). "Machinability investigations on hardened AISI 4340 steel using coated carbide insert." *International Journal of Refractory Metals and Hard Materials*, Elsevier Ltd, 33, 75–86.
- Umbrello, D., Ambrogio, G., Filice, L., and Shivpuri, R. (2007). "An ANN approach for predicting subsurface residual stresses and the desired cutting conditions during

hard turning.” *Journal of Materials Processing Technology*, 189(1–3), 143–152.

Venugopal, K. A., Paul, S., and Chattopadhyay, A. B. (2007). “Tool wear in cryogenic turning of Ti-6Al-4V alloy.” *Cryogenics*, 47(1), 12–18.

APPENDIX

Table 5.1 ANOVA for tangential cutting force (F_z) during dry condition

| F _z Dry | Sum of Squares | DoF | Mean Square | F-Value | P-value | % Cont |
|--------------------|----------------|-----|-------------|---------|----------|--------|
| Model | 2.9970E+05 | 9 | 33295.68 | 626.06 | < 0.0001 | |
| A-f | 1.09E+05 | 1 | 1.09E+05 | 2056.06 | < 0.0001 | 36.36 |
| B-V _c | 544.38 | 1 | 544.38 | 10.24 | 0.0053 | 0.18 |
| C-a _p | 1.67E+05 | 1 | 1.67E+05 | 3140.11 | < 0.0001 | 55.56 |
| AB | 74.3 | 1 | 74.3 | 1.4 | 0.2535 | 0.02 |
| AC | 14706.96 | 1 | 14706.96 | 276.53 | < 0.0001 | 4.89 |
| BC | 0.79 | 1 | 0.79 | 0.015 | 0.9044 | 0.00 |
| A ² | 528.15 | 1 | 528.15 | 9.93 | 0.0058 | 0.18 |
| B ² | 45.31 | 1 | 45.31 | 0.85 | 0.3689 | 0.02 |
| C ² | 382.19 | 1 | 382.19 | 7.19 | 0.0158 | 0.13 |
| Residual | 904.11 | 17 | 53.18 | | | 0.30 |
| Cor | | | | | | |
| Total | 3.01E+05 | 26 | | | | 100 |

Table 5.2 ANOVA for tangential cutting force (F_z) during wet condition

| F_z Wet | Sum of Squares | DoF | Mean Square | F-Value | P-value | % Cont |
|-----------|----------------|-----|-------------|---------|----------|--------|
| Model | 4.5645E+04 | 9 | 5071.65 | 59.89 | < 0.0001 | |
| A-f | 2.55E+04 | 1 | 2.55E+04 | 301.18 | < 0.0001 | 54.17 |
| B- V_c | 415.16 | 1 | 415.16 | 4.9 | 0.0408 | 0.88 |
| C- a_p | 1.61E+04 | 1 | 1.61E+04 | 189.67 | < 0.0001 | 34.11 |
| AB | 72.7 | 1 | 72.7 | 0.86 | 0.3671 | 0.15 |
| AC | 1751.15 | 1 | 1751.15 | 20.68 | 0.0003 | 3.72 |
| BC | 1.03 | 1 | 1.03 | 0.012 | 0.9134 | 0.00 |
| A^2 | 40.18 | 1 | 40.18 | 0.47 | 0.5002 | 0.09 |
| B^2 | 62.77 | 1 | 62.77 | 0.74 | 0.4013 | 0.13 |
| C^2 | 0.95 | 1 | 0.95 | 0.011 | 0.9171 | 0.00 |
| Residual | 1439.61 | 17 | 84.68 | | | 3.06 |
| Cor | | | | | | |
| Total | 4.71E+04 | 26 | | | | 100 |

Table 5.3 ANOVA for tangential cutting force (F_z) during cryogenic condition

| F_z Cryo | Sum of Squares | DoF | Mean Square | F-Value | P-value | % Cont |
|------------|----------------|-----|-------------|---------|----------|--------|
| Model | 4.4625E+04 | 9 | 4958.28 | 123.82 | < 0.0001 | |
| A-f | 6.78E+03 | 1 | 6.78E+03 | 169.28 | < 0.0001 | 14.96 |
| B- V_c | 190.39 | 1 | 190.39 | 4.75 | 0.0436 | 0.42 |
| C- a_p | 3.37E+04 | 1 | 3.37E+04 | 840.79 | < 0.0001 | 74.32 |
| AB | 5.88 | 1 | 5.88 | 0.15 | 0.7062 | 0.01 |
| AC | 2585.45 | 1 | 2585.45 | 64.56 | < 0.0001 | 5.71 |
| BC | 0.013 | 1 | 0.013 | 0.00032 | 0.986 | 0.00 |
| A^2 | 32.02 | 1 | 32.02 | 0.8 | 0.3837 | 0.07 |
| B^2 | 41.58 | 1 | 41.58 | 1.04 | 0.3225 | 0.09 |
| C^2 | 271.53 | 1 | 271.53 | 6.78 | 0.0185 | 0.60 |
| Residual | 680.77 | 17 | 40.05 | | | 1.50 |
| Cor | | | | | | |
| Total | 4.53E+04 | 26 | | | | 100 |

Table 5.4 ANOVA for surface roughness (Ra) during dry condition

| R _a Dry | Sum of Squares | DoF | Mean Square | F-Value | P-value | % Cont |
|--------------------|----------------|-----|-------------|----------|----------|--------|
| Model | 9.18 | 9 | 1.02 | 27.56 | < 0.0001 | |
| A-f | 6.34 | 1 | 6.34 | 171.3 | < 0.0001 | 64.63 |
| B-V _c | 1 | 1 | 1 | 27.03 | < 0.0001 | 10.19 |
| C-a _p | 0.59 | 1 | 0.59 | 15.93 | 0.0009 | 6.01 |
| AB | 0.2 | 1 | 0.2 | 5.5 | 0.0314 | 2.04 |
| AC | 0.023 | 1 | 0.023 | 0.61 | 0.4438 | 0.23 |
| BC | 0.77 | 1 | 0.77 | 20.89 | 0.0003 | 7.85 |
| A ² | 3.31E-04 | 1 | 3.31E-04 | 8.93E-03 | 0.9258 | 0.00 |
| B ² | 0.29 | 1 | 0.29 | 7.9 | 0.012 | 2.96 |
| C ² | 0.066 | 1 | 0.066 | 1.79 | 0.1989 | 0.67 |
| Residual | 0.63 | 17 | 0.037 | | | 6.42 |
| Cor Total | 9.81 | 26 | | | | 100 |

Table 5.5 ANOVA for surface roughness (Ra) during wet condition

| R _a Wet | Sum of Squares | DoF | Mean Square | F-Value | P-value | % Cont |
|--------------------|----------------|-----|-------------|----------|----------|--------|
| Model | 9.5 | 9 | 1.06 | 27.05 | < 0.0001 | |
| A-f | 6.71 | 1 | 6.71 | 171.95 | < 0.0001 | 66.04 |
| B-V _c | 0.86 | 1 | 0.86 | 22.01 | 0.0002 | 8.46 |
| C-a _p | 0.55 | 1 | 0.55 | 14.19 | 0.0015 | 5.41 |
| AB | 0.28 | 1 | 0.28 | 7.15 | 0.016 | 2.76 |
| AC | 0.03 | 1 | 0.03 | 0.78 | 0.3896 | 0.30 |
| BC | 0.92 | 1 | 0.92 | 23.68 | 0.0001 | 9.06 |
| A ² | 9.70E-04 | 1 | 9.70E-04 | 2.50E-02 | 0.8765 | 0.01 |
| B ² | 0.22 | 1 | 0.22 | 5.68 | 0.0291 | 2.17 |
| C ² | 0.04 | 1 | 0.04 | 1.03 | 0.3253 | 0.39 |
| Residual | 0.66 | 17 | 0.039 | | | 6.50 |
| Cor Total | 10.16 | 26 | | | | 100 |

Table 5.6 ANOVA for surface roughness (Ra) during cryogenic condition

| R _a Cryo | Sum of Squares | DoF | Mean Square | F-Value | P-value | % Cont |
|---------------------|----------------|-----|-------------|----------|----------|--------|
| Model | 8.93 | 9 | 0.99 | 32.57 | < 0.0001 | |
| A-f | 6.15 | 1 | 6.15 | 201.93 | < 0.0001 | 65.15 |
| B-V _c | 1 | 1 | 1 | 32.68 | < 0.0001 | 10.59 |
| C-a _p | 0.57 | 1 | 0.57 | 18.86 | 0.0004 | 6.04 |
| AB | 0.25 | 1 | 0.25 | 8.08 | 0.0113 | 2.65 |
| AC | 0.006186 | 1 | 0.006186 | 0.2 | 0.6579 | 0.07 |
| BC | 0.76 | 1 | 0.76 | 25.1 | 0.0001 | 8.05 |
| A ² | 4.51E-05 | 1 | 4.51E-05 | 1.48E-03 | 0.9697 | 0.00 |
| B ² | 0.27 | 1 | 0.27 | 8.98 | 0.0081 | 2.86 |
| C ² | 0.061 | 1 | 0.061 | 2.01 | 0.1739 | 0.65 |
| Residual | 0.52 | 17 | 0.03 | | | 5.51 |
| Cor Total | 9.44 | 26 | | | | 100 |

Table 5.7 ANOVA for tool tip temperature (T) during dry condition

| T Dry | Sum of Squares | DoF | Mean Square | F-Value | P-value | % Cont |
|------------------|----------------|-----|-------------|---------|----------|--------|
| Model | 4819.4 | 9 | 535.49 | 28.05 | < 0.0001 | |
| A-f | 122.42 | 1 | 122.42 | 6.41 | 0.0215 | 2.38 |
| B-V _c | 3894.64 | 1 | 3894.64 | 203.97 | < 0.0001 | 75.71 |
| C-a _p | 505.9 | 1 | 505.9 | 26.5 | < 0.0001 | 9.83 |
| AB | 20.16 | 1 | 20.16 | 1.06 | 0.3186 | 0.39 |
| AC | 32.34 | 1 | 32.34 | 1.69 | 0.2104 | 0.63 |
| BC | 379.81 | 1 | 379.81 | 19.89 | 0.0003 | 7.38 |
| A ² | 0.76 | 1 | 0.76 | 0.04 | 0.8439 | 0.01 |
| B ² | 373.63 | 1 | 373.63 | 19.57 | 0.0004 | 7.26 |
| C ² | 3.14 | 1 | 3.14 | 0.16 | 0.69 | 0.06 |
| Residual | 324.6 | 17 | 19.09 | | | 6.31 |
| Cor Total | 5144 | 26 | | | | 100 |

Table 5.8 ANOVA for tool tip temperature (T) during wet condition

| T Wet | Sum of Squares | DoF | Mean Square | F-Value | P-value | % Cont |
|------------------|----------------|-----|-------------|---------|----------|--------|
| Model | 4920.1 | 9 | 546.68 | 30.27 | < 0.0001 | |
| A-f | 149.59 | 1 | 149.59 | 8.28 | 0.0104 | 2.86 |
| B-V _c | 3525.42 | 1 | 3525.42 | 195.22 | < 0.0001 | 67.45 |
| C-a _p | 1015.93 | 1 | 1015.93 | 56.26 | < 0.0001 | 19.44 |
| AB | 37 | 1 | 37 | 2.05 | 0.1705 | 0.71 |
| AC | 18.9 | 1 | 18.9 | 1.05 | 0.3206 | 0.36 |
| BC | 229.57 | 1 | 229.57 | 12.71 | 0.0024 | 4.39 |
| A ² | 0.89 | 1 | 0.89 | 0.049 | 0.8266 | 0.02 |
| B ² | 94.5 | 1 | 94.5 | 5.23 | 0.0353 | 1.81 |
| C ² | 76.78 | 1 | 76.78 | 4.25 | 0.0548 | 1.47 |
| Residual | 307 | 17 | 18.06 | | | 5.87 |
| Cor Total | 5227.1 | 26 | | | | 100 |

Table 5.9 ANOVA for tool tip temperature (T) during cryogenic condition

| T Cryo | Sum of Squares | DoF | Mean Square | F-Value | P-value | % Cont |
|------------------|----------------|-----|-------------|---------|----------|--------|
| Model | 133.82 | 9 | 14.87 | 46.48 | < 0.0001 | |
| A-f | 7.35 | 1 | 7.35 | 22.96 | 0.0002 | 5.28 |
| B-V _c | 104.11 | 1 | 104.11 | 325.41 | < 0.0001 | 74.76 |
| C-a _p | 9.59 | 1 | 9.59 | 29.99 | < 0.0001 | 6.89 |
| AB | 0.079 | 1 | 0.079 | 0.25 | 0.6257 | 0.06 |
| AC | 0.19 | 1 | 0.19 | 0.59 | 0.4543 | 0.14 |
| BC | 12.15 | 1 | 12.15 | 37.97 | < 0.0001 | 8.72 |
| A ² | 0.007746 | 1 | 0.007746 | 0.024 | 0.8782 | 0.01 |
| B ² | 0.98 | 1 | 0.98 | 3.06 | 0.0985 | 0.70 |
| C ² | 0.2 | 1 | 0.2 | 0.63 | 0.4382 | 0.14 |
| Residual | 5.44 | 17 | 0.32 | | | 3.91 |
| Cor Total | 139.26 | 26 | | | | 100 |

Table 5.10 Experimental verses predicted (RSM and ANN) during dry condition

| Sl No | Cutting Force (F_z) | | | Surface Roughness (R_a) | | | Tool Tip Temperature (T) | | |
|-------|-------------------------|--------|--------|-----------------------------|------|------|--------------------------|-------|-------|
| | Exp | RSM | ANN | Exp | RSM | ANN | Exp | RSM | ANN |
| 1 | 85.95 | 81.40 | 110.74 | 3.54 | 3.65 | 3.61 | 39.60 | 43.52 | 41.17 |
| 2 | 125.90 | 131.68 | 66.41 | 4.27 | 4.17 | 4.27 | 40.12 | 43.63 | 41.80 |
| 3 | 167.05 | 164.98 | 164.54 | 5.12 | 4.70 | 4.95 | 42.56 | 43.03 | 43.19 |
| 4 | 66.55 | 74.40 | 107.63 | 3.31 | 3.36 | 3.38 | 55.86 | 56.03 | 54.24 |
| 5 | 123.05 | 125.97 | 66.08 | 3.88 | 3.95 | 3.83 | 57.98 | 56.81 | 57.20 |
| 6 | 166.89 | 160.60 | 162.38 | 4.25 | 4.54 | 4.25 | 58.87 | 56.90 | 58.98 |
| 7 | 65.00 | 66.08 | 81.82 | 3.43 | 3.42 | 3.43 | 62.58 | 59.55 | 60.43 |
| 8 | 120.20 | 121.08 | 102.25 | 4.21 | 4.18 | 4.24 | 63.84 | 62.12 | 63.63 |
| 9 | 164.89 | 159.29 | 165.61 | 4.93 | 4.97 | 4.95 | 64.25 | 64.07 | 64.21 |
| 10 | 144.15 | 136.54 | 136.60 | 4.12 | 4.02 | 4.13 | 40.59 | 41.10 | 40.89 |
| 11 | 219.35 | 221.09 | 210.95 | 4.28 | 4.50 | 4.29 | 45.26 | 42.82 | 45.26 |
| 12 | 281.75 | 290.14 | 279.09 | 4.79 | 4.98 | 4.85 | 46.85 | 43.89 | 44.81 |
| 13 | 142.83 | 129.41 | 117.79 | 3.83 | 3.60 | 3.79 | 60.87 | 56.56 | 60.07 |
| 14 | 217.69 | 215.24 | 148.40 | 4.02 | 4.14 | 3.70 | 61.89 | 58.95 | 61.54 |
| 15 | 279.86 | 285.62 | 210.77 | 4.68 | 4.69 | 4.67 | 62.48 | 60.71 | 61.67 |
| 16 | 115.50 | 120.73 | 117.95 | 3.34 | 3.30 | 3.41 | 66.58 | 68.01 | 64.12 |
| 17 | 214.69 | 209.99 | 213.33 | 4.12 | 4.02 | 4.16 | 67.56 | 72.19 | 80.41 |
| 18 | 276.89 | 283.95 | 279.61 | 4.81 | 4.76 | 4.84 | 67.98 | 75.82 | 72.37 |
| 19 | 198.45 | 207.65 | 203.84 | 4.37 | 4.60 | 4.46 | 42.69 | 40.13 | 41.96 |
| 20 | 326.25 | 326.46 | 329.10 | 5.17 | 5.03 | 5.11 | 44.85 | 43.46 | 44.73 |
| 21 | 442.35 | 431.26 | 434.66 | 5.45 | 5.47 | 5.41 | 45.27 | 46.21 | 44.86 |
| 22 | 195.92 | 200.39 | 215.18 | 4.25 | 4.04 | 4.21 | 56.70 | 58.54 | 57.47 |
| 23 | 321.45 | 320.47 | 332.15 | 4.59 | 4.54 | 4.64 | 58.50 | 62.54 | 57.01 |
| 24 | 424.45 | 426.60 | 436.06 | 5.09 | 5.05 | 5.24 | 59.86 | 65.98 | 60.72 |
| 25 | 193.61 | 191.34 | 195.94 | 3.19 | 3.39 | 3.30 | 75.89 | 77.92 | 74.46 |
| 26 | 318.25 | 314.86 | 421.64 | 4.05 | 4.06 | 4.06 | 86.23 | 83.71 | 86.99 |
| 27 | 422.87 | 424.57 | 420.81 | 4.77 | 4.76 | 4.72 | 97.50 | 89.01 | 76.47 |

Table 5.11 Experimental verses predicted (RSM and ANN) during wet condition

| Sl No | Cutting Force (F_z) | | | Surface Roughness (R_a) | | | Tool Tip Temperature (T) | | |
|-------|-------------------------|--------|--------|-----------------------------|------|------|--------------------------|-------|-------|
| | Exp | RSM | ANN | Exp | RSM | ANN | Exp | RSM | ANN |
| 1 | 79.56 | 87.62 | 80.39 | 3.28 | 3.35 | 3.32 | 35.90 | 36.36 | 37.20 |
| 2 | 115.60 | 118.15 | 89.41 | 4.02 | 3.87 | 4.01 | 37.90 | 35.95 | 38.17 |
| 3 | 142.95 | 144.72 | 137.16 | 4.77 | 4.40 | 4.78 | 37.80 | 36.31 | 41.93 |
| 4 | 89.11 | 83.11 | 83.77 | 3.06 | 3.10 | 3.11 | 39.56 | 44.84 | 39.66 |
| 5 | 114.87 | 112.38 | 112.13 | 3.56 | 3.70 | 3.27 | 40.78 | 45.33 | 42.00 |
| 6 | 133.10 | 137.63 | 143.39 | 3.98 | 4.30 | 3.98 | 45.23 | 46.64 | 46.29 |
| 7 | 85.64 | 83.34 | 83.53 | 3.14 | 3.15 | 3.13 | 55.58 | 52.50 | 55.69 |
| 8 | 113.98 | 109.21 | 108.22 | 3.96 | 3.97 | 3.99 | 58.63 | 55.41 | 60.00 |
| 9 | 132.28 | 130.92 | 137.22 | 4.87 | 4.79 | 4.76 | 61.20 | 59.24 | 60.87 |
| 10 | 110.00 | 105.78 | 110.82 | 3.84 | 3.77 | 3.51 | 41.90 | 42.09 | 41.40 |
| 11 | 139.75 | 148.14 | 145.55 | 4.08 | 4.24 | 4.10 | 42.87 | 42.91 | 43.88 |
| 12 | 214.00 | 187.04 | 203.73 | 4.55 | 4.71 | 4.64 | 44.83 | 44.55 | 46.55 |
| 13 | 109.21 | 101.12 | 95.16 | 3.59 | 3.37 | 3.52 | 58.84 | 52.86 | 45.00 |
| 14 | 138.91 | 142.21 | 143.77 | 3.81 | 3.92 | 3.72 | 59.90 | 54.58 | 56.13 |
| 15 | 169.80 | 179.80 | 171.07 | 4.48 | 4.47 | 4.53 | 60.10 | 57.17 | 61.83 |
| 16 | 90.18 | 100.93 | 87.21 | 3.08 | 3.03 | 3.09 | 65.50 | 66.68 | 66.71 |
| 17 | 136.93 | 138.63 | 133.37 | 3.89 | 3.80 | 3.88 | 65.69 | 70.83 | 67.41 |
| 18 | 167.56 | 172.68 | 171.20 | 4.56 | 4.57 | 4.64 | 67.97 | 75.94 | 72.56 |
| 19 | 122.40 | 124.74 | 128.54 | 4.01 | 4.34 | 4.08 | 40.50 | 40.66 | 41.01 |
| 20 | 179.30 | 178.92 | 168.35 | 4.92 | 4.77 | 4.84 | 41.87 | 42.71 | 38.67 |
| 21 | 221.70 | 230.16 | 218.73 | 5.17 | 5.19 | 5.07 | 43.60 | 45.63 | 44.21 |
| 22 | 120.84 | 119.93 | 136.02 | 4.06 | 3.80 | 4.07 | 52.89 | 53.73 | 52.85 |
| 23 | 175.35 | 172.84 | 212.70 | 4.39 | 4.31 | 4.55 | 56.88 | 56.68 | 58.63 |
| 24 | 220.60 | 222.76 | 220.37 | 4.85 | 4.81 | 4.83 | 58.19 | 60.54 | 60.91 |
| 25 | 118.96 | 119.33 | 117.84 | 2.93 | 3.08 | 3.06 | 72.76 | 73.71 | 69.73 |
| 26 | 174.63 | 168.84 | 173.02 | 3.74 | 3.79 | 3.56 | 78.96 | 79.08 | 80.44 |
| 27 | 218.96 | 215.23 | 203.24 | 4.52 | 4.51 | 4.51 | 92.58 | 85.48 | 90.63 |

Table 5.12 Experimental verses predicted (RSM and ANN) during cryogenic condition

| Sl No | Cutting Force (F_z) | | | Surface Roughness (R_a) | | | Tool Tip Temperature (T) | | |
|-------|-------------------------|--------|--------|-----------------------------|------|------|--------------------------|-------|-------|
| | Exp | RSM | ANN | Exp | RSM | ANN | Exp | RSM | ANN |
| 1 | 71.90 | 73.64 | 72.00 | 2.13 | 2.19 | 2.20 | 34.95 | 34.43 | 34.85 |
| 2 | 73.70 | 80.23 | 73.71 | 2.75 | 2.66 | 2.73 | 35.15 | 35.23 | 35.08 |
| 3 | 85.33 | 82.38 | 78.88 | 3.51 | 3.15 | 3.49 | 36.55 | 36.13 | 34.32 |
| 4 | 66.65 | 68.81 | 66.70 | 1.83 | 1.90 | 1.82 | 34.35 | 35.67 | 35.32 |
| 5 | 72.36 | 75.75 | 72.35 | 2.39 | 2.45 | 2.09 | 36.15 | 36.42 | 36.14 |
| 6 | 84.78 | 78.27 | 84.79 | 2.76 | 3.01 | 2.84 | 37.65 | 37.29 | 37.09 |
| 7 | 65.54 | 65.85 | 65.75 | 1.92 | 1.93 | 1.77 | 37.95 | 37.45 | 37.90 |
| 8 | 71.89 | 73.76 | 71.88 | 2.71 | 2.68 | 2.68 | 38.25 | 38.10 | 38.22 |
| 9 | 83.83 | 77.29 | 83.88 | 3.42 | 3.44 | 3.40 | 38.55 | 38.84 | 38.56 |
| 10 | 106.14 | 96.22 | 83.38 | 2.63 | 2.54 | 2.65 | 34.25 | 34.14 | 34.33 |
| 11 | 121.50 | 117.17 | 121.47 | 2.77 | 2.99 | 2.82 | 34.45 | 34.82 | 34.40 |
| 12 | 131.09 | 134.31 | 131.24 | 3.29 | 3.45 | 3.73 | 34.65 | 35.59 | 34.66 |
| 13 | 97.36 | 91.37 | 79.55 | 2.33 | 2.12 | 2.27 | 36.55 | 35.90 | 36.54 |
| 14 | 115.09 | 112.68 | 115.00 | 2.52 | 2.64 | 2.52 | 37.25 | 36.54 | 37.25 |
| 15 | 119.36 | 130.19 | 117.54 | 3.19 | 3.18 | 3.20 | 37.65 | 37.27 | 37.66 |
| 16 | 87.92 | 88.36 | 87.65 | 1.85 | 1.79 | 1.74 | 38.95 | 39.11 | 38.95 |
| 17 | 113.69 | 110.64 | 113.44 | 2.61 | 2.51 | 2.55 | 39.65 | 39.63 | 38.60 |
| 18 | 117.96 | 129.16 | 118.03 | 3.29 | 3.26 | 3.53 | 39.85 | 40.25 | 39.84 |
| 19 | 125.22 | 132.26 | 125.02 | 2.86 | 3.09 | 2.76 | 34.35 | 34.22 | 34.43 |
| 20 | 165.65 | 167.57 | 165.83 | 3.67 | 3.52 | 3.61 | 34.85 | 34.77 | 34.66 |
| 21 | 202.95 | 199.70 | 190.87 | 3.94 | 3.96 | 3.87 | 35.55 | 35.42 | 35.55 |
| 22 | 124.83 | 127.38 | 144.14 | 2.73 | 2.53 | 2.73 | 36.35 | 36.51 | 36.30 |
| 23 | 164.15 | 163.06 | 179.17 | 3.07 | 3.03 | 3.05 | 36.65 | 37.02 | 36.65 |
| 24 | 198.50 | 195.56 | 173.04 | 3.59 | 3.55 | 3.53 | 37.65 | 37.63 | 37.66 |
| 25 | 122.68 | 124.33 | 122.54 | 1.68 | 1.85 | 1.70 | 40.85 | 41.13 | 40.82 |
| 26 | 163.79 | 160.97 | 163.48 | 2.54 | 2.55 | 2.50 | 41.65 | 41.53 | 41.67 |
| 27 | 197.54 | 194.48 | 197.54 | 3.28 | 3.27 | 3.47 | 42.35 | 42.02 | 42.17 |

LIST OF PUBLICATIONS AND CONFERENCE

| Sl. No. | Title of the paper | Authors (in the same order as in the paper. Underline the Research Scholar's name) | Name of the Journal/ Conference, Vol., No., Pages | Month, Year of Publication | Category* |
|---------|--|--|--|----------------------------|-----------|
| 1 | Investigation of machinability characteristics on EN47 steel for cutting force and tool wear using optimization technique | <u>Vasu M.</u> H Shivananda Nayaka, | Material Research Express. (SCIE-1.151) https://doi.org/10.1088/2053-1591/aac67f | 2018 | 1 |
| 2 | Comparative study of coated and uncoated tool inserts with dry machining of EN47 steel using Taguchi L ₉ optimization technique | <u>Vasu M.</u> H Shivananda Nayaka, | AIP conference series Proceedings (Scopus) Vol 1943, Issue 1, P 020063. https://doi: 0.1063/1.5029639 | 2018 | 1 |
| 3 | Investigation of Cutting Force Tool Tip Temperature and Surface Roughness during Dry Machining of Spring Steel | <u>Vasu M.</u> H Shivananda Nayaka, | Materials Today Proceedings (Scopus), Vol 5, Issue 2, Part 2, P 7141-7149. https://doi.org/10.1016/j.matpr.2017.11.379 . | 2018 | 1 |
| 4 | Comparative study of turning process on EN47 spring steel | <u>Vasu M.</u> H Shivananda Nayaka, | Materials Today Proceedings (Scopus), | 2018 | 1 |

| | | | | | |
|---|--|---|--|------|---|
| | with different nose radii using statistical technique | | Vol 5, Issue 9, Part 1, P 16893-16903. https://doi.org/10.1016/j.matpr.2018.04.092 . | | |
| 5 | Turning process on EN47 spring steel with different tool nose radii using OFAT approach | <u>Vasu M,</u> H Shivananda Nayaka, | Advances in Modelling and Analysis A (Scopus), Vol. 55, No. 2, June,2018, P 43-46 https://doi.org/10.18280/ama_a.550201 . | 2018 | 1 |
| 6 | Investigation of Cutting Force Tool Tip Temperature and Surface Roughness during Dry Machining of Spring Steel | <u>Vasu M,</u> H Shivananda Nayaka, | International Conference on Emerging Trends in Materials and Manufacturing Engineering, March 10 th -12 th 2017. NIT Tiruchirappalli, Tamilnadu, India. | 2017 | 3 |
| 7 | Comparative study of turning process on EN47 spring steel with different nose radii using statistical technique | <u>Vasu M,</u> H Shivananda Nayaka, | International Conference on Advances in Materials & Processing: Challenges & Opportunities Nov 30 th - Dec 2 nd 2017. IIT Roorkee, India | 2017 | 3 |
| 8 | Comparative study of coated and uncoated tool inserts with dry machining of EN47 steel using Taguchi L ₉ optimization technique | <u>Vasu M,</u> H Shivananda Nayaka, | Advances in International Conference on Design, Materials & Manufacture, Jan 29 th to 31 st Jan -2018 NITK Surathkal. | 2018 | 3 |

| | | | | | |
|----|--|---|---|------|---|
| 9 | Comparative Study of Turning Process on EN47 Spring Steel with Different Nose Radii Using OFAT Approach | H Shivananda Nayaka, <u>Vasu M.</u> | 7 th International Engineering Symposium, Kumamoto University, March 7th -9th (2018). Japan. | 2018 | 3 |
| 10 | Machinability studies on EN47 Spring Steel of turning process by optimization technique during dry and wet condition | <u>Vasu M.</u> H Shivananda Nayaka, | 8 th International Engineering Symposium, Kumamoto University, March 13th -15th (2019). Japan. | 2019 | 3 |

*Category:

- 1: Journal paper, full paper reviewed.
- 2: Journal paper, Abstract reviews.
- 3: Conference/Symposium paper, full paper reviewed.
- 4: Conference/Symposium paper, abstract reviewed.
- 5: others (including papers in Workshops, NITK Research Bulletins, Short notes etc.)

Vasu M

Research Scholar

Name & Signature, with Date

Dr. H Shivananda Nayaka

Research Guide

Name & Signature, with Date

BIO-DATA

Name: Vasu. M
Father's Name: Mallesha. M
Date of Birth: 30-January-1987
Nationality: Indian
Marital Status: Married

Address:

Permanent Address

S/o Mallesha M, Ningamma Nilaya,
#654/2, 1st Main, B B Garden Road,
Fort Mohalla, Agrahara,
Mysuru-570004

Present Address

Research Scholar,
Department of Mechanical Engineering
National Institute of Technology
Karnataka.
Surathkal, Mangalore-575025

Mobile Number: +91-9611-604-276
E-mail id: vasu.m.manu@gmail.com

Educational Qualification:

| Course | Institution | University | Batch | Percentage |
|--|--|------------|-------|----------------|
| Ph. D. (Mechanical Engineering) | National Institute of Technology Karnataka. Surathkal. | NITK | 2019 | 6.69 (CGPA) |
| M.Tech. (Manufacturing Engineering) | National Institute of Technology Karnataka. Surathkal. | NITK | 2012 | 7.00 (CGPA) |
| B.E. (Industrial Engineering & Management) | Sri Siddhartha Institute of Technology, Tumkur. | VTU | 2010 | 65.70% |

Publication Details

| Papers Published | Under Review | Conference | Workshops/ Symposium | Awards and Recognitions |
|-------------------------|---------------------|-------------------|---------------------------------|--|
| 5 | 2 | 3 | 5 | 1. MHRD Scholarship for perusing MTech and Ph.D. |

I declare that the above information is true and correct to the best of my knowledge.

(VASU. M)